

A STUDY OF NITRIC OXIDE AND HYDROGEN PRODUCTION BASED ON CHEMICAL LOOPING

Submitted in partial fulfilment of the requirements for the degree of
Doctor of Philosophy

of the

Indian Institute of Technology, Bombay, India

and

Monash University, Australia

by

Sonal Keshawrao Thengane

(IITB: 114174003; [REDACTED])

Under the guidance of

Prof. Santanu Bandyopadhyay

Prof. Sagar Mitra

**Indian Institute of Technology Bombay
India**

Prof. Andrew Hoadley

Prof. Sankar Bhattacharya

**Monash University
Australia**



*The course of study for this award was developed jointly by
the Indian Institute of Technology, Bombay and Monash University, Australia
and given academic recognition by each of them.*


The programme was administered by The IITB-Monash Research Academy

(2016)

APPROVAL SHEET

This thesis/dissertation/report entitled “A study of Nitric Oxide and Hydrogen production based on Chemical Looping” by Sonal Keshawrao Thengane is approved for the degree of Doctor of Philosophy.

External Examiner



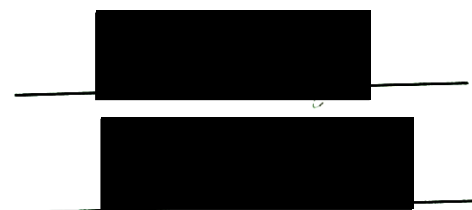
Internal Examiner



IITB Supervisor (s)



Monash Supervisor (s)



Chairman



Date : 20/6/2016

Place : Mumbai

DECLARATION

I declare that this written submission represents my ideas in my own words and where others' ideas or words have been included, I have adequately cited and referenced the original sources. I also declare that I have adhered to all principles of academic honesty and integrity and have not misrepresented or fabricated or falsified any idea/data/fact/source in my submission. I understand that any violation of the above will be cause for disciplinary action by the Institute and can also evoke penal action from the sources which have thus not been properly cited or from whom proper permission has not been taken when needed.

Notice 1

Under the Copyright Act 1968, this thesis must be used only under the normal conditions of scholarly fair dealing. In particular no results or conclusions should be extracted from it, nor should it be copied or closely paraphrased in whole or in part without the written consent of the author. Proper written acknowledgement should be made for any assistance obtained from this thesis.

Notice 2

I certify that I have made all reasonable efforts to secure copyright permissions for third-party content included in this thesis and have not knowingly added copyright content to my work without the owner's permission.



Student Name: **Sonal Keshawrao Thengane**

IITB ID: 114174003



Date: 20 June 2016

ABSTRACT

Hydrogen is considered as a fuel of the future with several potential benefits whereas nitric oxide has varied medical and pharmaceutical applications in addition to being the major intermediate in the production of nitric acid which has itself extended applications. The conventional processes employ highly exothermic catalytic oxidation of ammonia to produce nitric oxide, and energy intensive steam methane reforming of natural gas to produce hydrogen. These fossil fuel based commercial processes are effective, but face future challenges due to the depletion of fossil resources and atmospheric emissions. There have been several efforts in the direction of improvement of these processes energetically and economically, however, there have been no significant changes in the main process reactions. As hydrogen is the starting precursor for ammonia and hence nitric oxide production, the cost-benefit analysis is performed for different hydrogen producing technologies where the benefits are evaluated using multi-criteria decision making approach such as Analytic Hierarchy Process. Water splitting by a chemical looping approach proved to be the best renewable technology for the chosen perspective of selecting a cost effective environmentally benign technology. In the present work, a chemical looping based process is proposed for production of nitric oxide and hydrogen with a major focus on the reaction of ammonia with different metal oxides. Nitric oxide and hydrogen are produced by reduction of metal oxide by ammonia and the metal oxide is regenerated by oxidation thus completing the cycle. Based on the method of regeneration, the two chemical looping based processes are possible, namely chemical looping using air oxidation (CLAO) and chemical looping using hydrolysis (CLHYD).

The objective of the thesis is to carry out both thermodynamic and experimental studies of the proposed chemical looping based processes to produce nitric oxide and hydrogen. The thermodynamic feasibility analysis and the experimental constraints resulted in the selection of cupric oxide (CuO), ferric oxide (Fe₂O₃) and cobalt oxide (Co₃O₄) for reaction with ammonia at 825 °C, 830 °C and 530 °C, respectively. The experimental results confirm the feasibility of the ammonia-metal oxide reaction for each of these metal oxides with conversions as high as 90 % in semi-batch mode reactor. The effect of varying the different parameters such as temperature, ammonia concentration, and particle size on the yield of nitric oxide is reported for the case of CuO and a reaction mechanism is proposed to explain

these results. This simultaneous production of nitric oxide and hydrogen in endothermic manner can prove to be a better alternative for conventional exothermic oxidation of ammonia in presence of platinum catalyst at 900 °C. The proposed chemical looping based processes are simulated in Aspen Plus and are compared with the steam methane reforming (SMR) approach for nitric oxide production on the basis of energy and exergy analysis. The exergy efficiency for three processes, namely, SMR, CLHYD and CLAO including steam generation potential is calculated to be 36.9 %, 62.9 % and 66.5 % respectively. The chemical looping approach is found to be exergetically more efficient and environmentally more benign than the reforming based process. The chemical looping based processes offer the advantages such as operation at lower pressures, avoidable expensive catalysts, independent of fossil fuels as feed, negligible nitrous oxide (N₂O) emission, and the hydrogen product that can be totally or partially used for production of ammonia. The proposed process scheme for nitric oxide and hydrogen production holds the potential for significant reductions in cost, energy and environmental emissions.

ACKNOWLEDGEMENT

I take this opportunity in expressing my sincere gratitude to all the people who have their direct or indirect contributions in making this thesis possible. First and foremost I express my profound sense of reverence to my main supervisors Prof. Santanu Bandyopadhyay and Prof. Andrew Hoadley for their constant guidance, support and motivation throughout the course in both India and Australia. Prof. Santanu has inspired me to become an independent researcher making me explore and develop my potential of critical thinking and analysis. The joy and enthusiasm he has for research is contagious and the frequent walk and talk discussions with him helped me to develop a sense of belonging and interest in the research topic. Prof. Andrew demonstrated a perfect combination of an enthusiastic hard-working supervisor and a very good human being who kept on positively inspiring me with his immense support and consistent evaluation during the entire course. He believed in me and constantly motivated me to give my best in the research and thesis writing. I take pride in dedicating this work to both of my supervisors.

I am extremely thankful to my loving and caring co-supervisors Prof. Sankar Bhattacharya and Prof. Sagar Mitra for their consistent support, valuable guidance and encouragement. I would like to gratefully acknowledge the generous financial support of the Orica Mining Services, Newcastle, Australia. My special thanks must go to Greg Rigby and Milinda Ranasinghe, the external mentors from Orica Mining Services who helped and guided me during my visit to their industrial plants and research labs in Australia. I am also indebted to Prof. Sanjay Mahajani, Prof. Balasubramaniam Kavaipatti, and Prof. Akshat Tanksale, the members of my research progress committee for their precious comments during the annual seminars which helped me to present ideas in simple and clear way.

My heartfelt thanks go to Prof. Murali Shastri and Prof. Mohan Krishnamoorthy, CEOs of IITB-Monash Research Academy for their constant support and encouragement in India and Australia. I wish to sincerely thank the staff of the Academy (Kuheli, Jayashree, Nancy, Mamta, Rahul and so on), Energy Science and Engineering Department (Leena, Sharmila, Pawarji, Meenakshi), and Monash University (Kim, Ron, Ross, Harry, Martin, Trent) for all their support and co-operation. My time at IIT Bombay and Monash University was made enjoyable in large part due to friends, namely, Prashant, Ashish, Niteen, Prachi and

colleagues such as Krishnapriya, Sharmen, Tristan, Ishan, Pratham, Bayzid, Nishith who became a part of my life. There are many more and I thank each and everyone from bottom of my heart for their kind help and love.

I would like to thank my mom Mangala for her love, trust and encouragement during tough times. I dedicate this work in the memory of my late dearest younger brother Chetan for his loving memories and my late father Dr. K. D. Thengane who raised me with a love of science and supported me in all my pursuits. Last but not the least I owe my gratitude to my loving, supportive, encouraging, and patient fiancée Madhukriti whose faithful support during the final stages of this Ph.D. is much appreciated.

Thank you.

Date: 20 June 2016

Sonal Keshawrao Thengane
IITB-Monash Research Academy

CONTENTS

<i>List of Figures</i>	x
<i>List of Tables</i>	xiii
<i>Nomenclature</i>	xv
CHAPTER 1 INTRODUCTION	
1.1 Hydrogen and Nitric Oxide	1
1.2 Objective	4
1.3 Dissertation Structure	4
CHAPTER 2 LITERATURE REVIEW	
2.1 Nitric Oxide Production	6
2.2 Hydrogen Production	7
2.3 Chemical Looping based Processes	11
2.4 Research Gaps	13
CHAPTER 3 EVALUATION OF HYDROGEN PRODUCTION TECHNOLOGIES	
3.1 Hydrogen Production Technologies	15
3.2 Methodology	16
3.2.1 Costs	19
3.2.2 Benefits	21
3.3 Results and Discussion	25
3.4 Conclusions	27
CHAPTER 4 AMMONIA OXIDATION BY CHEMICAL LOOPING	
4.1 Introduction	29
4.2 Oxidation of Ammonia	30
4.3 Chemical Looping based Ammonia Oxidation	32
4.4 Thermodynamic Feasibility	34
4.5 Conclusions	37

CHAPTER 5 MATERIALS AND METHODS	
5.1 Experimental Set up	39
5.2 Procedure	41
5.3 Reactor Designs	42
5.4 Instrumentation	44
5.5 Issues and Constraints	46
CHAPTER 6 EXPERIMENTAL RESULTS AND DISCUSSION	
6.1 Results	48
6.2 Discussion	53
6.2.1 N ₂ O formation	58
6.3 Experiments with Reactor 4	61
6.3.1 Results and Discussion	62
6.4 Conclusions	66
CHAPTER 7 THERMODYNAMIC ANALYSIS	
7.1 Introduction	67
7.2 Process Simulation	69
7.3 Methodology	74
7.4 Results	75
7.5 Discussion	81
7.6 Conclusions	86
CHAPTER 8 CONCLUSIONS AND FUTURE WORK	
8.1 Main Contributions	87
8.2 Future Work	88
APPENDIX A	89
APPENDIX B	91
APPENDIX C	105
REFERENCES	106
LIST OF PUBLICATIONS	115

LIST OF FIGURES

Figure 1.1 Conventional processing scheme for nitric acid production	2
Figure 1.2 Chemical looping based process scheme for NO and H ₂ production	4
Figure 2.1 Chemical looping set-up for hydrogen production and carbon capture	11
Figure 3.1 Simplified block diagrams for different hydrogen production processes: (a) Steam Methane Reforming (SMR), (b) Coal Gasification (CG), (c) Partial Oxidation of hydro-carbons (POX), (d) Biomass Gasification (BG), (e) PV-based, Wind-based, and Hydro-based electrolysis (PV-EL, W-EL, and H-EL), (f) Water Splitting by Chemical Looping (WS-CL)	18
Figure 3.2 Hierarchy tree structure for the evaluation of eight hydrogen production processes using AHP	24
Figure 3.3 Cost-Benefit analysis results: (a) AHP for assumed criteria weights, (b) AHP for equal criteria weights	27
Figure 4.1 Conventional nitric acid production	29
Figure 4.2 Chemical looping based process schemes for NO and H ₂ production (a) Hydrolysis case (b) Air oxidation case	33
Figure 5.1 Reactor system for chemical looping based NO and H ₂ production	38
Figure 5.2 Schematic of the experimental set-up	40
Figure 5.3 Different types of reactor (a) Reactor 1(normal) (b) Reactor 1 (after hole formation) (c) Reactor 2 (d) Reactor 3 (e) Reactor 4 (before and after tapping)	43
Figure 5.4 Mass Flow Controllers for Ammonia, Air and Nitrogen (a) Ammonia (0-30 ml/min) (b) Air and Nitrogen (0-5 l/min)	45
Figure 5.5 Ammonia flow meter (0-30 ml/min)	46
Figure 5.6 Digital weighing balance (0-50 g)	46
Figure 5.7 Gas analysers with specifications (a) Testo 340 (b) iBRID MX6	46
Figure 6.1 Preliminary experimental results for different metal oxides (a) Co ₃ O ₄ (10 g, 530 °C) (b) Fe ₂ O ₃ (10 g, 830 °C) (c) CuO (15 g, 825 °C) (Operating conditions: 1100 ppm NH ₃ (2.3 ml/min NH ₃ and 2100 ml/min))	49
Figure 6.2 Effect of ammonia concentration (a) 1100 ppm (b) 1600 ppm (c) 2300 ppm (Operating conditions: 15 g CuO (100-120 micron), 825 °C, 2100 ml/min N ₂)	50
Figure 6.3 Effect of temperature (a) 575 °C (b) 700 °C (c) 825 °C (d) 860 °C (Operating conditions: 15 g CuO (100-120 micron), 2300 ppm NH ₃ (4.8 ml/min NH ₃ and 2100 ml/min N ₂))	51

Figure 6.4 Effect of particle size (a) 100-120 micron (b) 40-60 micron (c) 1-10 micron (Operating conditions: 15 g CuO, 825 °C, 1100 ppm NH ₃ (2.3 ml/min NH ₃ and 2100 ml/min N ₂))	52
Figure 6.5 Temperature measurements (Operating conditions: 15 g CuO, 825 °C, 1100 ppm NH ₃ (2.3 ml/min NH ₃ and 2100 ml/min N ₂))	52
Figure 6.6 HSC results for equilibrium composition of oxides of copper (Feed parameters: 1 kmol CuO, 0.1 kmol Cu ₂ O, 0.1 kmol Cu, 1000 kmol N ₂)	54
Figure 6.7 Proposed reaction mechanism for ammonia and CuO	55
Figure 6.8 H ₂ /NO for different metal oxides	57
Figure 6.9 N ₂ O analysis results for CuO, Fe ₂ O ₃ and Co ₃ O ₄	59
Figure 6.10 Experimental results for decomposition of NH ₃ (a) Al ₂ O ₃ : 1 ml/min NH ₃ , 2000 ml/min N ₂ , T = 825 °C (b) Reactor without metal oxide: 1 ml/min NH ₃ , 2000 ml/min N ₂ , T = 825 °C	61
Figure 6.11 Highest NO conversion results (Reactor 2) (a) Co ₃ O ₄ (b) CuO (c) Fe ₂ O ₃ (d) Mn ₃ O ₄ (Operating conditions: 1000 ppm NH ₃ (2.1 ml/min NH ₃ and 2100 ml/min N ₂))	63
Figure 6.12 Experimental results for Co ₃ O ₄ (a) Effect of temperature on NO yield: 3.5 ml/min NH ₃ , 2.1 l/min N ₂ (b) Effect of NH ₃ concentration on NO yield: 2.1 l/min N ₂ , T = 530 °C	64
Figure 6.13 Experimental results for CuO (a) Effect of temperature on NO yield: 2.1 ml/min NH ₃ , 2.1 l/min N ₂ (b) Effect of NH ₃ concentration on NO yield: 2.1 l/min N ₂ , T = 750 °C	64
Figure 6.14 Experimental results for Fe ₂ O ₃ (a) Effect of temperature on NO yield: 2.1 ml/min NH ₃ , 2.1 l/min N ₂ (b) Effect of NH ₃ concentration on NO yield: 2.1 l/min N ₂ , T = 830 °C	65
Figure 6.15 Experimental results for effect of particle size on NO yield (a) CuO: 2.1 ml/min NH ₃ , 2.1 l/min N ₂ , T = 750 °C (b) Fe ₂ O ₃ : 2.1 ml/min NH ₃ , 2.1 l/min N ₂ , T = 830 °C	65
Figure 7.1 Energy and exergy balance for a system	68
Figure 7.2 Reactions in each process for NO production (a) SMR (b) CLHYD (c) CLAO	70
Figure 7.3 Schematic block diagram for NO production (a) SMR (b) CLHYD (c) CLAO	73
Figure 7.4 Grand Composite Curve for SMR based process	78
Figure 7.5 Grand Composite Curve for CLHYD process (Fe ₂ O ₃ /Fe ₃ O ₄)	78
Figure 7.6 Grand Composite Curve for CLAO process (Fe ₂ O ₃ /Fe ₃ O ₄)	79
Figure 7.7 Exergy input, output and losses from the major components in each process (a) SMR process (b) CLHYD process (c) CLAO process	83
Figure 7.8 Percentage contributions of individual process components towards total process exergy loss	84

Figure 7.9 Effect of NO conversion on exergy efficiency of CL based processes	85
---	----

List of Figures (Appendix)

Figure B.1 Flowchart for exergy loss calculation of HEN	92
Figure B.2 Aspen Plus simulation flowsheet for SMR case	93
Figure B.3 Aspen Plus simulation flowsheet for CLHYD case	97
Figure B.4 Aspen Plus simulation flowsheet for CLAO case	101
Figure C.1 Effect of temperature (Operating conditions: 15 g CuO (100-120 micron), 2300 ppm NH ₃ (4.8 ml/min NH ₃ and 2100 ml/min N ₂))	105

LIST OF TABLES

Table 3.1 Data collected from the literature for different hydrogen production processes	21
Table 3.2 Calculated data for year 2013 for different hydrogen production processes with plant capacity of 254.6 tonnes H ₂ /day	21
Table 3.3 CO ₂ equivalent emissions and energy efficiency data for hydrogen production technologies	22
Table 3.4 Pair wise comparison matrix for five criteria using AHP for Case 1	25
Table 3.5 Pair wise comparison matrix for eight alternatives for energy efficiency	26
Table 3.6 Final scores using AHP for Case 1	26
Table 3.7 Final scores using AHP for Case 2	27
Table 4.1 Calculations for thermodynamic feasibility of some metal oxide cases	36
Table 5.1 Selected metal oxides for reaction with ammonia	39
Table 5.2 Specifications of chemicals and gases used	40
Table 6.1 HSC Chemistry results for desorption and additional reactions	56
Table 6.2 Possible reactions between ammonia and copper oxide forming N ₂ O	59
Table 6.3 Calculations for change in weight of metal oxides	60
Table 7.1 Major operating parameters and assumptions for simulated processes	72
Table 7.2 Stream data for SMR, CLHYD and CLAO processes	77
Table 7.3 Chemical exergy values for chemical species at 25°C	79
Table 7.4 Exergy efficiency calculations for overall processes	80

List of Tables (Appendix)

Table A.1 GHG emissions	89
Table A.2 Scalability	89
Table A.3 Raw material and utilities consumption	90
Table A.4 Waste disposal and non GHG emissions	90
Table B.1 Aspen Plus stream summary for SMR case	94
Table B.2 Overall Exergy Loss for SMR based process	95

Table B.3 Individual Component Exergy Loss for SMR based process	95
Table B.4 HEN Exergy Loss for SMR based process	96
Table B.5 Aspen Plus stream summary for CLHYD case	98
Table B.6 Overall Exergy Loss for CLHYD based process	99
Table B.7 Individual Component Exergy Loss for CLHYD based process	99
Table B.8 HEN Exergy Loss for CLHYD based process	100
Table B.9 Aspen Plus stream summary for CLAO case	102
Table B.10 Overall Exergy Loss for CLAO based process	103
Table B.11 Individual Component Exergy Loss for CLAO based process	103
Table B.12 HEN Exergy Loss for CLAO based process	104

NOMENCLATURE

C_C	Capital cost (₹ and A\$)
C_{EA}	Equivalent annual cost (₹ and A\$)
C_{FD}	Feedstock cost (₹/y and A\$/y)
C_{FO}	Fixed operating cost (₹/y and A\$/y)
CI	Consistency index
C_{known}	Cost of plant for known capacity (₹ and A\$)
C_{new}	Cost of plant for selected capacity (₹ and A\$)
C_O	Operating cost (₹/y and A\$/y)
CR	Consistency ratio
CRF	Capital recovery factor (y^{-1})
C_{VO}	Variable operating cost (₹/y and A\$/y)
ϵ	Exergy factor
Ex	Exergy (kW)
Ex_C	Chemical exergy (kW)
Ex_D	Exergy destroyed (kW)
Ex_P	Physical exergy (kW)
Ex_{prod}	Exergy of desired product (kW)
Ex_Q	Exergy associated with heat transfer Q (kW)
Ex_W	Exergy associated with exchange of work (kW)
ΔEx	Change in exergy (kW)
f	Capital cost factor
g	Gaseous
ΔG	Gibbs free energy (kJ)
ΔG_o	Standard Gibbs free energy (kJ)
ΔH	Heat/Enthalpy of formation (kJ)
ΔH_o	Standard Heat of formation (kJ)
ΔH_r	Heat of reaction (kJ)
i	initial
I	Chemical engineering plant cost index
l	Liquid
mC_p	Heat capacity flowrate

<i>mix</i>	mixing
<i>n</i>	Number of attributes
<i>oxi</i>	oxidised
<i>p</i>	present
<i>P</i>	Consumer price index
<i>Q</i>	Heat of adsorption (kJ)
<i>r</i>	Discount rate (%)
<i>R</i>	Ratio of new plant capacity to the known capacity
<i>red</i>	reduced
<i>RI</i>	Random index
<i>s</i>	Solid
<i>S</i>	Entropy (kJ/molK)
ΔS	Change in entropy (kJ/molK)
<i>t</i>	Economic life (y)
T_o	Reference temperature ($^{\circ}\text{C}$)
<i>T</i>	Temperature ($^{\circ}\text{C}$)
T_e	Equilibrium temperature ($^{\circ}\text{C}$)
T_r	Actual reaction (real) temperature ($^{\circ}\text{C}$)
ΔT_{\min}	Minimum driving force (temperature difference)
<i>x</i>	H_2/NO ratio
w_i	Priority value
λ_{\max}	Maximum eigen value
η_C	Carnot factor

Abbreviations

AHP	Analytic hierarchy process
Al_2O_3	Aluminium oxide
AN	Ammonium nitrate
BG	Biomass gasification
CAN	Calcium ammonium nitrate
CG	Coal gasification
CH_4	Methane

CLAO	Chemical looping using air oxidation
CLHYD	Chemical looping using hydrolysis
CLC	Chemical looping combustion
CO	Carbon monoxide
CO ₂	Carbon dioxide
Co ₃ O ₄	Tricobalt Tetraoxide / Cobalt oxide
Cu	Copper
CuO	Copper (II) oxide
Cu ₂ O	Copper (I) oxide / Cuprous oxide
FeO	Iron (II) oxide / Ferrous oxide
Fe ₂ O ₃	Iron (III) oxide / Ferric oxide
Fe ₃ O ₄	Iron (II, III) oxide
GCC	Grand composite curve
GHG	Greenhouse gas
H ₂	Hydrogen
H-EL	Hydro-based electrolysis
HEN	Heat exchanger network
HNO ₃	Nitric acid
H ₂ O	Water
HP	High Pressure
H ₂ S	Hydrogen sulphide
HTS	High temperature shift
LCA	Life cycle analysis
LP	Low Pressure
LTS	Low temperature shift
MCDM	Multi-criteria decision making
MFC	Mass flow controller
Mn ₃ O ₄	Manganese (II,III) oxide
MO	Metal oxide
NH ₃	Ammonia
NiO	Nickel oxide
NO	Nitric oxide
NO ₂	Nitrogen dioxide
N ₂ O	Nitrous oxide

N ₂	Nitrogen
O ₂	Oxygen
POX	Partial oxidation of hydrocarbons
Pt/Rh	Platinum/Rhodium
PV-EL	Photovoltaic-based electrolysis
SMR	Steam methane reforming
Th	Thermocouple
W-EL	Wind-based electrolysis
WS-CL	Water splitting by chemical looping

Units

atm	atmosphere
°C	Celsius
GJ/t	Giga Joule per tonne
g	gram
g/L	gram per litre
hr	hour
kJ	kilo Joule
kmol	kilo mole
km ² /kW	kilo metres square per kilowatt
kW _{th}	kilowatt thermal
K	Kelvin
l/min	litres per minute (LPM)
ml/min	milliliters per minute
MW _{th}	megawatt thermal
ppm	parts per million
s	second
scfd	standard cubic feet per day
t/y	tonnes per year
y	year
µm	micrometer

CHAPTER 1

INTRODUCTION

This chapter introduces the state of the art of production of hydrogen and nitric oxide by different routes along with the motivation and the objective of the present study followed by the chapter wise structure of the thesis.

1.1 Hydrogen and Nitric Oxide

Hydrogen is considered as a fuel of the future that can be produced from renewable energy systems with several potential applications as a feedstock and as a utility. The hydrogen generation market is expected to grow from an estimated 6.31 trillion ₹ (114.75 billion A\$) in 2014 to 8.44 trillion ₹ (153.5 billion A\$) by 2019 (Markets and Markets [M&M] Analysis 2014). In 2014, the refining sector was the biggest hydrogen consumer with 48 % of total consumption share followed by the ammonia industry with 43% share (M&M Analysis 2014). The diverse areas of applications of hydrogen includes refining, production of chemicals, metals and fertilizers, food processing, electronics, fuel cells, pharmaceuticals, aerospace, plant utilities, glass production, welding, and laboratories, etc. (Armaroli & Balzani 2011). Nitric oxide is an important intermediate in the chemical industry especially in the production of nitric acid in addition to various medical and pharmaceutical applications (Market Research 2014). Nearly 80 % of the total world consumption of nitric acid occurs in the fertilizer industry as ammonium nitrate (AN) and calcium ammonium nitrate (CAN) whereas non-fertilizer application accounts for about 20 %, with production of chemicals such as nitrobenzene, adipic acid and nitrochlorobenzenes (Chemical Economics Handbook 2015). After the year 2006, the annual production of nitric acid in the US alone has been more than 6 million tonnes (IHS 2015).

The producers of industrial chemicals such as hydrogen, ammonia, nitric acid, and ammonium nitrate increasingly have a responsibility to investigate manufacturing methods having less impact on the environment and efficient energy utilization. Figure 1.1 represents the commercially accepted conventional process for the production of nitric acid starting with steam methane reforming (SMR) of natural gas to produce hydrogen, which is reacted to

produce ammonia followed by catalytic oxidation of ammonia to produce nitric oxide, which in turn is hydrolysed to produce nitric acid (Thiemann et al. 2012). This process relies on fossil fuel (natural gas) and is efficient, but has atmospheric emissions in different stages of the process.

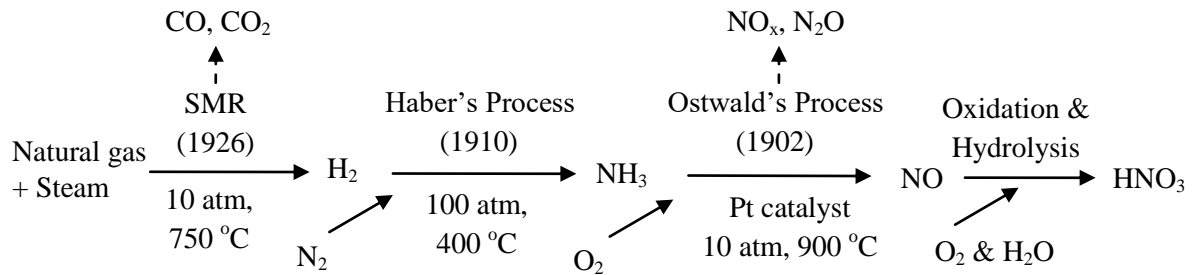


Figure 1.1 Conventional processing scheme for nitric acid production

The SMR process producing hydrogen from hydrocarbons, mostly methane or natural gas has energy efficiency of about 80 % but emits gases such as carbon monoxide (CO), carbon dioxide (CO₂) and hydrogen sulfide (H₂S) (Cetinkaya et al. 2011). Hydrogen obtained from SMR process is combined with nitrogen to produce ammonia via the Haber-Bosch process. The thermodynamic minimum energy consumption based on reaction stoichiometry is around 18.58 GJ/t of ammonia but the real process has much higher energy consumption due to requirements of high temperature, high pressure, excess reactants and impure natural gas (Noelker et al. 2011). A recent study evaluating energy efficiency of nearly 50 ammonia plants reported energy consumption to vary from 23.8 GJ/t to 51.9 GJ/t NH₃ for the production capacities ranging from 0.09 million t/y to 0.75 million t/y (Tavares et al. 2013). However, amongst the reforming plants using natural gas as feed, the best is reported to have energy efficiency rates ranging from 29.5 GJ/t to 30.6 GJ/t NH₃ (Eller et al. 2012; Tavares et al. 2013). The extensive research and progress in process engineering have led to improvements in efficiency, converter design and energy recovery in the synthesis section, however, still the research is going on to find options for reducing natural gas and energy consumption in addition to environmental emissions. The ammonia is then transferred to produce nitric acid by Ostwald's process. The presence of excess air (normally 10 % ammonia and 90 % air) and Pt/Rh catalyst at high temperature of 900 °C, 10 atm pressure results in almost complete conversion of ammonia to oxides of nitrogen (Scientific American Supplement 1913). There have been several efforts in the direction of improvement of these processes energetically and economically, however, there have been no significant changes in

main process reactions. Despite the high conversion achieved in the ammonia oxidation step to produce nitric oxide, there is still potential for a better process that gives a higher overall conversion in when considering the whole reaction pathway, whilst also minimising the production of N_2O and NO_x emissions.

Hydrogen appears to be a main precursor in nitric acid production as it produces ammonia which is crucial in further process. From the several alternatives for the production of hydrogen, electrolysis and thermochemical processes are at the forefront amongst renewable approaches. Thermochemical cyclic processes are often termed as chemical looping based processes and have the potential to produce multiple desired products in parallel reactors. The chemical looping has emerged as one of the attractive options to produce pure hydrogen by thermochemical water splitting and to improve CO_2 capture by chemical looping combustion (CLC) at potentially reduced cost and energy penalty compared to other technologies (Moghtaderi 2012). To the present date, several chemical looping combustion projects ranging from 10 kW_{th} to 3 MW_{th} have been demonstrated, with over 2000 hours of operational experience (Kolbitsch et al. 2009; Lyngfelt 2014). Since the discovery of first two-step Fe_3O_4/FeO water-splitting cycle, more than 280 thermochemical cycles have been proposed for hydrogen production with few such as Mn_3O_4/MnO , Co_3O_4/CoO , ZnO/Zn , In_2O_3/In , NiO/Ni , etc. investigated in detail (Charvin et al. 2008; Abanades et al. 2006). Recently, some studies reported the extended application of chemical looping in different areas such as solar-hybrid CLC of dimethyl ether (Han et al. 2012), production of commercial chemicals such as ammonia (Galvez et al. 2007), etc.

The general chemical looping scheme involves reduction of metal oxide by a reducing agent followed by regeneration of consumed metal oxide by oxidation mostly in parallel entrained flow reactors. Metal oxides are characterized as potential oxygen carriers for chemical looping based reactions where a reducing agent can be hydrogen, carbon monoxide, and hydrocarbons. The requirement of H_2 as a precursor for NH_3 and hence NO emphasizes the need of developing a chemical looping based process that could produce NO and H_2 simultaneously. In addition, the kinetics and mechanisms of catalytic and non-catalytic oxidation of ammonia have been studied since the early 1900's. This gives rise to the possibility of exploring the potential of ammonia as a reducing agent in a chemical looping process. Therefore, the application of the chemical looping approach can be extended to the formation of feedstock for mineral acids such as nitric acid (HNO_3) where NH_3 can be

oxidised by an oxygen carrier such as metal oxide instead of air or pure oxygen as shown in Figure 1.2.

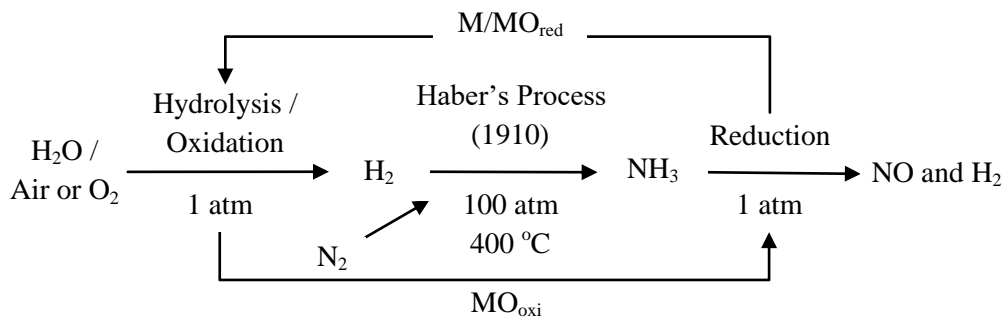


Figure 1.2 Chemical looping based process scheme for NO and H₂ production

1.2 Objective

The objective of the study is to investigate an energy efficient process for the production of nitric oxide and hydrogen, in particular, for ammonia and nitric acid plants. The work presented in this thesis can be summarized as follows:

- To propose a chemical looping based reaction scheme for nitric oxide and hydrogen production
- To study the feasibility of the proposed reaction between ammonia and metal oxides theoretically and experimentally
- To propose a suitable reaction pathway for the reaction between ammonia and metal oxide
- To compare the proposed chemical looping based processes with steam methane reforming on the basis of energy and exergy analysis

1.3 Dissertation Structure

The dissertation comprises of eight chapters including the theoretical, experimental and simulation study for chemical looping based production of nitric oxide and hydrogen.

Chapter 1 provided an introduction to the topic highlighting the potential of chemical looping concept in nitric oxide and hydrogen production followed by the objective of the thesis.

Chapter 2 presents a literature survey, which reviews the various processes for nitric oxide and hydrogen production. A separate section is attributed to the literature review on chemical looping based processes in the chemical production sector.

Chapter 3 reports the cost-benefit analysis of eight different hydrogen producing technologies where the benefits are evaluated using multi-criteria decision making method such as Analytic Hierarchy Process (AHP).

Chapter 4 proposes the chemical looping based process for nitric oxide and hydrogen production and reports the thermodynamic feasibility analysis for different metal oxide based cycles.

Chapter 5 discusses the instrumentation and materials required for experimental study of reaction of ammonia with different metal oxides. The experimental set up, procedure, and different types of reactors and gas analysers used are explained in this chapter.

Chapter 6 discusses the results of the experimental study of reaction between ammonia and selected metal oxides, in particular, Copper oxide (CuO).

Chapter 7 presents the comparison of chemical looping based processes with conventional SMR approach for 1 mole/s NO production on the basis of energy and exergy analysis. Each of the processes is simulated using Aspen Plus to extract the stream data for thermodynamic calculations.

Finally Chapter 8 reports the conclusions drawn from the work done and the recommendations for future work.

CHAPTER 2

LITERATURE REVIEW

The different processes to produce nitric oxide and hydrogen are reviewed individually in this chapter followed by a brief section on chemical looping based processes.

2.1 Nitric Oxide Production

Nitric oxide or nitrogen monoxide (NO) is an important intermediate in the chemical industry and is a by-product of combustion, as in automobile engines, fossil fuel power plants, and is produced naturally during the electrical discharges of lightning in thunderstorms (Joesten et al. 2006). As presented in Chapter 1, Ostwald's process is the most common commercial method of NO production by the catalytic combustion of ammonia at 800-900 °C in presence of platinum (Thiemann et al. 2012). The process was patented in 1902 but the first commercial implementation was carried out in 1906 (Hunt 1958).



The Birkeland–Eyde process of nitrogen fixation into nitric acid was one of the competing industrial processes in 1903 (Thiemann et al. 2012). The process involved reaction of nitrogen and oxygen to form NO at about 3000 °C with up to 4 % yield of NO ('Birkeland-Eyde Process' n.d.). However, the process is very energy intensive and relatively inefficient. The same reaction is carried out by lightning, providing a natural source for converting atmospheric nitrogen to soluble nitrates (Leigh 2004). In the 1910s and 1920s, it was gradually replaced by a combination of the Haber-Bosch process that produced ammonia and the Ostwald process that produced nitric acid through NO as intermediate.



In 1950s a new method was proposed to prepare nitric oxide from heating a dry powdered mixture of potassium nitrite, potassium nitrate, chromic oxide and ferric oxide above 300 °C (Ray & Ogg 1956). Though the process produced 99.78% pure nitric oxide, it was not

explored further for commercial purpose due to the complex procedure and several pre-experiment requirements. The other attempts are mainly focused on Ostwald's process to obtain high NO concentration and eliminate or reduce the chances of getting any impurities especially nitrous oxide (N₂O) either by adding intermediate cooling and separation stages (Jockers et al. 1970; Echegaray et al. 2000) or by modified catalysts (Theodore 1995).

Recently in 2014 there has been a process proposed for nitric oxide (NO) production from the reaction of water-soluble chemical reactants microencapsulated in polymer matrices (Chen et al. 2014). The process proposed mainly for medical application involves a mixture of microencapsulated nitrite salt, acid, and reducing agent which is activated by water to produce NO via a nitrous acid intermediate. Kebede et al. (2013) studied the photo-oxidation of ammonia on TiO₂ as a source to produce NO and NO₂ under atmospheric conditions. They analysed a mechanism by which O₂ addition to NH₂ generates an aminoperoxy radical that undergoes water-assisted proton transfer and isomerization to ultimately yield NO and H₂O. This was a laboratory level study focussed mainly on studying the kinetics of NH₃ oxidation under ambient conditions and not on NO production.

As discussed above, there have been few processes to produce NO but most of them except the Ostwald's process are feasible mostly at laboratory scale. The major step in Ostwald's process is the oxidation of NH₃ which is normally produced from steam methane reforming process thereby making H₂ an important precursor for both NO and NH₃. This emphasises the need and importance of developing a process that could produce H₂ and NO simultaneously.

2.2 Hydrogen Production

Hydrogen can act as a possible solution as an important energy carrier that can be produced from both fossil fuels and renewable sources (Koroneos et al. 2005). The route by which hydrogen is produced would be the determining factor for its environmental performance. The demand for hydrogen is expected to significantly increase in the near future owing to the growing needs of the oil refining and chemical industries, as well as new applications such as synthetic fuel, bio-fuel production, and use in fuel cells (Dufour et al. 2011; Mansilla et al. 2010). Life cycle analysis (LCA) is the systematic methodology that includes all the life

cycle stages from extraction of raw materials to final wastes management (Dufour et al. 2011). Several LCA have been performed on hydrogen storage, production and use, and integrated systems (Neelis 2004; Koroneos 2004). Dufour et al. (2011) determined the critical aspects to ensure the feasibility of hydrogen producing processes such as water photosplitting, solar two-step thermochemical cycles, and methane decomposition in comparison to conventional processes using life cycle analysis.

There are studies that have undertaken a life cycle assessment approach to investigate the environmental aspects of hydrogen production by natural gas steam reforming and renewable sources and reported the benefits and the drawbacks of the competing hydrogen production technologies (Koroneos 2004). One of the studies have quantified and compared the carbon dioxide equivalent emissions and energy equivalents using comprehensive LCA for five methods of hydrogen production, namely steam reforming of natural gas, coal gasification, water electrolysis via wind and solar electrolysis, and thermochemical water splitting with a Cu-Cl cycle (Cetinkaya et al. 2011). Thermochemical water splitting process was found to be most beneficial in terms of CO₂ equivalent emissions and fossil based processes were more advantageous in terms of production capacity. Granovskii et al. (2006) examined various hydrogen production methods and use of hydrogen in fuel cell vehicles to compare them with a base case (gasoline use in an internal combustion engine). It was concluded that wind and solar electrolysis are advantageous by resulting in less air pollution compared to natural gas reforming method. Spath and Mann (2001) presented several LCA studies to determine the major impact category of the process so that environmental impacts can be minimized: a coal to electricity process, hydrogen production via steam methane reforming, and wind/electrolysis. Mueller-Langer et al. (2007) investigated the hydrogen production processes based on natural gas steam reforming, coal and biomass gasification, and water electrolysis from a techno-economic viewpoint while satisfying the criteria for sustainability, i.e. economic competitiveness, environmental protection, and security of energy supply. The study reported steam reforming of natural gas as the most favourable hydrogen production method, but with concerns over greenhouse gas emissions and the potential rise in natural gas prices. Gasification of coal coupled with carbon dioxide capture could be competitive while biomass gasification can be a viable option provided that the existing challenges such as gas cleaning, scale up and continuous production are overcome. Hydrogen production from electrolysis is unlikely to be an economically competitive option due to high electricity prices, though electrolysis may find some niche applications. Bartels et al. (2010)

investigated the economics of producing hydrogen from both conventional and alternative energy resources and found coal, nuclear, and natural gas to be the most economical sources of hydrogen with an estimated cost of 18-92.4 ₹/kg (0.45-2.31 A\$/kg), 90.8 ₹/kg (2.27 A\$/kg), and 125.2-160.4 ₹/kg (3.13-4.01 A\$/kg) respectively.

Primary drawbacks of LCA include the requirement of detailed inventory data and the use of other researchers' data for comparison of different alternatives. Some researchers have evaluated the hydrogen production methods on the basis of thermodynamic analysis (i.e., energy and exergy efficiencies) (Koroneos & Rovas 2012; Rosen & Scott 1998). These approaches may prove beneficial to compare the processes in thermodynamic regard, but they cannot be used for overall comparison of technologies as a whole (i.e., to include factors such as emission, cost, scalability, etc.). However, LCA and thermodynamic methods do not provide any economic assessment, and it is difficult for these approaches to include both qualitative and quantitative attributes together for critical comparison of different options. Most of these studies consider only the production costs and environmental emissions. There are other parameters also affecting the LCA study of hydrogen production such as operation and maintenance issues, safety issues, waste disposal, transportation, manpower, etc. In addition, when there are several alternative technologies, the choice of technology problem should be viewed as a technology-ranking problem, where the rankings would be arrived at through multi-criteria analysis that is capable of handling both quantitative and qualitative criteria.

The multi-criteria decision making (MCDM) has emerged as a tool for analysing complex problems with the potential to critically evaluate the alternatives for different criteria to select the most suitable alternative(s) (Kabir et al. 2013). These alternatives may need to be further explored in-depth for their final implementation. The Analytic Hierarchy Process (AHP) proposed by Saaty (1980) is a very popular approach that can take care of both quantitative and qualitative criteria. The AHP has found its widest applications in the areas of planning, evaluation of technology investment decisions, resource allocation, conflict resolution, etc. (Saaty & Vargas 2000). AHP has been used in several engineering applications such as the emissions from power plants (Chatzimouratidis & Pilavachi 2007), hydrogen fuelling systems for transportations (Winebrake & Creswick 2003), evaluation of liquid bio-fuels (Papalexandrou et al. 2008) and for hydrogen energy technology (Chui et al. 2005; Lee et al. 2008). There are only a few studies which used AHP to study different hydrogen production

processes. Pilavachi et al. (2009) evaluated seven hydrogen production methods using AHP for the criteria of CO₂ emissions, operation and maintenance cost, capital cost, feedstock cost and hydrogen production cost. The potential of AHP is not fully utilized in this case as it did not include any qualitative factors, but only the quantitative attributes which could have been easily compared without AHP. Chui et al. (2005) performed LCA on 11 different hydrogen production pathways for the criteria of energy consumption, fossil fuel usage, and greenhouse gas (GHG) emissions. Electrolysis using renewable electricity proved to be the best followed by SMR process. Recently, Heo et al. (2012) evaluated six different hydrogen production methods using fuzzy AHP under the concepts of benefits, opportunities, costs, and risks. The SMR process proved to be the optimal one with initial investment and market size as deciding factors.

Amongst the hydrogen production processes, there is extensive research on renewable approaches, especially the water splitting process. The cost of electricity is one of the major factors and hence the source from which the electricity would be obtained for water splitting can prove to be a deciding factor for the future of this technology. Solar energy can be effectively utilized to produce hydrogen, in the form of heat (thermochemical), light (photoelectrochemical, photosynthetic or photocatalytic), and electricity (electrolysis) (Dufour et al. 2011). In contrast to direct thermolysis of H₂O, the two-step thermochemical cycles using metal oxide redox reactions bypass the H₂-O₂ separation problem and operate at relatively lower temperature. Metal oxides act as oxygen carriers in this process where H₂ and O₂ are preferably formed in different steps and in different reactors. Thermal decomposition of water, in particular, water splitting using redox systems, has emerged as one of the most attractive approaches for the direct production of pure hydrogen (Perkins & Weimer 2004). The process is also known as chemical looping since all the components except for water are regenerated and the oxidation-reduction cycle is continued with the production of hydrogen and oxygen (Steinfeld et al. 1999). As evident from the previous discussion very few processes exist for NO production to be compared on multi-criteria basis. However, there exist enough number of fossil fuel based and renewable processes for H₂ production. Considering the industrial applications of H₂ as fuel in fuel cells and importance of H₂ as a feedstock for the production of NH₃ and hence NO, it is essential to select the appropriate process to produce H₂. The next chapter reports the evaluation of different hydrogen production technologies on the basis of a cost-benefit analysis using AHP.

2.3 Chemical Looping based Processes

Chemical looping has been an area of extensive research since the 1980s due to its potential applications in the water splitting to produce hydrogen (Figure 2.1a) and carbon dioxide capture technologies (Figure 2.1b) (Adanez et al. 2012). In Figure 2.1b, the products depend on the reducing agent (e.g. CH_4 , H_2 , CO , etc.) used. More than 282 thermochemical cycles have been proposed for hydrogen production till now, out of which very few are found to be promising (Bamberger & Richardson 2000). Some of them are two step metal oxides based cycles while some are multi-step (meaning three or more steps). The two step metal oxide process with some exceptions of three or four step cycles has been proved to be one of the most viable options amongst all chemical looping approaches to split water thermochemically.

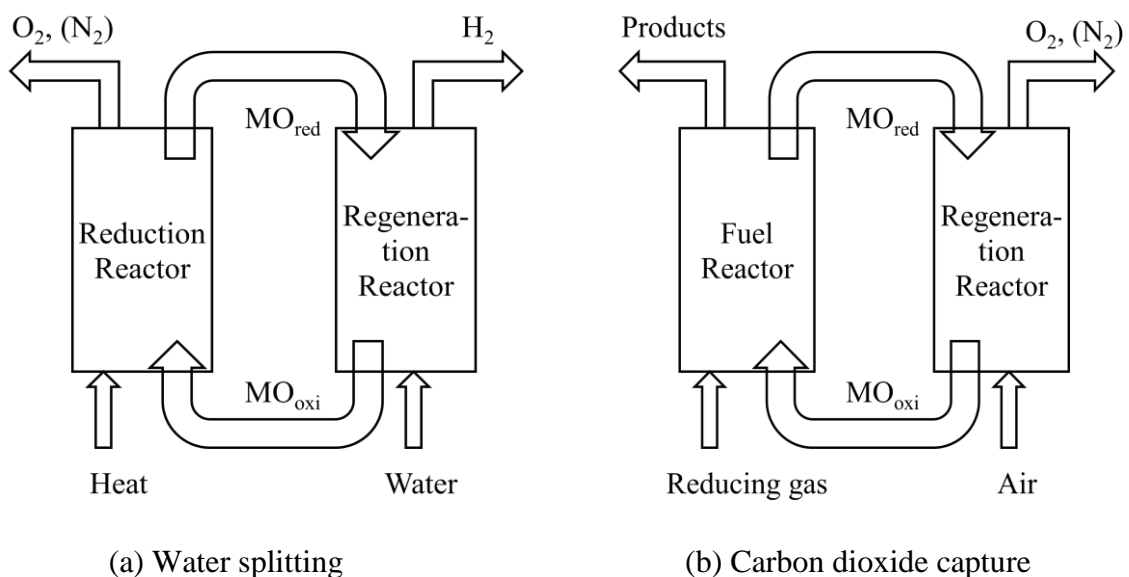


Figure 2.1 Chemical looping set-up for hydrogen production and carbon dioxide capture

In metal oxide based processes, during the first step (Equation (2.3), water splitting) the reduced and hence activated material (e.g. metal or a metal oxide) is oxidized by water to produce hydrogen at lower temperatures ($30 - 600\text{ }^\circ\text{C}$). During the second step (Equation (2.4), regeneration) the material is reduced thermally or/and chemically to be available for reuse, delivering some of the oxygen from its lattice at high temperatures ($800 - 2200\text{ }^\circ\text{C}$) (Roeb et al. 2006; Steinfeld 2005). Since the process runs in a loop, any step can occur first depending on the metal oxides used.



Since 1977, many cycles such as $\text{Mn}_3\text{O}_4/\text{MnO}$, $\text{Co}_3\text{O}_4/\text{CoO}$, $\text{Nb}_2\text{O}_5/\text{NbO}_2$, ZnO/Zn , $\text{In}_2\text{O}_3/\text{In}$, SnO_2/Sn , etc. have been proposed, but Fe based cycles have always been at the forefront. Charvin et al. (2008) developed and screened a database of over 280 cycles to select the most suitable option for coupling with concentrated solar thermal energy. ZnO/Zn , $\text{Fe}_3\text{O}_4/\text{FeO}$ and $\text{Fe}_2\text{O}_3/\text{Fe}_3\text{O}_4$ cycles were selected because of their high potential, the amount of available data on the reactions involved and their level of development. Extensive research has been carried out for FeO based thermochemical cycles either for water splitting or for CO_2 capture over the last 30 years. FeO based cycles are thought to be of prime importance for our study too for several reasons. As per the study by Charvin et al. (2008) the optimised global process efficiency from solar energy to hydrogen is estimated to reach 17.4 %, 18.6 % and 20.8 % for $\text{Fe}_3\text{O}_4/\text{FeO}$ (magnetite/wustite), $\text{Fe}_2\text{O}_3/\text{Fe}_3\text{O}_4$ and ZnO/Zn cycles, respectively whereas the economic assessment gave a hydrogen production cost ranging from 380.8 ₹/kg (9.52 A\$/kg) and 704 ₹/kg (17.6 A\$/kg) for, respectively a 55 MW_{th} and 11 MW_{th} solar power plant operating for 40 years. Abanades et al. (2006) performed the screening of thermochemical cycles for hydrogen production by concentrated solar energy and selected about 30 cycles for further investigation. The metal oxide cycles were selected and evaluated on different criteria such as number of steps, temperature ranges, toxicity of materials, etc.

Chemical looping combustion (CLC) is emerging as an attractive option for carbon dioxide capture as it avoids the need of gas separation equipment or additional energy for gas separation. The system usually comprises of two interconnected fluidized bed reactors, an air reactor and a fuel reactor; where metal oxide particles are used as oxygen carriers (Lyngfelt 2014). This technology was first proposed mainly for the gaseous fuels combustion and has recently been considered for solid fuels such as coal. Numerous projects employing chemical looping have been implemented at different scales in different parts of the world. Tong et al. (2013) demonstrated the continuous high purity hydrogen generation from a syngas chemical looping 25 kW_{th} sub-pilot unit at The Ohio State University, Columbus, US with 100 % carbon capture. Cormos (2011) investigated the plant concepts with natural gas and syngas-based chemical looping methods to produce 500 MW of hydrogen covering ancillary power consumption with an almost 100 % carbon dioxide capture.

The chemical looping approach has been explored for its potential to integrate with other processes such as gas reforming, solid fuel gasification, and power generation. Recently, some studies reported the extended application of chemical looping in production of chemicals of industrial importance. Galvez et al. (2007) proposed the carbothermal reduction of Al_2O_3 by C or CH_4 in N_2 to AlN at about 1400°C and syngas followed by steam-hydrolysis of AlN to Al_2O_3 and NH_3 below 375°C . It should be noted that both reaction steps proceed at 1 bar, without added catalysts skipping the energy-intensive production of hydrogen. Edrisi et al. (2014) proposed the chemical looping approach to provide feedstock for ammonia synthesis producing pure streams of H_2 , N_2 and CO_2 in three different reactors. A significant reduction in investment cost is anticipated with 30 % rise in production ratio due to less number of units in addition to benefits of carbon capture and storage. In another study, Edrisi et al. (2014) investigated the simultaneous production of hydrogen, nitrogen and carbon dioxide streams from methane and iron based oxygen carrier in chemical looping reactor. Michalsky and Pfromm (2011) suggested synthesis of NH_3 from N_2 and H_2O through a solar thermochemical reaction cycle using Chromium oxide. The techno-economic feasibility and thermodynamic performance of Mo-based solar thermochemical NH_3 synthesis was also checked and evaluated (Michalsky et al. 2012).

2.4 Research Gaps

From the literature review, the identified scope of research is listed as follows:

- Hydrogen is required for ammonia and hence nitric oxide production. There are several studies comparing hydrogen production processes using LCA, energy efficiency and thermodynamic analysis, but very few using MCDM methods such as AHP. Hence, there is a need for the cost-benefit analysis of different hydrogen production technologies including chemical looping using AHP.
- There are only two commercial processes for the chemical production of nitric oxide since 1902. At present, only Ostwald's process is employed for nitric oxide production which is efficient, but suffers from the emission of N_2O , a strong greenhouse gas, and the consumption of fossil fuels. Thus there is scope for exploring the possibility of a new process reaction that would form nitric oxide (NO) in ecofriendly manner.

- The domain of chemical looping based processes is mainly restricted to carbon dioxide capture and to a lesser extent hydrogen production. In case of carbon capture, the choice of reducing agents ranges from hydrogen to hydrocarbons in addition to carbon monoxide. Though a lot of research has been done on part of oxygen carriers, the potential of these metal oxides in reducing atmospheres such as ammonia to produce NO has not been explored. There is hardly any chemical looping based approach proposed as a method for direct production of NO and H₂ except a few associated with ammonia production.
- As the production of NO by chemical looping is a new process, there are many design variables that need to be evaluated. Thermodynamic analysis, process simulation and mathematical modelling are capable of helping with the selection of these variables. The subsequent chapters would address these research gaps to meet the objective of the present study.

CHAPTER 3

EVALUATION OF HYDROGEN PRODUCTION TECHNOLOGIES

Nitric oxide is widely used as an intermediate in nitric acid production and hence ammonium nitrate that have extensive applications. Though there are only two processes reported for the commercial scale production of nitric oxide, there are several alternatives to produce hydrogen which is an important molecule for both ammonia and nitric oxide production. This highlights the need to evaluate different hydrogen production technologies on a multi-criteria basis as explained in the previous chapter. The present chapter comprehensively assesses eight of the most common hydrogen production processes in terms of a cost-benefit analysis including both economic and environmental aspects. Five different criteria namely, greenhouse gas emissions, raw material and utilities consumption, energy efficiency, scalability, as well as waste disposal and atmospheric emissions are evaluated under benefits category using the Analytic Hierarchy Process (AHP). Cost is a separate attribute against which the results obtained for benefits using AHP are plotted to give the final trade-offs so as to find a cost-effective and environmentally benign hydrogen production technology.

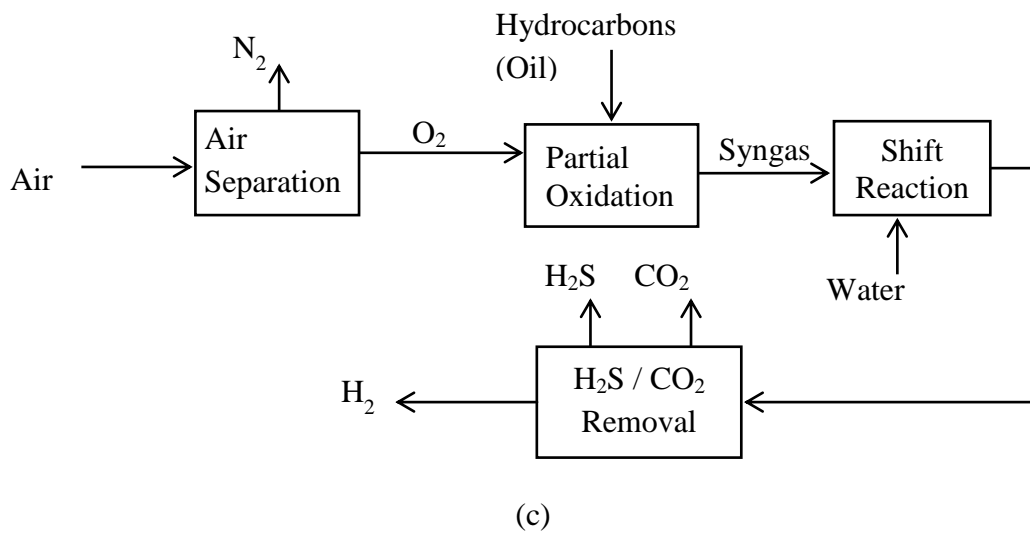
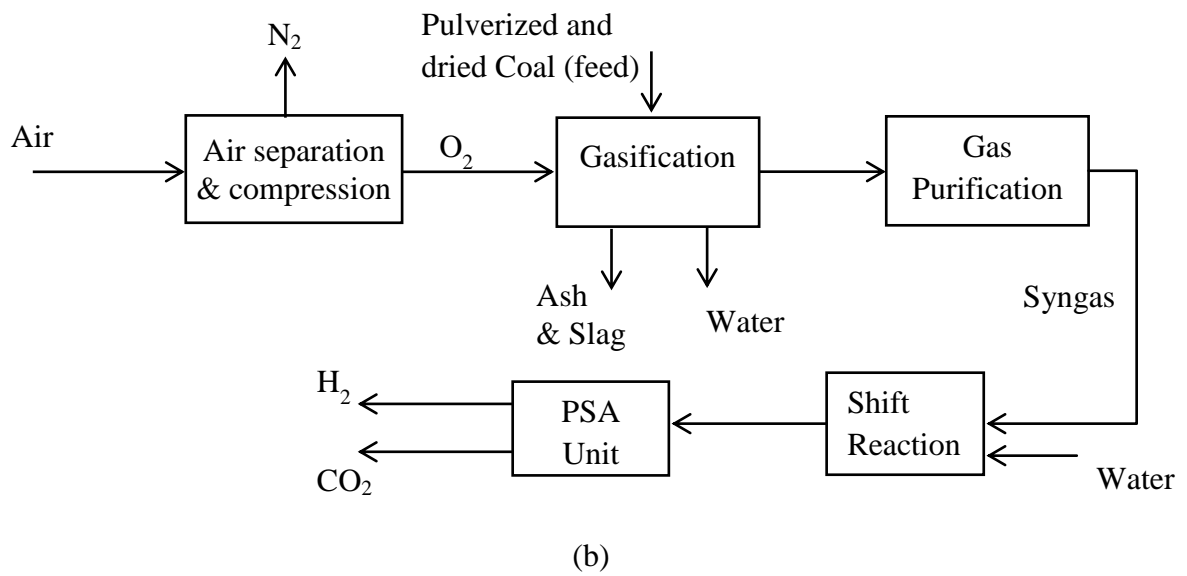
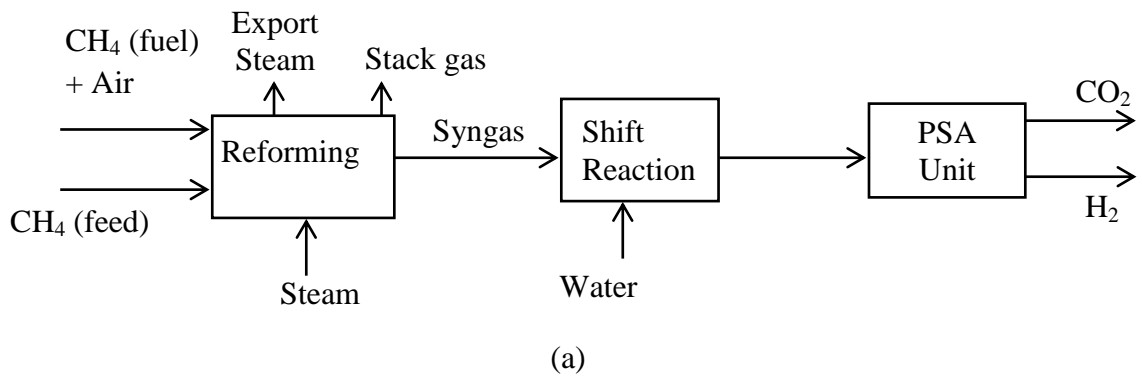
3.1 Hydrogen Production Technologies

Eight out of the several hydrogen production technologies including both renewable based and fossil based are selected for the assessment study. Figure 3.1 shows the simplified process block diagrams for the eight hydrogen production processes: steam methane reforming (SMR), coal gasification (CG), partial oxidation of hydrocarbons (POX), biomass gasification (BG), photovoltaic-based electrolysis (PV-EL), wind-based electrolysis (W-EL), hydro-based electrolysis (H-EL), and water splitting by chemical looping (WS-CL). Natural gas, heavy oil, and coal are currently the main feed stock used for commercial hydrogen production. The technology for hydrogen production from each of these feed stocks is well advanced, and significant experience exists in the operation of the plants using these technologies (Bartels et al. 2010). The non-hydrocarbon processes normally use the energy source to produce hydrogen using either electricity or heat or a thermo-chemical process to split water into hydrogen and oxygen. Biomass gasification is still a developing technology and research is currently being done on the use of biomass to produce hydrogen from more

advanced thermo-chemical and biological approaches (Bartels et al. 2010). Water splitting by chemical looping or thermo-chemical water splitting using metal-metal oxide cycles can be categorized under renewable based approaches of hydrogen production. The process considered in this category is the thermo-chemical water splitting using Zn/ZnO (Steinfeld 2002). The details of each of these technologies are available in the literature (Bartels et al. 2010; Steinberg & Cheng 1989; Ramsden et al. 2009; Perkins & Weimer 2004). There exist few other processes for hydrogen production such as dry reforming of methane, photobiological process, etc. that are not considered in the present study. All the selected technologies are considered without CO₂ sequestration, and are compared for the capacity of 254.6 tonnes H₂/day (i.e., 100×10^6 scfd H₂ per day) (Steinberg & Cheng 1989). To ensure that all plants operate 24 hours per day, the PV-based electrolysis technology is assumed to be supplemented by an equal amount of conventional electricity and the wind-based electrolysis technology is assumed to be supplemented with 20% conventional electricity. These values are assumed on the basis of the inconsistent nature of these renewable sources and the selected plant capacity for the hydrogen production. In both cases, the additional electricity is assumed to have been generated by a pulverized coal power station.

3.2 Methodology

Considering the main objective of this section to generate the trade-offs from a cost-benefit analysis for different alternatives of hydrogen production, the two major attributes are the costs associated with each technology and the benefits. The cost is a quantitative attribute representing the normalized equivalent annual cost (C_{EA}) which includes the factors such as capital cost, fixed operating cost, and variable operating cost. The criteria selected under the benefits category are the greenhouse gas (GHG) emissions, raw material and utilities consumption, energy efficiency, scalability, waste disposal and non GHG atmospheric emissions. These five criteria are chosen to evaluate the fossil and renewable based hydrogen production processes on the basis of energy, environmental performance, resource utilization, and possibility of commercialization.



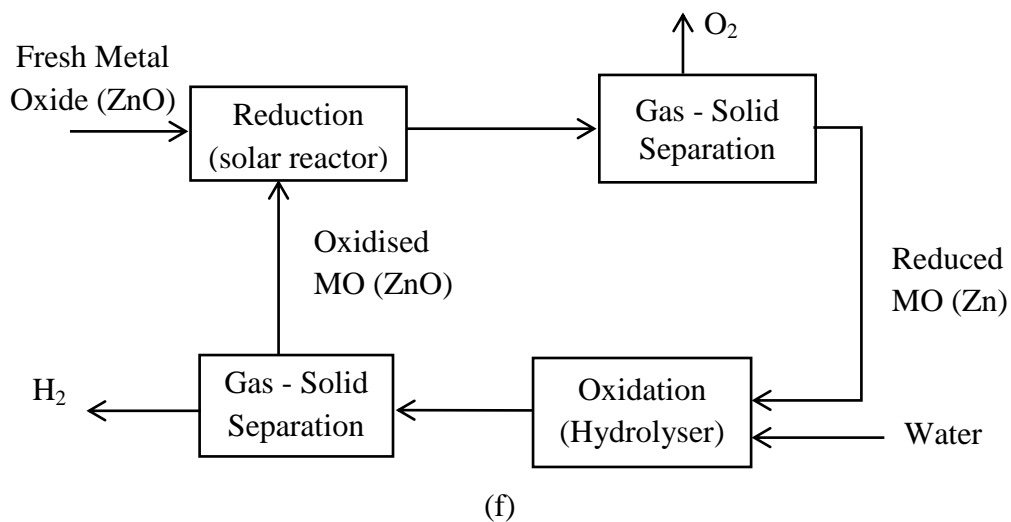
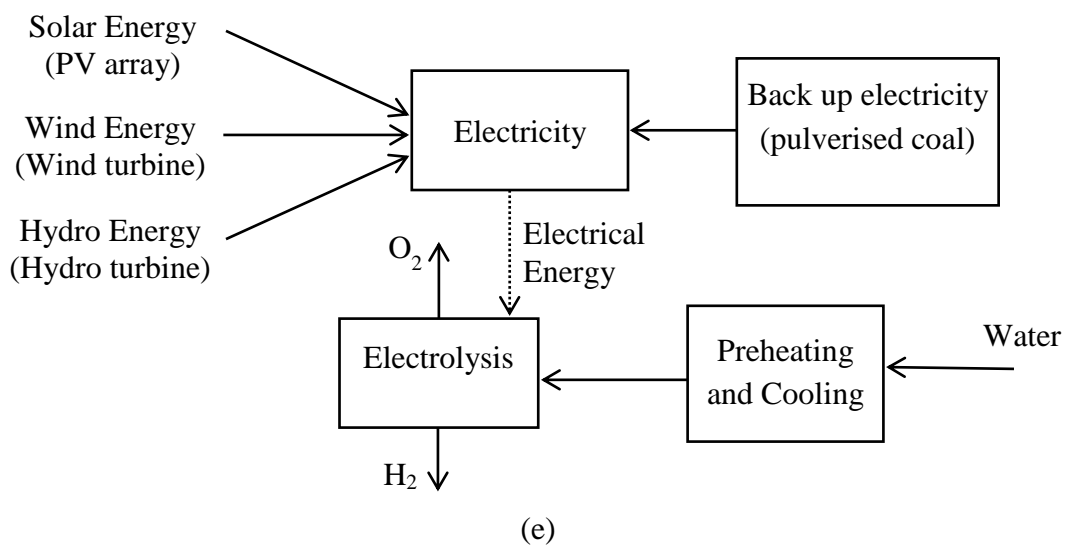
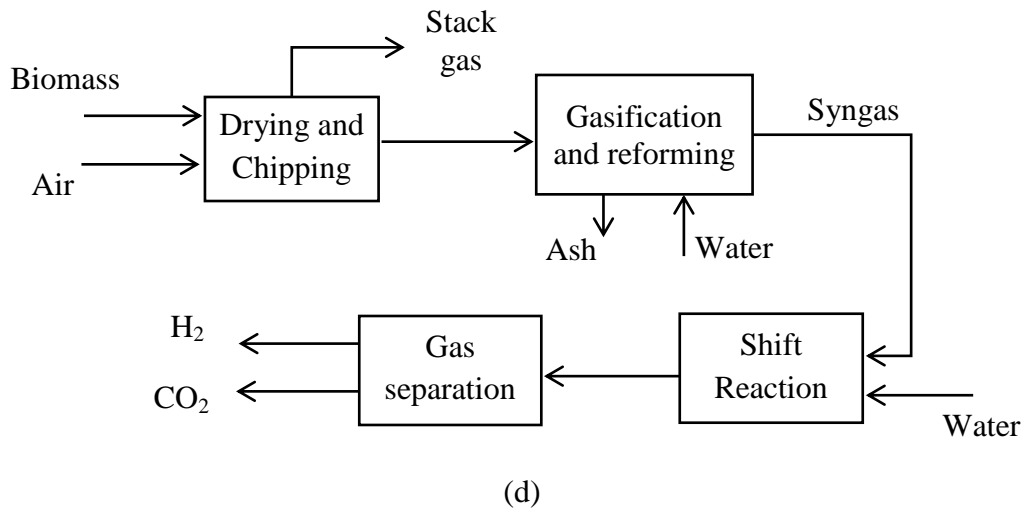


Figure 3.1 Simplified block diagrams for different hydrogen production processes: (a) Steam Methane Reforming (SMR), (b) Coal Gasification (CG), (c) Partial Oxidation of hydrocarbons (POX), (d) Biomass Gasification (BG), (e) PV-based, Wind-based, and Hydro-based electrolysis (PV-EL, W-EL, and H-EL), (f) Water Splitting by Chemical Looping (WS-CL)

3.2.1 Costs

The different costs that are considered for each of the chosen technologies include the capital cost, the fixed operating costs and the variable operating costs. The storage and distribution costs for hydrogen, costs relating to the release of GHGs, and credits relating to revenue from the sale of byproducts are not considered as these are relatively small compared to the capital and the operating costs of hydrogen production. Furthermore, GHG emission and waste disposal are considered as the environmental performance related criteria under the attribute of benefits. The capital cost (C_C) is considered taking into account the cost of the equipment, the land and the installation of the unit. The fixed operating cost refers to the cost of labor, property taxes, insurance, and administrative expenses in the hydrogen production process. The variable operating cost refers to the cost of feedstock (C_{FD}), utilities, electricity, waste treatment, and some other miscellaneous costs. In order to carry out the evaluation, the different costs need to be updated to a common year considering the appropriate price indexes (Chemical Engineering Online 2015). The equations for capital cost and operating cost are as follows:

$$C_{Cp} = C_{Ci} (I_p/I_i) \quad (3.1)$$

where, C_{Cp} is the present capital cost (i.e., the indexed cost for the present year), C_{Ci} is the initial capital cost (i.e., cost for the year the data were collected), and I is the chemical engineering plant cost index.

$$C_{Op} = C_{Oi} (P_p/P_i) \quad (3.2)$$

where, C_{Op} is the present operating cost (i.e., the indexed cost for the present year), and C_{Oi} is the initial operating cost (i.e., cost for the year the data were collected), and P is the consumer price index.

The next step is to calculate the costs for chosen capacity of plant (C_{new}) as basis for evaluation using six-tenths factor rule as per Equation (3.3) where R is the ratio of new plant capacity to the known capacity and value of the factor f is 0.6 (Peters et al. 2003).

$$C_{new} = C_{known} \times R^f \quad (3.3)$$

In order to categorize all the costs under a single term with constant units, it is necessary to annualize all the costs together. The equivalent annual cost (C_{EA}) is the cost per year of owning and operating an asset over its entire lifespan and is calculated by Equation (3.4).

$$C_{EA} = (C_C \times CRF_{r,t}) + C_o \quad (3.4)$$

where CRF is the capital recovery factor for an economic life t and discount rate r .

$$CRF_{r,t} = \frac{r(r+1)^t}{(r+1)^t - 1} \quad (3.5)$$

The fixed and variable operating costs are reported on an annual basis whereas the capital cost is a onetime investment for the plant. The plant economic life is assumed to be 20 years with a discount rate of 5% for all the technologies. Assuming the fixed operating cost (C_{FO}) and variable operating cost (C_{VO}) on a real value basis, thus constant over the plant life, the equivalent annual cost (C_{EA}) is calculated by using Equation (3.6).

$$C_{EA} = (C_C \times CRF_{r,t}) + C_{FO} + C_{VO} \quad (3.6)$$

Different costs for each of the alternatives are tabulated in Table 3.1. As these data for different technologies are for different plant capacities in different years, Table 3.2 shows the data calculated for the year 2013 in Indian currency using Equations (3.1) – (3.5) for a plant capacity of 254.6 tonnes H_2 /day. The feedstock cost (C_{FD}) is included in the variable operating cost, but shown separately so as to facilitate the comparison of the chosen technologies based on their feedstock. In the case of technologies based on electrolysis, the feedstock cost is basically the electricity cost that is also included in the variable operating costs considering electricity as a utility required during production process and this is the only parameter which distinguishes the three technologies of PV-EL, W-EL and H-EL.

Table 3.1 Data collected from the literature for different hydrogen production processes

Process	Data Year	Plant Capacity (kg H ₂ /day)	C _C (US M\$)	C _{FO} (US M\$/year)	C _{VO} (US M\$/year)	C _{FD} (US M\$/year)
SMR (Ramsden et al. 2009)	2005	379000	180.5	6.9	144.4	136.2
CG (Ramsden et al. 2009)	2005	284000	450.5	23.1	33.6	29.7
POX (Steinberg & Cheng 1989)	1989	254600	204.5	16.5	102.21	34.78
BG (Ramsden et al. 2009)	2005	155000	160.5	10.4	43.2	27.4
PV-EL (Ramsden et al. 2009), (Zhao et al. 2008)	2005 2013	52000	123.5	5.4	81	79.59
W-EL (Ramsden et al. 2009), (Li 2013)	2005 2013	52000	123.5	5.4	38	36.39
H-EL (Ramsden et al. 2009), (Li 2013)	2005 2013	52000	123.5	5.4	30	28.43
WS-CL (Steinfeld 2002)	2002	5580	60.38	10.27	1	0.9

Table 3.2 Calculated data for year 2013 for different hydrogen production processes with plant capacity of 254.6 tonnes H₂/day

Process	C _C (M₹)	C _{FO} (M₹/year)	C _{VO} (M₹/year)	C _{FD} (M₹/year)	C _{EA} (M₹/year)	Normalized C _{EA}
SMR	10042.83	377.58	7907.23	7458.5	9091.28	0.52
CG	29803.94	1503.94	2188.03	1933.98	6083.38	0.35
POX	19030.98	1805.78	11186.0	3806.1	14519.1	0.83
BG	15270.24	973.69	4045.10	2565.6	6244.21	0.36
PV-EL	22627.41	973.69	14605.9	14352.4	17395.3	1.00
W-EL	22627.41	973.69	6851.96	6561.2	9641.35	0.55
H-EL	22627.41	973.69	5409.78	5126.0	8199.17	0.47
WS-CL	49964.19	7672.4	747.02	672.43	12428.41	0.71

3.2.2 Benefits

The five criteria selected under the benefits category are greenhouse gas emissions, raw material and utilities consumption, energy efficiency, scalability, and waste disposal along

with non-GHG atmospheric emissions. The greenhouse gas emissions and energy efficiency are quantitative criteria having numerical values (reported in Table 3.3) whereas the rest are qualitative and depend on the judgment of the decision maker. The greenhouse gases emitted during the process are estimated on the basis of LCA methodology using CO₂ equivalent as a measure of global warming potential (Cetinkaya et al. 2011; Koroneos et al. 2005). The energy efficiencies are calculated as the ratio of the energy of hydrogen produced based on its lower heating value (LHV) to the energy of input, considering fuel and/or heat and/or electricity as the external energy inputs (Ramsden et al. 2009). Scalability represents the potential of a technology to be scaled up to a level of the production capacity taken as a basis for cost calculations. It is decided considering the factors such as current status of the technology, plant area in km²/kW, and the existing average capacity factors of each technology (Afgan & Carvalho 2002). The raw material and utilities include the source, type and amount of the major feedstock, hot and cold utilities, additional fuel, water, etc. The last criterion of waste disposal and non-GHG atmospheric emissions includes the type and amount of solid or liquid wastes generated and their methods of disposal along with the possible flue gases released during the mainstream hydrogen production process.

Table 3.3 CO₂ equivalent emissions and energy efficiency data for hydrogen production technologies

Hydrogen production process	CO ₂ equivalent emissions (kg/MJ)	Energy Efficiency (%)
SMR	0.080 (Koroneos et al. 2005)	77.5 (Kalamaras & Efstathiou 2013)
CG	0.076 (Cetinkaya et al. 2011)	55.8 (Ataei & Yoo 2010)
POX	0.136 (Kothari et al. 2008)	67.5 (Kalamaras & Efstathiou 2013)
BG	0.020 (Koroneos et al. 2005)	42.5 (Kalamaras & Efstathiou 2013)
PV-EL	0.040 (Koroneos et al. 2005)	31.2 (Afgan & Carvalho 2002)
W-EL	0.005 (Koroneos et al. 2005)	33.8 (Afgan & Carvalho 2002)
H-EL	0.010 (Koroneos et al. 2005)	52 (Afgan & Carvalho 2002)
WS-CL	0.012 (Koroneos et al. 2005)	21 (Steinfeld 2002)

These criteria, selected under the benefits category, are evaluated for their weights using AHP. Since the original AHP was introduced by Saaty, there have been numerous modifications in the methodology. Different studies applied various modifications of AHP. The detail study evaluating hydrogen production technologies using three different forms of AHP is reported in the literature (Thengane et al. 2014). The analytic hierarchy process (AHP), introduced by Saaty is a common decision-making methodology based on additive synthesis. AHP utilizes a tree structure of objective, criteria (sub-criteria), and alternatives in order to simplify complex decision-making problems resulting in simplified sub-problems (Chui et al. 2005). Figure 3.2 displays the evaluation tree of eight hydrogen production processes with respect to five criteria falling under the benefits attribute. The step by step methodology for AHP is available in literature (Saaty 1990; Alonso & Lamata 2006).

For every pair wise comparison matrix, the consistency index (CI) is calculated using the maximum eigen value (λ_{max}) and the number of attributes (n).

$$CI = \frac{\lambda_{max} - 1}{n - 1} \quad (3.7)$$

The preferences are acceptable if the consistency ratio (CR) is less than 0.1 which is given by Equation (3.8) where RI is the random index reported by Saaty (1980).

$$CR = \frac{CI}{RI} \quad (3.8)$$

In AHP based approaches, the pair wise comparison matrices are generated using the data obtained from the surveys. However, in this specific study concerning hydrogen production processes, the relative importance of alternatives for each criterion is logically assumed using Saaty's scale of 1/9–9 on the basis of data available in literature (Ramsden et al. 2009) either for each criterion or for the parameters on which those criteria depend. For example, the process with highest emission would rank last with scale value 1 and the process with highest efficiency would rank first with scale value 9. The scale values for other alternatives would be decided based on their qualitative or quantitative importance relative to highest or lowest ranked process. Acceptability of the assumed values for each pair wise comparison is finally checked against the CR. For the objective of finding the cost-effective environmentally benign hydrogen production technology, the selection criteria are evaluated as two different

cases. In Case 1 priority is given to future sustainability and environmental concerns. On the other hand, in Case 2 equal priority is given to all the criteria. The pair wise comparison matrix for the selected five criteria using classical AHP for Case 1 is shown in Table 3.4. Application of AHP results in importance of different criteria for Case 1. GHG emissions are at foremost in deciding the future sustainability of a technology with respect to environment. Hence, the highest importance of 45 % is assigned to GHG emissions criterion on account of the increasing global concerns of climate change and environmental regulations. Raw material and utilities are assigned 30 % importance as they contribute to major portion of the operating costs as well as emissions in case of hydrogen production. The nature, source and mode of utilising feedstock and other ancillary material decides the extent of environmental and economic impact. The energy efficiency is allotted 14 % weight considering the wastage of energy as a significant factor affecting effective environ-economic practice. The criterion of waste disposal and non-GHG emissions being considerably less significant than other criteria is allotted 4 % importance. The criterion is given less importance as most of the processes do not encounter solid and liquid waste disposal problem. Furthermore, the non-GHG emissions are relatively less harmful for environment. Scalability is assigned 7 % importance to account the difficulties in actual implementation of renewable based approaches at assumed plant capacity.

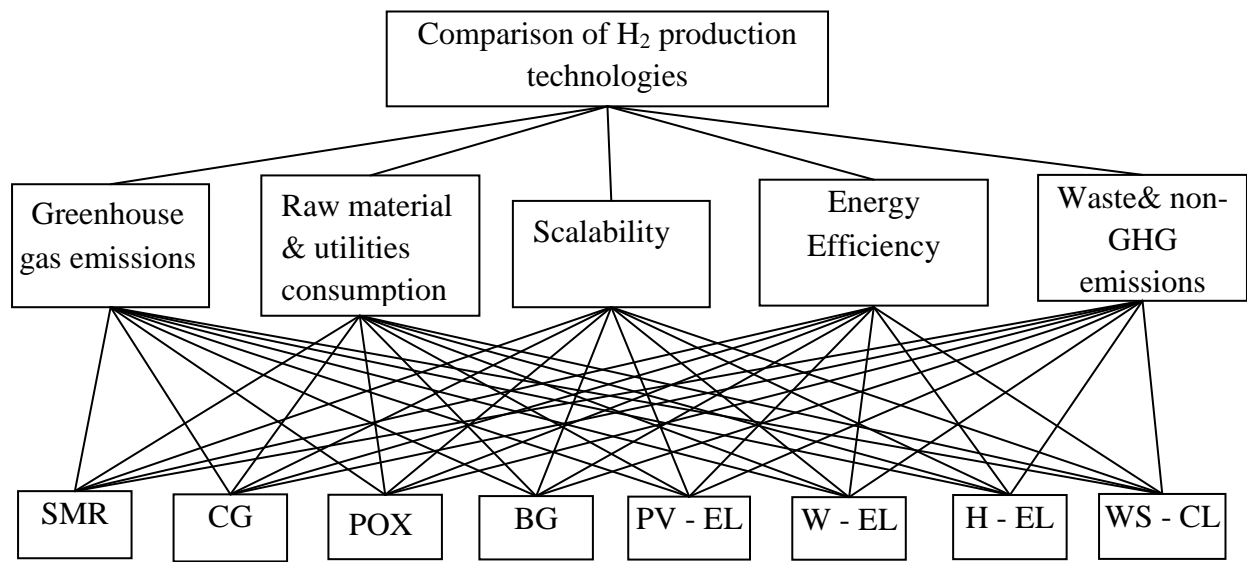


Figure 3.2 Hierarchy tree structure for the evaluation of eight hydrogen production processes using AHP

Table 3.4 Pair wise comparison matrix for five criteria using AHP for Case 1

Criteria	GHG emissions	Raw material & utilities	Energy Efficiency	Scalability	Waste & emissions	Weights
GHG emissions	1	2	4	6	7	0.45
Raw material & utilities	1/2	1	3	5	6	0.30
Energy Efficiency	1/4	1/3	1	3	4	0.14
Scalability	1/6	1/5	1/3	1	2	0.07
Waste & emissions	1/7	1/6	1/4	1/2	1	0.04
$\lambda_{\max} = 5.14$		C.I. = 0.03			C.R. = 0.03	

3.3 Results and Discussion

Table 3.5 shows the pair wise comparison matrix for eight alternatives for the criterion of energy efficiency. The similar matrices for rest of the criteria are reported in Appendix A. Each of these matrices is also checked for their consistency. Tables 3.6 and 3.7 represent the final scores obtained after synthesis using AHP for Case 1 and Case 2 respectively. The last column display the scores attained by each of the technologies in descending order of importance. The higher value indicates the higher preference for the alternative. Wind-based electrolysis (W-EL) and water splitting by chemical looping (WS-CL) appears to be most beneficial in Case 1 whereas only WS-CL appears to be most beneficial in Case 2 when all the criteria are equally important. This implies that amongst the renewable options, only water splitting by chemical looping holds the potential to be most beneficial irrespective of the weightage to different criteria.

Figure 3.3 shows the cost-benefit trade-offs for the selected eight hydrogen production technologies for two cases using three different AHP approaches. For Case 1 of AHP, wind-based electrolysis, hydro-based electrolysis, and water splitting by chemical looping proves to be the most beneficial technologies having the higher final scores. For Case 2, water splitting by chemical looping, SMR, wind-based electrolysis, and hydro-based electrolysis proves to be the most beneficial technologies. The PV-based electrolysis method is the most expensive alternative and relatively less beneficial than most of the other renewable technologies. This makes it less desirable for the chosen plant capacity. Similarly the coal

gasification, biomass gasification, and partial oxidation of heavy oils scores relatively low on the benefits scale making them the less preferred alternatives amongst the fossil based technologies. The benefits of the fossil based technologies seem to increase while the benefits of the renewable based technologies decrease in Case 2. In both cases, WS-CL amongst the renewable approaches is the only technology that appeared beneficial and cost competitive with the fossil based hydrogen production technologies. The wind-based and hydro-based hydrogen production technologies though beneficial, have more than twice the equivalent annual cost compared to water splitting by chemical looping and SMR. In addition, in Case 2, the scores of wind and hydro-based electrolysis drop down unlike WS-CL. The overall cost-benefit trade-offs clearly imply that the water splitting by chemical looping should be the technology of first choice for hydrogen production.

Table 3.5 Pair wise comparison matrix for eight alternatives for energy efficiency

	SMR	CG	POX	BG	PV-EL	W-EL	H-EL	WS-CL	Weights
SMR	1	3	2	5	7	6	4	8	0.3316
CG	1/3	1	1/2	3	5	4	2	6	0.1576
POX	1/2	2	1	4	6	5	3	7	0.2310
BG	1/5	1/3	1/4	1	3	2	1/2	4	0.0713
PV-EL	1/7	1/5	1/6	1/3	1	1/2	1/4	2	0.0329
W-EL	1/6	1/4	1/5	1/2	2	1	1/3	3	0.0480
H-EL	1/4	1/2	1/3	2	4	3	1	4	0.1034
WS-CL	1/8	1/6	1/7	1/4	1/2	1/3	1/4	1	0.0243
$\lambda_{\max} = 8.29$			C.I. = 0.04			C.R. = 0.03			

Table 3.6 Final scores using AHP for Case 1

Alternatives	GHG emissions (0.45)	Raw material & utilities (0.30)	Energy Efficiency (0.14)	Scalability (0.07)	Waste & emissions (0.04)	Final Scores
W-EL	0.3328	0.1572	0.0480	0.0355	0.1736	0.2136
WS-CL	0.1605	0.3313	0.0243	0.1449	0.3568	0.2000
H-EL	0.2330	0.2307	0.1034	0.0508	0.1736	0.1995
SMR	0.0276	0.0477	0.3316	0.3284	0.0356	0.0965
BG	0.1102	0.0709	0.0713	0.0258	0.0202	0.0835
PV-EL	0.0765	0.1059	0.0329	0.0743	0.1135	0.0806
POX	0.0203	0.0236	0.2310	0.2311	0.0511	0.0661
CG	0.0391	0.0327	0.1576	0.1093	0.0757	0.0601

Table 3.7 Final scores using AHP for Case 2

Alternatives	GHG emissions (0.2)	Raw material & utilities (0.2)	Energy Efficiency (0.2)	Scalability (0.2)	Waste & emissions (0.2)	Final Scores
WS-CL	0.1605	0.3313	0.0243	0.1449	0.3568	0.2036
H-EL	0.2330	0.2307	0.1034	0.0508	0.1736	0.1583
SMR	0.0276	0.0477	0.3316	0.3284	0.0356	0.1542
W-EL	0.3328	0.1572	0.0480	0.0355	0.1736	0.1494
POX	0.0203	0.0236	0.2310	0.2311	0.0511	0.1114
CG	0.0391	0.0327	0.1576	0.1093	0.0757	0.0829
PV-EL	0.0765	0.1059	0.0329	0.0743	0.1135	0.0806
BG	0.1102	0.0709	0.0713	0.0258	0.0202	0.0597

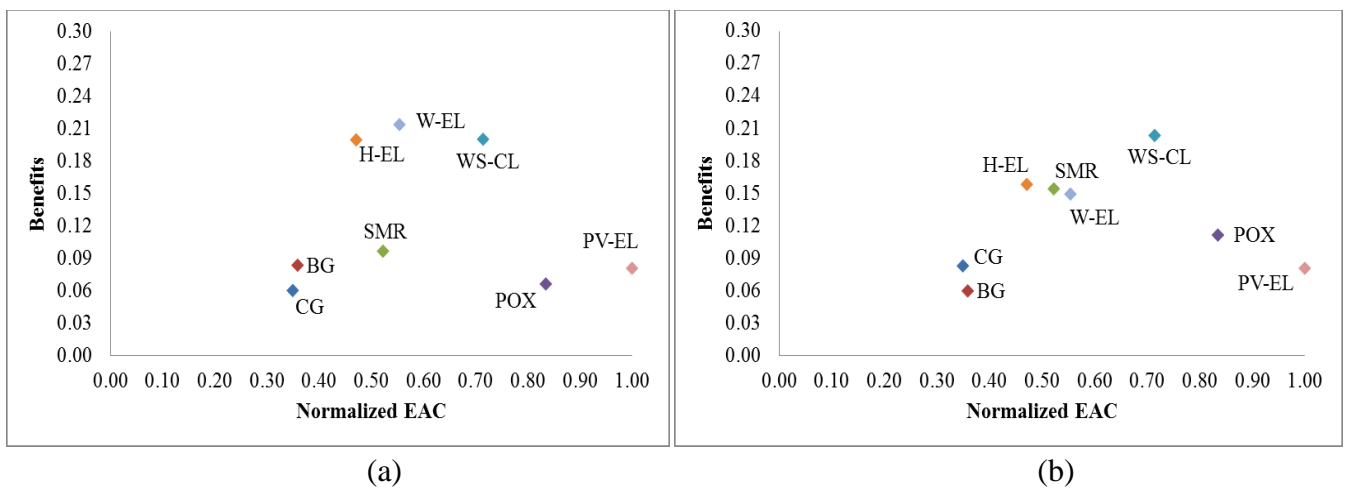


Figure 3.3 Cost-Benefit analysis results: (a) AHP for assumed criteria weights, (b) AHP for equal criteria weights

3.4 Conclusions

The eight different technologies of hydrogen production are compared on the basis of cost-benefit analysis. AHP method is used to evaluate different criteria under the benefits category for two different cases. From the results of the cost-benefit analysis, water splitting by chemical looping (WS-CL) technology appears to be the most promising one for hydrogen production for the selected objective as a decision maker. However, it should be noted that the results are based on the weights assumed for each criterion and the pair wise comparison matrix. The final scores and rankings of various technologies depend on the weights, pair wise comparison matrix, and the AHP-based approach used for carrying out calculations and

analysis. Therefore it is highly recommended to use the results obtained by the AHP-based approach for making final decisions under the guidance of an expert in the field instead of directly selecting the results of AHP. The AHP based approach can prove to be an efficient tool for decision makers and particularly for technology selection in the hydrogen production sector, which would otherwise be difficult because of the diverse range of possible technologies. For the chosen perspective in present study, the most beneficial and hence desirable technology is water splitting by chemical looping. This qualitatively justifies the selection of chemical looping approach to propose a process for NO and H₂ production in next chapter.

CHAPTER 4

AMMONIA OXIDATION BY CHEMICAL LOOPING

This chapter discusses the advances in ammonia oxidation study and proposes the reaction of ammonia with different metal oxides to produce NO and H₂, followed by the thermodynamic feasibility check for the same.

4.1 Introduction

The catalytic and non-catalytic oxidation of ammonia by different oxygen carriers has been studied extensively. The commercial significance of oxidation of ammonia lies mainly in the production of nitric oxide for nitric acid production and medical applications. The current world production of nitric acid is about 60 million tonnes, 85 % of which is used in the fertilizer industry for producing ammonium nitrate (The Essential Chemical Industry n.d.). The conventional process for the production of nitric acid begins with steam methane reforming (SMR) of natural gas to produce hydrogen, which is desulfurised and reacted to produce ammonia followed by catalytic oxidation of ammonia to produce nitric oxide (NO) which is further hydrolysed to produce nitric acid (Thiemann et al. 2012). This process relies on fossil fuel (natural gas), which although efficient is not environmentally benign due to the atmospheric emissions in almost every stage of the process. The ammonia-air ratio of about 1:10 and Pt/Rh catalyst at high temperature of 900 °C, 10 bar pressure results in almost complete conversion of ammonia to oxides of nitrogen (Thiemann et al. 2012; Scientific American Supplement 1913).

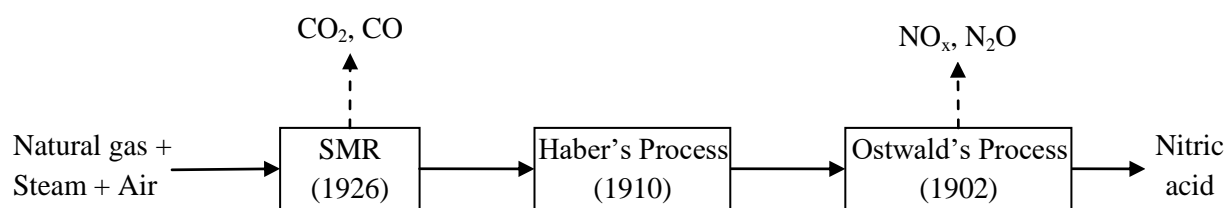


Figure 4.1 Conventional nitric acid production

There have been several efforts in improving energy and economics of SMR based process, however, there have been no significant changes in the NO forming reactions except for the

catalysts and operating conditions. The other attempts focused mainly on improving nitric oxide (NO) selectivity and mitigate the environmental emissions such as nitrous oxide (N₂O) in particular. The traditional oxidation of NH₃ by air or oxygen in exothermic manner at high temperatures results in lot of energy being unused. Hence, the replacement of air or oxygen by other oxygen carrier such as metal oxide that would react with NH₃ endothermically is a worthwhile option to be considered.

Chemical looping process employs metal oxides as oxygen-carrier for the conversion of the fuel; the reduced metal oxide is then regenerated by oxidation thus completing the cycle mostly in fluidized bed reactors (Adanez et al. 2012). The concept has been explored for its potential to integrate with processes such as gas reforming, solid fuel gasification, and power generation. As discussed in the literature review, the application of chemical looping has been extended to other areas such as combustion and production of different chemicals. The chemical looping approach has been used to provide feedstock for ammonia synthesis producing pure streams of H₂, N₂ and CO₂ in three different reactors (Edrisi et al. 2014). The synthesis of NH₃ from N₂ and H₂O is also proposed through a solar thermochemical reaction cycle using Chromium (Michalsky & Pfromm 2011). The application of chemical looping approach can be extended to the formation of feedstock for mineral acids such as nitric acid (HNO₃) where NH₃ can be oxidised by an oxygen carrier such as metal oxide in place of air or pure oxygen.

This chapter proposes a chemical looping based process scheme in which NO and H₂ are produced from reaction of ammonia with metal oxide, and the reduced metal oxide is regenerated either by hydrolysis or by air oxidation. The metal oxide regeneration step of the proposed process scheme by hydrolysis (Steinfeld 2002; Charvin et al. 2007) as well as by air oxidation (Zhu et al. 2002; Fontijn & Kurzius 1971) has been reported in literature. The present chapter reports the thermodynamic feasibility of the proposed reaction of ammonia with different metal oxides to produce NO and H₂.

4.2 Oxidation of Ammonia

Ammonia oxidation process is different from other reactions of oxidation of inorganic species such as H₂, hydrogen chloride (HCl), CO, sulfur dioxide (SO₂), etc. It is possible to obtain

each of the three products (N₂, N₂O, NO) in various ratios depending on the catalyst used and the appropriate operating conditions (Il'chenko 1976). The general oxidation of ammonia in presence of air or oxygen proceeds mainly by following three paths:



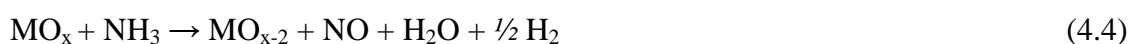
Zawadzki (1950) proposed an imide (NH) mechanism where NH is formed first to either react with atomic oxygen to form nitroxyl (HNO) with further conversion to N₂ or nitrous oxide (N₂O), or react with molecular O₂ to produce NO. In case of non-catalytic oxidation, the fraction of ammonia reacted decreases rapidly on increasing ammonia concentration thereby indicating a zero (or negative) order (Stephens & Pease 1950). Most of the metal oxide catalysts form all three products in different proportions at around 400-500 °C, however, some catalysts are selective to specific product. In first industrial nitric acid plant, pure platinum gauzes served as the catalyst selectively producing NO which was later replaced by platinum–rhodium alloys with 5 to 10 % of rhodium (Sadykov et al. 2000). Though many different metal oxides and alloys have been tried since then, Pt-Rh alloys are the most often used catalyst even in the present day industrial plants. The oxidation of ammonia on platinum gauzes at 10 atm pressure and 800–950 °C temperature produces mainly molecular N₂ and NO in an exothermic reaction (Connor 1967). There is still no agreement amongst the theories predicting the side reactions affecting the process selectivity of ammonia oxidation. In recent years, the two other insights have been proposed into the reaction mechanism of NH₃ oxidation. First is the selective catalytic oxidation (SCO) by a direct route involving a hydrazinium-type intermediate reported mainly for the transition metal oxide catalysts such as CuO/Al₂O₃, CuO/TiO₂, Fe₂O₃/TiO₂, CrO_x/TiO₂, and CoO_x/TiO₂ (Darvell et al. 2003; Amores et al. 1997). Second is a two-step internal selective catalytic reduction (iSCR) mechanism in which major fraction of NH₃ is oxidised to NO_x species that subsequently react with NH₃ to form N₂ (Chmielarz et al. 2005; 2006). Several noble metal catalysts, such as Ag (powder), Pt, Pt/Al₂O₃, Pd/Al₂O₃, Pt-ZSM-5, Pd-ZSM-5, Rh/Al₂O₃, and Rh-ZSM-5, have been suggested to follow this iSCR route (Jabłońska et al. 2012). The

decomposition of NO to N₂ and O₂ has also been explored as a possible side reaction to explain the decrease in conversion of NH₃ to NO.

In most of the above mentioned studies, ammonia reacts with metal oxides in presence of oxygen or air. Miyamoto et al. (1978) studied the synergistic effect of mixing oxidised metal oxide with Pt/Al₂O₃ for ammonia oxidation and found that the addition of Pt improved the selectivity to N₂ formation but did not change the activity of metal oxide reacting with ammonia. Kosaki et al. (1979) investigated the role of lattice oxygen and absorbed oxygen in different metal oxides while studying oxidation of ammonia and proposed formation of NO as an intermediate which further reacts with NH₃ to form partial oxidation products such as N₂ and N₂O. Ammonia oxidation to N₂ by metal oxide-Pt/Al₂O₃ mixture involves two types of active sites, viz. metal oxide site for conversion of NH₃ to NO_x and N₂, and Pt metal site for NO_x reacting with NH₃ to form N₂ (Kosaki et al. 1982). These studies report the reaction of ammonia with different metal oxides but did not clearly mention the overall reaction taking place in the reactor. The major focus of these studies is to convert the entire NH₃ and NO_x to the safe form of N₂. In addition, the possibility of getting hydrogen as an additional product with NO_x such as NO has not been considered in any of these works. The next section describes the proposed chemical looping process producing NO and H₂ from ammonia and metal oxides.

4.3 Chemical Looping based Ammonia Oxidation

Chemical looping involves the reduction of oxygen carrier such as metal oxides by a reducing gas such as ammonia followed by oxidation of the reduced metal oxide back to its oxidized state. A new process is proposed based on the concept of chemical looping using metal oxides as oxygen carrier to facilitate the continuous production of NO and H₂ along with regeneration of the metal oxide. Figure 4.2 shows two reaction schemes for this new process where the difference is in the method of regeneration of the metal oxide. From some preliminary experiments, it was found that H₂ was co-produced with NO in a ratio of about 0.5. This leads to the following chemical reactions:





The reaction (4.4) is the reduction step where the metal oxide is reduced by ammonia to the metal or reduced metal oxide producing NO, H₂ and H₂O. The ratio H₂ to NO ($x=0.5$ in equation 4.4) is one of the important outcomes of this work and is discussed in more detail in later sections.

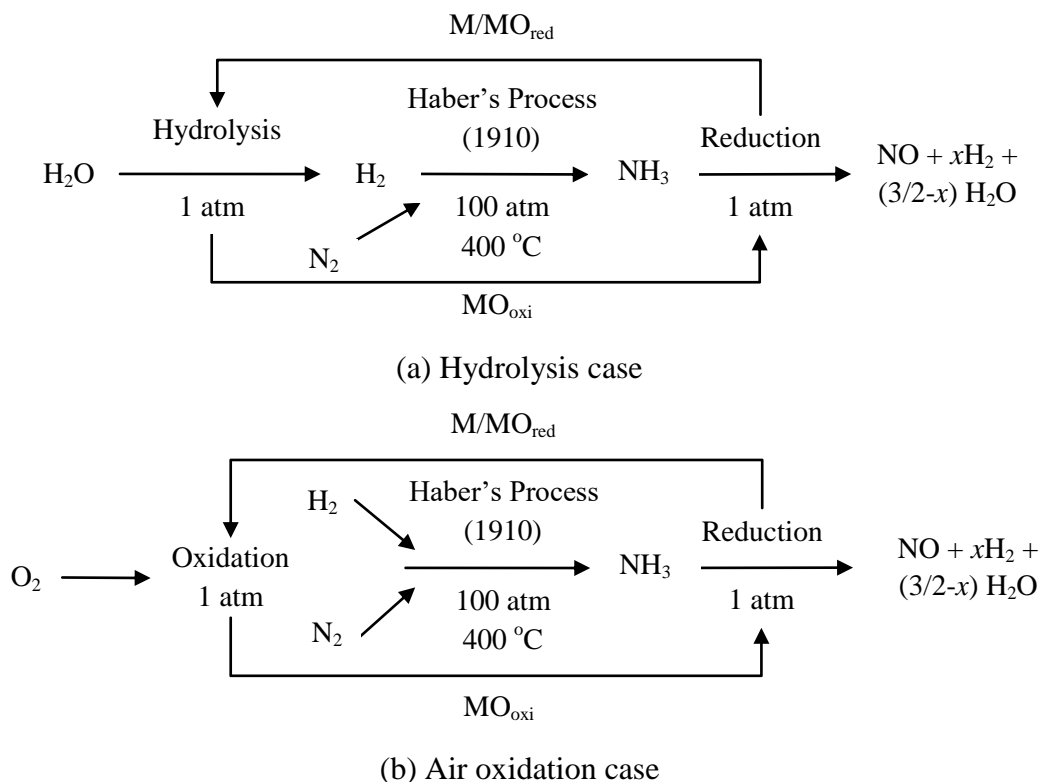


Figure 4.2 Chemical looping based process schemes for NO and H₂ production (a) Hydrolysis case, (b) Air oxidation case

In reaction (4.5a), the metal or reduced metal oxide is hydrolyzed with steam releasing hydrogen at a wide range of temperatures depending on the metal oxide (Abanades et al. 2006). In reaction (4.5b), metal oxide is reoxidised in excess air or oxygen usually at relatively higher temperatures than hydrolysis. The two processes would be referred to as chemical looping using hydrolysis (CLHYD) and chemical looping using air oxidation (CLAO) at further instances. CLAO offers the advantage of carrying re-oxidation reaction at temperatures higher than reduction step whereas CLHYD offers the advantage of surplus hydrogen production. Both the reactions in the proposed processes can be operated at lower

pressures without the need for expensive catalysts. The hydrogen produced in Reaction (4.4) or (4.5a) can be utilized for total or partial production of ammonia in a renewable manner. The reaction of ammonia with metal oxide is endothermic whereas the regeneration reactions are exothermic thereby providing an opportunity for intra process heat exchange. Though the minimum number of steps is preferred in chemical looping processes, the proposed reaction to produce NO and H₂ can also be employed with multi-step thermochemical cycles. There are several other factors such as the availability, cost and properties of oxygen carriers that need to be accounted for selecting a particular cycle.

4.4 Thermodynamic Feasibility

Before performing the experimental investigation, it is important to check the thermodynamic feasibility of the reaction so as to find the approximate operating conditions. Table 4.1 represent the calculations for thermodynamic feasibility of different metal oxide cycles using the reaction equations tab of the software package HSC Chemistry Version 7.1 by Outotec. The reaction stoichiometry is adjusted to balance the reaction equation based on 1 mole NO formation. ΔH_0 and ΔG_0 are the heats of reaction and the change in Gibbs free energy at standard conditions of 1 atm, 25 °C. The temperature at which a reaction becomes spontaneous is found by applying the Gibbs equation where ΔG is change in Gibbs free energy, ΔH is heat of reaction, T is temperature and ΔS is change in entropy.

$$\Delta G = \Delta H - T\Delta S \qquad \Delta G < 0 \text{ for thermodynamic feasibility} \qquad (4.6)$$

T_e is the equilibrium temperature at which the reaction just becomes spontaneous for ΔG equals to zero at T_e . The real temperature (T_r) is the temperature at which the reaction is assumed to occur in forward direction for Gibbs free energy of -50 kJ. The ΔG value close to -50 kJ is a reasonable criterion for a reaction to go to 100 % conversion, as the majority of chemical reactions start becoming feasible as soon as ΔG becomes negative. Fe based oxides are considered to be one of the most suitable candidates for conventional chemical looping processes owing to their properties and cheaper availability. Considering the different oxidation states that Fe can exist, there are multiple cycles possible with Fe based oxides each occurring at different temperatures. However, in this study the thermodynamic feasibility of other metal oxides which might react with ammonia are also checked. The calculations are

shown for reduction step with ammonia followed by both the methods of regeneration of metal oxide. The regeneration by hydrolysis in case of CuO and Co_3O_4 is multi-step involving electrolysis step (Abanades et al. 2006) and hence only the air oxidation step is reported in the table. For the purpose of these calculations, the value of x (the H_2 to NO ratio) in equation 4.4 is assumed to be 0.5 (Values of x lower than 0.5 will be more exothermic and spontaneous and hence is a conservative value from a feasibility perspective).

From Table 4.1, $\text{Fe}_2\text{O}_3/\text{Fe}_3\text{O}_4$, CuO/Cu and $\text{Co}_3\text{O}_4/\text{CoO}$ cycles appear to be feasible below temperatures of $1000\text{ }^\circ\text{C}$ (this being the maximum temperature limit of the experimental setup) making them potential candidates to be selected for the experimental study. The preliminary experiments are performed using Fe_2O_3 , CuO and Co_3O_4 over a wide range of temperatures close to those calculated using thermodynamic simulation to decide the reaction temperature with ammonia for each metal oxide. In case of Fe based oxides, the FeO/ Fe_3O_4 and FeO/ Fe_2O_3 cycles have ammonia-metal oxide reaction temperatures more than $1000\text{ }^\circ\text{C}$ unlike $\text{Fe}_2\text{O}_3/\text{Fe}_3\text{O}_4$ and hence are not considered for experimental investigation. It can be seen that the hydrolysis step is slightly exothermic whereas the air oxidation step is highly exothermic and the reduction step is highly endothermic at T_r . Hence, there is a need to find the optimum temperature for each reaction so as to minimize the temperature difference thus providing scope for improvement in process heat exchange. For this reason, in the case of metal oxide regeneration by air oxidation, the temperature for the re-oxidation of the metal oxide is set at a value higher than the NH_3 oxidation temperature, as it is assumed that the metal oxide will not only supply oxygen, but also the heat required by the endothermic reaction of the NH_3 oxidation step. Indium, Nickel and Tin based oxides are interesting candidates, as the hydrolysis reaction (reaction 4a) is feasible at a relatively high temperature compared to other metal oxides. However, In_2O_3 , NiO and SnO_2 could not be selected for the experimental study as the NH_3 oxidation reaction temperatures are much higher than $1000\text{ }^\circ\text{C}$. In case of metal oxide regeneration by hydrolysis, the process can provide surplus hydrogen which can be used for the total production of NH_3 . However, there is also a need to supply external heat for the highly endothermic reduction of metal oxide by ammonia. In the case of regeneration by air oxidation, the proposed process looks promising from an energy point of view as the exothermic regeneration reaction is feasible over a wide range of temperatures and if a higher temperature is selected than the reduction reaction, the metal oxide oxidation can provide the heat for the endothermic reduction reaction.

Table 4.1 Calculations for thermodynamic feasibility of some metal oxide cases

No.	Reaction Set	ΔH_o (kJ)	ΔG_o (kJ)	T_e (°C)	T_r (°C)	ΔH_r (kJ)	ΔG (kJ)
1.	$2 \text{Fe}_3\text{O}_{4(s)} + \text{NH}_{3(g)} \rightarrow 6 \text{FeO}_{(s)} + \text{NO}_{(g)} + \text{H}_2\text{O}_{(g)} + 0.5 \text{H}_{2(g)}$	492.7	395.6	1377	1550	462.3	-47.9
a	$6 \text{FeO}_{(s)} + 2 \text{H}_2\text{O}_{(g)} \rightarrow 2 \text{Fe}_3\text{O}_{4(s)} + 2 \text{H}_{2(g)}$	-114.6	-64	447	125	-113.5	-51.4
b	$6 \text{FeO}_{(s)} + \text{O}_{2(g)} \rightarrow 2 \text{Fe}_3\text{O}_{4(s)}$	-598.2	-521.2		1600	-568	-174
2.	$2 \text{Fe}_2\text{O}_{3(s)} + \text{NH}_{3(g)} \rightarrow 4 \text{FeO}_{(s)} + \text{NO}_{(g)} + \text{H}_2\text{O}_{(g)} + 0.5 \text{H}_{2(g)}$	458.3	360.6	1157	1325	437.0	-49.9
a	$4 \text{FeO}_{(s)} + 2 \text{H}_2\text{O}_{(g)} \rightarrow 2 \text{Fe}_2\text{O}_{3(s)} + 2 \text{H}_{2(g)}$	-80.2	-29	217	100	-79.5	-16.2
b	$4 \text{FeO}_{(s)} + \text{O}_{2(g)} \rightarrow 2 \text{Fe}_2\text{O}_{3(s)}$	-563.9	-563		1375	-541	-159
3.	$\text{In}_2\text{O}_{3(s)} + \text{NH}_{3(g)} \rightarrow \text{In}_2\text{O}_{(g)} + \text{NO}_{(g)} + \text{H}_2\text{O}_{(g)} + 0.5 \text{H}_{2(g)}$	785.4	645.4	1487	1600	726.9	-44.4
a	$\text{In}_2\text{O}_{(g)} + 2 \text{H}_2\text{O}_{(g)} \rightarrow \text{In}_2\text{O}_{3(s)} + 2 \text{H}_{2(g)}$	-407.4	-313.7	1202	1000	-359.1	-49.5
b	$\text{In}_2\text{O}_{(g)} + \text{O}_{2(g)} \rightarrow \text{In}_2\text{O}_{3(s)}$	-891.1	-770.9		1650	-830	-180
4.	$2 \text{NiO}_{(s)} + \text{NH}_{3(g)} \rightarrow 2 \text{Ni}_{(s)} + \text{NO}_{(g)} + \text{H}_2\text{O}_{(g)} + 0.5 \text{H}_{2(g)}$	373.8	297.6	1217	1425	360.6	-50.3
a	$2 \text{Ni}_{(s)} + 2 \text{H}_2\text{O}_{(l)} \rightarrow 2 \text{NiO}_{(s)} + 2 \text{H}_{2(g)}$	92.2	51.2	533	975	-11.6	-10
b	$2 \text{Ni}_{(s)} + \text{O}_{2(g)} \rightarrow 2 \text{NiO}_{(s)}$	-479.4	-423.2		1450	-465.2	-173.3
5.	$6 \text{Fe}_2\text{O}_{3(s)} + \text{NH}_{3(g)} \rightarrow 4 \text{Fe}_3\text{O}_{4(s)} + \text{NO}_{(g)} + \text{H}_2\text{O}_{(g)} + 0.5 \text{H}_{2(g)}$	389.6	290.5	833	965	407.9	-48.7
a1	$4 \text{Fe}_3\text{O}_{4(s)} + 12 \text{NaOH}_{(l)} \rightarrow 12 \text{NaFeO}_{2(s)} + 4 \text{H}_2\text{O}_{(g)} + 2 \text{H}_{2(g)}$	114.7	-59.9		500	-92.51	-189.4
a2	$12 \text{NaFeO}_{2(s)} + 6 \text{H}_2\text{O}_{(g)} \rightarrow 6 \text{Fe}_2\text{O}_{3(s)} + 12 \text{NaOH}_{(l)}$	137.7	152.4		100	155.7	154.1
b	$4 \text{Fe}_3\text{O}_{4(s)} + \text{O}_{2(g)} \rightarrow 6 \text{Fe}_2\text{O}_{3(s)}$	-495.2	-416.1		1000	-509.5	-135.2
6.	$2 \text{CuO}_{(s)} + \text{NH}_{3(g)} \rightarrow 2 \text{Cu}_{(s)} + \text{NO}_{(g)} + \text{H}_2\text{O}_{(g)} + 0.5 \text{H}_{2(g)}$	209.1	133.6	557	760	200.6	-49
	$2 \text{Cu}_{(s)} + \text{O}_{2(g)} \rightarrow 2 \text{CuO}_{(s)}$	-315	-259	1525	800	-302	-123
7.	$4 \text{CuO}_{(s)} + \text{NH}_{3(g)} \rightarrow 2 \text{Cu}_2\text{O}_{(s)} + \text{NO}_{(g)} + \text{H}_2\text{O}_{(g)} + 0.5 \text{H}_{2(g)}$	186.4	101.1	385	575	177	-51
	$2 \text{Cu}_2\text{O}_{(s)} + \text{O}_{2(g)} \rightarrow 4 \text{CuO}_{(s)}$	-292	-226	1200	900	-272	-50
8.	$2 \text{Co}_3\text{O}_{4(s)} + \text{NH}_{3(g)} \rightarrow 6 \text{CoO}_{(s)} + \text{NO}_{(g)} + \text{H}_2\text{O}_{(g)} + 0.5 \text{H}_{2(g)}$	286.8	179.1	467	590	309.8	-49.1
	$6 \text{CoO}_{(s)} + 1.5 \text{O}_{2(g)} \rightarrow 2 \text{Co}_3\text{O}_{4(s)}$	-392	-305	977	600	-412	-114
9.	$\text{SnO}_{2(s)} + \text{NH}_{3(g)} \rightarrow \text{Sn}_{(s)} + \text{NO}_{(g)} + \text{H}_2\text{O}_{(g)} + 0.5 \text{H}_{2(g)}$	471.8	390	1417	1575	510.6	-46.4
a	$\text{Sn}_{(s)} + 2 \text{H}_2\text{O}_{(g)} \rightarrow \text{SnO}_{2(s)} + 2 \text{H}_{2(g)}$	-93.7	-58.4	585	200	-89.2	-38.7
b	$\text{Sn}_{(s)} + \text{O}_{2(g)} \rightarrow \text{SnO}_{2(s)}$	-577	-516	2325	1600	-618	-176

4.5 Conclusions

The chemical looping based process to produce NO and H₂ is proposed and the thermodynamic feasibility check is performed in this chapter. From the results of thermodynamic feasibility analysis, it can be inferred that ammonia can react with different metal oxides at different operating conditions to form NO and H₂. Fe₂O₃/Fe₃O₄, CuO/Cu and Co₃O₄/CoO cycles are found to be feasible below temperatures of 1000 °C making them potential candidates to be selected for the experimental study. The proposed reaction of ammonia with metal oxide is endothermic and hence expected to be thermodynamically efficient in comparison to highly exothermic conventional oxidation of ammonia in nitric acid plant. The metal oxide regeneration step by hydrolysis or by air oxidation is well established and reported in the literature. However, the reduction of metal oxides by ammonia as a means to produce NO and H₂ using chemical looping has not yet been reported. The next chapter discusses the experimental set up, procedure and the instrumentation used in the experimental investigation of the proposed reaction of ammonia with selected metal oxides.

CHAPTER 5

MATERIALS AND METHODS

The traditional chemical looping based system is comprised of two interconnected fluidized bed reactors (Figure 5.1), in which the metal oxide particles are used as oxygen carriers between the two reactors (Lyngfelt 2014). The regeneration section in which reduced metal oxide is oxidised back to its normal state by air or water has already been studied by several authors. In the proposed process for NO and H₂ production, the main objective is to confirm the experimental feasibility of the reaction between ammonia and metal oxide as per the reaction given by equation 4.4. Hence, a series of experiments are carried out to test the feasibility of the selected metal oxides from the results of thermodynamic analysis for their reaction with ammonia. These metal oxides are chosen for experimental investigation considering the limitations of the maximum temperature limit of the furnace of 1000 °C. In addition, copper, cobalt and iron based oxides have been of considerable research interest in the field of selecting oxygen carriers for chemical looping.

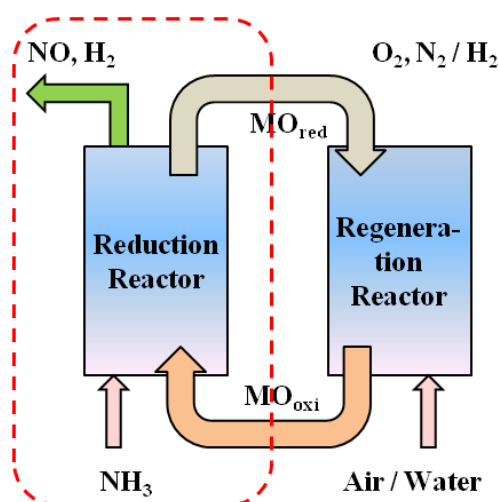


Figure 5.1 Reactor system for chemical looping based NO and H₂ production

Table 5.1 shows the metal oxides that are selected for reaction with ammonia in the proposed chemical looping based scheme. Fe₂O₃, CuO and Co₃O₄ are explored for studying the effect of different operating parameters on conversion of ammonia to nitric oxide (NO). Al₂O₃ is selected to study the decomposition of ammonia into nitrogen and hydrogen owing to its inert nature towards ammonia below 3000 °C. The next sections discuss in detail about the experimental set up, procedure and the instrumentation employed in the experimental study.

Table 5.1 Selected metal oxides for reaction with ammonia

No.	Reaction Set	ΔH_o (kJ)	ΔG_o (kJ)	T_e (°C)	T_r (°C)	ΔH_r (kJ)	ΔG (kJ)
1.	$6 \text{Fe}_2\text{O}_{3(s)} + \text{NH}_{3(g)} \rightarrow 4 \text{Fe}_3\text{O}_{4(s)} + \text{NO}_{(g)} + \text{H}_2\text{O}_{(g)} + 0.5 \text{H}_{2(g)}$	389.6	290.5	833	965	407.9	-48.7
2.	$2 \text{CuO}_{(s)} + \text{NH}_{3(g)} \rightarrow 2 \text{Cu}_{(s)} + \text{NO}_{(g)} + \text{H}_2\text{O}_{(g)} + 0.5 \text{H}_{2(g)}$	209.1	133.6	557	760	200.6	-49
3.	$4 \text{CuO}_{(s)} + \text{NH}_{3(g)} \rightarrow 2 \text{Cu}_2\text{O}_{(s)} + \text{NO}_{(g)} + \text{H}_2\text{O}_{(g)} + 0.5 \text{H}_{2(g)}$	186.4	101.1	385	575	177	-51
4.	$2 \text{Co}_3\text{O}_{4(s)} + \text{NH}_{3(g)} \rightarrow 6 \text{CoO}_{(s)} + \text{NO}_{(g)} + \text{H}_2\text{O}_{(g)} + 0.5 \text{H}_{2(g)}$	286.8	179.1	467	590	309.8	-49.1
5.	$\text{Al}_2\text{O}_{3(s)} + 2 \text{NH}_{3(g)} \rightarrow 2 \text{Al}_{(s)} + \text{NO}_{(g)} + \text{H}_2\text{O}_{(g)} + \text{H}_{2(g)}$	1403	1303	3230	3300	1817	-50.2

5.1 Experimental Set up

In the present study the objective is to verify the reaction of ammonia with metal oxide and hence, the experiments are carried out in a single fluidised bed reactor functioning in a semi batch mode. The fixed amount of metal oxide is placed into the reactor at the beginning of experiment and is not allowed to escape from the reactor. Figure 5.2 shows the schematic diagram of the experimental set-up used for the study. The rig consists of three mass flow controllers (MFCs) for ammonia, nitrogen and air followed by a gas mixer before the inlet of the reactor placed inside the furnace. An additional NH_3 rotameter calibrated from 2.3 to 10 ml/min of NH_3 flowrate is mounted on the ammonia gas line before the NH_3 MFC as an additional check on the flowrate of NH_3 . The electric furnace is equipped with a proportional-integral-derivative (PID) temperature controller with the maximum limit of 1000 °C. The quartz reactor has two distributor plates placed 10 cm apart having the diameter of 4 cm and thickness of 0.5 cm with a side inlet for transferring the metal oxide powder into and out of the reactor. The reactor has two outlets, one of which is connected to the exhaust and the other is connected to the inlet of the gas detector for analysing the gaseous composition.

Two similar quartz reactors used for experiments are labelled as Reactor 1 (normal reactor) and Reactor 4 (with tapered hole in lower distributor plate). The main sets of experiments are performed using Reactor 1 for different metal oxides with more focussed experiments for the

case of CuO to study the effect of different operating parameters on the product yield. The additional experiments are performed using Reactor 4 which required tapping at regular intervals to avoid agglomeration of metal oxide particles around the hole in the distributor. The reactor is cleansed using acid base treatment followed by distilled water wash and oven drying for each run. The gas analysers Testo 340 and iBRID MX6 are obtained to measure NH₃, NO and H₂ from Testo and Industrial Scientific, Melbourne respectively. The gas samples collected in 1 litre gas bags during peak conversions are sent to GHG Emissions Analysis laboratory for N₂O analysis. The specifications of different metal oxides and gases used in the experiments are mentioned in Table 5.2.

Table 5.2 Specifications of chemicals and gases used

Chemicals / Gases	Supplier (Particle size / Cylinder size)	Purity
CuO and Fe ₂ O ₃	Sigma Aldrich (10 micron) Chem Supply (70 micron)	99.50 %
Co ₃ O ₄ and Al ₂ O ₃	Sigma Aldrich (70 micron)	99.50 %
Ammonia	Air Liquide (G size)	99.95 %
Nitrogen	Air Liquide (G size)	99.99 %
Air	Air Liquide (G size)	99.00 %

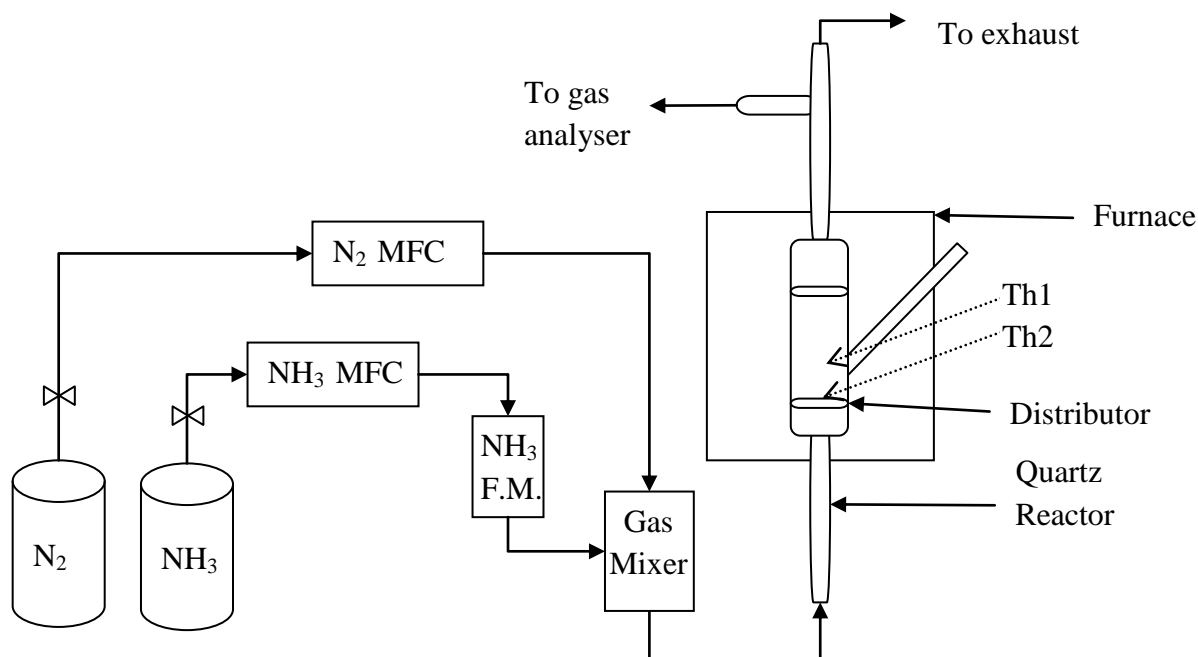


Figure 5.2 Schematic of the experimental set-up

5.2 Procedure

Before the start of every run, the quartz reactor is thoroughly cleansed using acid base treatment and air dried in an oven to remove the moisture. The different particle sized metal oxides are separated using micro sieves and stored in separate bottles. The desired amount of metal oxide powder is weighed using a digital weighing balance (error: ± 0.01 g) and transferred onto the bottom sinter plate using funnel through the side entrance nozzle of the reactor. The reactor is shaken to adjust the metal oxide powder for uniform distribution and the side arm of reactor is tightly closed by a silicon cork. The two thermocouples, Th1 and Th2 are placed inside the reactor such that Th1 touches the metal oxide particles and Th2 lies in the centre of the fluidising zone i.e. nearly 5 cm above the bottom distributor plate as shown in Figure 5.2. The entire reactor is placed vertically inside the furnace with inlet tubing connected to the outlet of the gas manifold and outlet tubing to the exhaust. One of the two outlets is connected to the inlet of the portable gas analyser. Each end of the reactor is quite far (nearly 15 cm) from the hot insulated furnace and hence silicon tubing is employed for gas entering and leaving the reactor. The furnace is set to the appropriate temperature for the corresponding metal oxide.

The experiment is started by first flowing nitrogen at a sufficient rate to fluidise the metal oxide particles. Once the set temperature is attained at a constant value for about 2 minutes, the ammonia flow is started and maintained at a fixed rate, so as to allow a specific concentration, around 1000 ppm to 1100 ppm ammonia into the reactor. The pressure just before the inlet of reactor is measured to be around 120 kPa. The flowrates of gases are controlled by the digital mass flow controllers and the outlet gas is sent to the gas analyser which measures the concentrations of different gases continuously at 1 second interval. The mass flow controllers are purged with nitrogen for about 5 minutes before and after each run. The ammonia flow meter is also purged by nitrogen before and after every run. The portable Testo 340 gas analyser calibrated for 3000 ppm NO with 95 % accuracy is used to measure NO concentration and the Industrial Scientific's iBRID MX6 gas analyser calibrated up to 50 ppm for each gas with 98 % accuracy is used to measure NO, H₂ and NH₃. The gas analysers are started with the experiment; however, the readings are noted only after starting the NH₃ flow. The gas samples are also collected in gas bags at appropriate intervals during the peak conversions for the purpose of determining the N₂O composition. After the experiment is completed, the ammonia gas flow is stopped and the furnace is switched off

allowing nitrogen to flow through the reactor for about 60 minutes until the reactor cools down. When the furnace temperature falls below 50 °C, the reactor is removed out and weighed with stopper removed to check the difference in the mass of metal oxide. Finally the entire metal oxide powder is taken out of the reactor and the reactor is cleaned as mentioned earlier for next run.

5.3 Reactor Designs

The experiments are carried out in a cylindrical shaped quartz reactor with one inlet at bottom, two outlets at top, two distributor plates within and a side arm for feeding metal oxide. The total vertical length of the reactor is 60 cm with 25 cm long cylindrical zone having diameter 4 cm that fits inside the furnace. The distributor plates are 0.5 cm thick and are placed 10 cm apart thereby creating the zone for fluidization and reaction. The 20 cm long side arm at an angle of 45° is provided for feeding metal oxide powder into the reactor. Out of the four different reactors, only two reactors labeled as Reactor 1 and Reactor 4 are used for the experiments. The only difference between them is that the bottom distributor plate of Reactor 4 is inclined towards a tapered hole in the centre to facilitate the spouted bed fluidisation of metal oxide particles on tapping the reactor at even intervals. Before designing Reactor 4, two other designs (Reactor 2 and Reactor 3) were also checked for NO conversions but were rejected due to very poor and intermittent conversions. Reactor 2 had a flat bottom distributor plate with 5 mm diameter hole leading to formation of vortex whereas Reactor 3 had an inclined hole at the corner leading to deposition of particles on one side of reactor wall. In both cases, most of the particles appeared to be in dead zone. These reactors with hole were purposefully designed after noticing the hole in the bottom distributor of Reactor 1 considering it to be the reason for efficient gas-solid contact and high conversion in later experiments. The formation of tapered hole sloping downwards must have taken place over a period of time as Reactor 1 was consistently used in experiments and encountered numerous cleaning and washing. The extent of agglomeration or cake formation tended to decrease in the experiments done with Reactor 1 after formation of hole. However, Reactors 2 and 3 did not facilitate efficient gas-solid contact as aimed and could not achieve good conversions. The video was recorded for different reactors to understand the extent of gas-solid interaction at room temperature. Figure 5.3 shows the schematic of different reactor designs tried for the experimental study. Figure 5.3(a) and (b) show the two versions of

Reactor 1 before and after formation of hole in the bottom distributor plate. Figure 5.3(c) and (d) show the rejected reactor designs due to poor reaction conversions. Figure 5.3(e) shows the Reactor 4 filled with Fe_2O_3 in addition to its photographic images before tapping and after tapping.

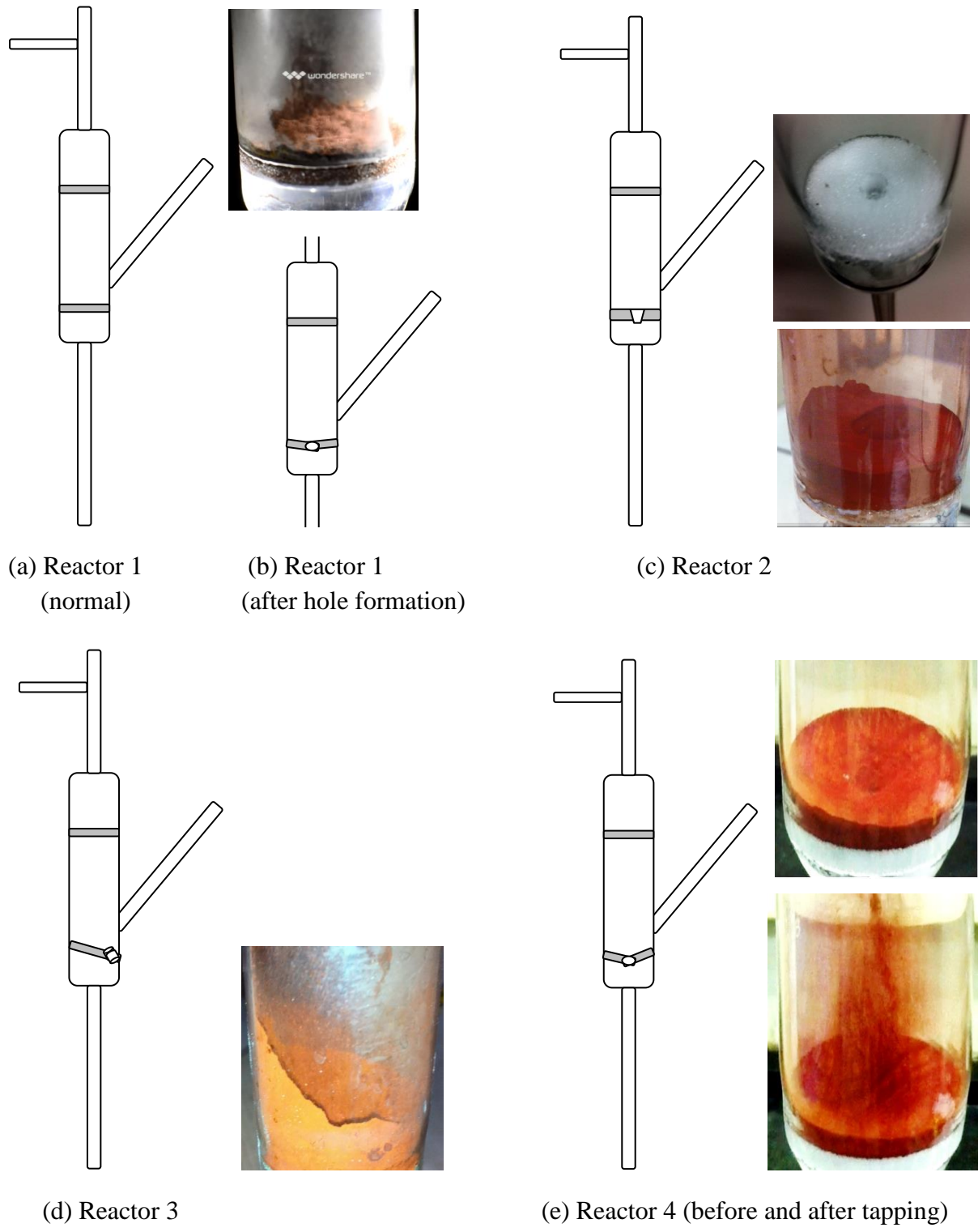


Figure 5.3 Different types of reactor

Agglomeration of solid particles is the most encountered problem in chemical looping based processes and this necessitated the use of regular tapping for the differently designed reactor (Reactor 4). As per the studies reported, the aggregation of solid particles in fluidized reactors can be resolved by different techniques such as vibrating the reactor (Wank et al. 2004), using sound waves (Zhu et al. 2004), or by micro nozzles (Quevedo et al. 2010). The introduction of external excitations such as vibration or oscillating magnetic field by premixing some magnetic particles helps to improve the fluidization of particles and hence the gas-solid interaction (Nam et al. 2004). Quevedo et al. (2010) made use of micronozzles producing a jet with high velocity, turbulence, and shear to break-up large nanoagglomerates, and promote smooth fluidisation. The common methods of mixing a solid and fluids in a container include use of agitation, shaking the container, sparging gases to move liquid, ultrasonic waves and several combinations of these methods (Niazi 2012). This served as the motivation behind designing Reactor 4 as shown in Figure 5.3(e) where gravity-driven fluidisation is supported by inclined surface pointing towards the hole in the centre. The hole functioned as the microjet nozzle for spouting of metal oxide particles coming over the surface of the hole. However, the particles in Reactor 4 settled down forming a stable vortex within a minute allowing the gas to flow through the hole without getting into contact with metal oxide. This necessitated the need for manual or mechanical tapping of the reactor at regular intervals of time to ensure continuous mixing. The pictures in the Figure 5.3(e) show the Fe_2O_3 particles in static and spouted mode respectively at room temperature condition.

5.4 Instrumentation

The major digital instruments involved in the experimental study are the gas analyzers, mass flow controllers (MFCs) and the weighing balance. The MFC used for nitrogen and air are ordered from AalBorg Australia for the flow range of 1 to 5 litres per minute (LPM). The MFC used for ammonia is ordered from Sierra Instruments, Australia calibrated for the flow range of 0 – 30 ml/min. The ammonia MFC needed to be purged for 5 minutes by nitrogen gas before and after every time ammonia is passed through it. The SmartTrak 100 MFC ordered for ammonia measurement could also measure the flowrates of other gases such as air, nitrogen, oxygen and carbon dioxide. Figure 5.4 shows the MFCs used in the experimental study. Considering the sensitivity of ammonia in the reaction study, an

additional flow meter shown in Figure 5.5 ordered from John Morris Scientific, Australia calibrated for 0-30 ml/min NH₃ is mounted before the MFC.

Figure 5.6 shows the digital weighing balance used for measuring appropriate quantity of different metal oxides up to the second decimal point in grams. The two portable gas analyzers used in the experimental study are shown in Figure 5.7 with their maximum ranges of gases. The Testo 340 gas analyser calibrated for 3000 ppm NO with 95 % accuracy can be used to measure NO concentration of up to 10000 ppm. The Industrial Scientific's iBRID MX6 gas analyser calibrated upto 50 ppm for each gas with 98 % accuracy can be used to measure NO, H₂ and NH₃. Hence, for every experiment, the readings for NO are taken from Testo 340 whereas the readings for H₂ and NH₃ are noted from iBRID MX6. The calibration certificates are obtained from the suppliers every 3 months. Since these gas analyzers could not measure N₂O, the gas samples are collected in gas bags at appropriate intervals during the peak conversions and sent to the Greenhouse Gas Laboratory of Chemistry Department for N₂O analysis.



(a) Ammonia (0-30 ml/min)

(b) Air and Nitrogen (0-5 l/min)

Figure 5.4 Mass Flow Controllers for Ammonia, Air and Nitrogen



Figure 5.5 Ammonia flow meter
(0-30 ml/min)



Figure 5.6 Digital weighing balance
(0-50 g)



Gas	Range (ppm)
NO	0-10000
O ₂	0-100000
NO _x	0-10000

(a) Testo 340



Gas	Range (ppm)
NO	0-1000
O ₂	0-100000
NO ₂	0-1000
NH ₃	0-500
H ₂	0-1000

(b) iBRiD MX6

Figure 5.7 Gas analysers with specifications

5.5 Issues and Constraints

There existed some experimental issues which limited the number of experiments and might have resulted in inaccuracies in some of the readings. The gas analysers were calibrated to lower ranges of gases restricting the inlet ammonia concentration to nearly 1000 ppm in most of the experiments. The maximum error in the readings of gas analysers is expected to be about 2-5 %. The flowmeters and MFCs are assumed to remain calibrated for the duration of three months until the next calibration is done by the supplier servicemen. This would also add to nearly 1 % of discrepancy in the flowrates. The idea of having Reactor 4 with a

tapered hole and inclined distributor plate did not give the NO conversions as expected. This resulted in the need for manual tapping of the reactor portion outside the furnace so as to ensure continuous mixing. Though the conversions increased as expected in spouted fluidised mode, the product gas concentration profiles obtained are not smooth and continuous. It was also difficult to measure the exact change in weight of metal oxides as it was not always possible to remove the entire particles out of the reactor after each run. The error in weight change measurement is expected to be in the range of 0.1 to 0.2 g. The voids of the distributor plate were sometimes blocked and were difficult to be cleaned thereby restricting the fluidisation and hence the gas – solid mixing.

The next chapter presents the experimental results for different metal oxides selected from thermodynamic feasibility analysis, and a reaction mechanism based on the parametric study for the case of CuO.

CHAPTER 6

EXPERIMENTAL RESULTS AND DISCUSSION

The proposed chemical looping based process scheme produces NO and H₂ from the reaction of ammonia with metal oxide, and the reduced metal oxide is regenerated either by hydrolysis or by air oxidation. The regeneration steps of the proposed process scheme; hydrolysis (Steinfeld 2002; Charvin et al. 2007) and air oxidation (Zhu et al. 2002; Fontijn & Kurzius 1971) have been reported in the literature and hence, the present work is focussed on the reaction of ammonia with different metal oxides to produce NO and H₂. Chapter 4 reported the thermodynamic feasibility analysis for the proposed process and identified the potential metal oxides for experimental study. The set up, methodology and instrumentation required for the experimental investigation are discussed in Chapter 5. The series of experiments are performed for the most feasible metal oxides in a semi batch reactor. These experiments test the feasibility of the ammonia-metal oxide reaction for cupric oxide (CuO), ferric oxide (Fe₂O₃) and cobalt oxide (Co₃O₄) at 825 °C, 830 °C and 530 °C, respectively. The present chapter discusses the experimental results obtained for main reactor (Reactor 1) and proposes a reaction mechanism based on the experimental results. Based on the preliminary results and also the temperature constraints of the reactor furnace, CuO was selected for further detailed experimental study. The effect of varying the different parameters such as temperature, ammonia concentration, and particle size on the yield of nitric oxide is reported for the case of CuO and a reaction mechanism is proposed to explain these results. Finally the results of an additional set of experiments performed with modified reactor (Reactor 4) are also discussed.

6.1 Results

This section reports the experimental results obtained for reaction of different metal oxides and ammonia using main reactor (Reactor 1). Figure 6.1 shows the experimental results for different metal oxides confirming the feasibility of the proposed reaction. The measured product concentrations (ppm) of NO, H₂ and the reactant NH₃ are plotted for each second of the duration of the experiments, typically one to two hours until the NO product concentration had significantly declined. The ammonia is found to react with metal oxides:

and Co_3O_4 , Fe_2O_3 and CuO at $530\text{ }^\circ\text{C}$, $830\text{ }^\circ\text{C}$ and $825\text{ }^\circ\text{C}$ respectively with peak conversions to NO of 92 %, 86 % and 90 % respectively. These temperatures are broadly in agreement with the temperatures T_r in Table 4.1, which were $590\text{ }^\circ\text{C}$, $965\text{ }^\circ\text{C}$ and $760\text{ }^\circ\text{C}$ respectively, noting that the value of the H_2 to NO ratio x influences these temperatures. The particle size of metal oxides used in these experiments is in the range of 100 – 120 micron for CuO and Fe_2O_3 but 50 micron for Co_3O_4 .

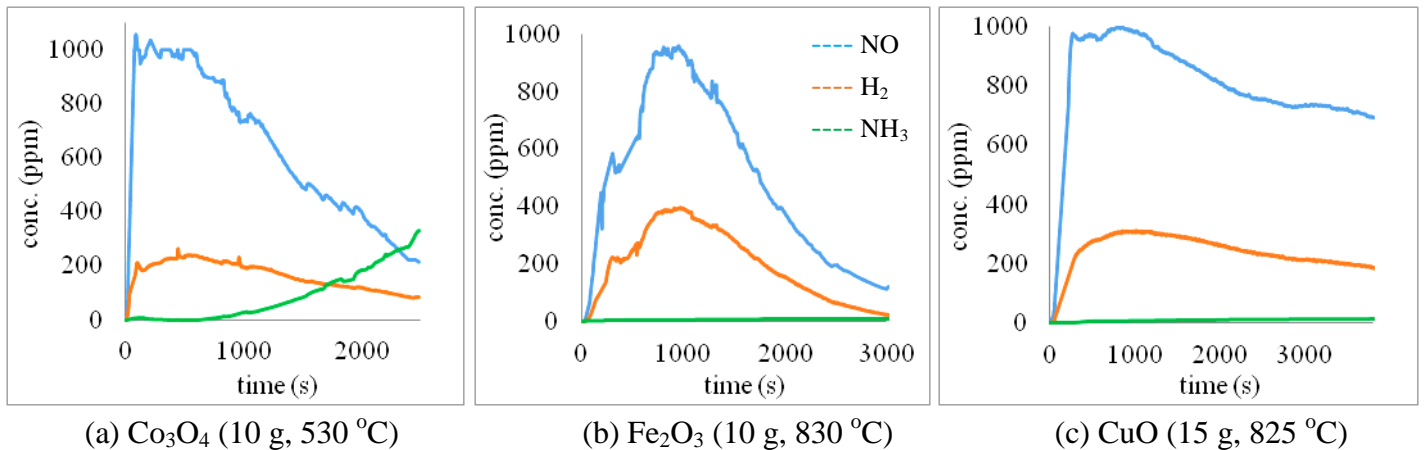


Figure 6.1 Preliminary experimental results for different metal oxides
(Operating conditions: 1100 ppm NH_3 (2.3 ml/min NH_3 and 2100 ml/min N_2))

Some important observations from the concentration profiles in Figure 6.1 are:-

- the rapid increase in the NO concentration to a maximum for CuO and Co_3O_4 , but the slower response in the case of Fe_2O_3
- an exponential decay in the NO concentration after the peak conversion is achieved
- early NH_3 breakthrough in the case of Co_3O_4 , but no breakthrough for CuO and Fe_2O_3 till an hour with slight indication only when the NO concentration has fallen to a low value after an hour
- x , the H_2 to NO ratio is between 0.2 and 0.4 for these experiments

In each run, a part of the metal oxides appeared in an agglomerated state after they were removed from the reactor. The agglomeration would restrict the availability of oxygen from metal oxide thereby leading to a decline in conversion with time. The peak conversions are obtained for about 20 minutes in case of each of the metal oxides. There are several factors affecting the conversion of NH_3 into NO such as temperature, concentration and flowrates of

feed gas, particle size of metal oxide, pressure, gas-solid contact, etc. which need to be addressed to understand the probable reaction mechanism. The effect of some of these factors (temperature, ammonia concentration, particle size) has been experimentally investigated for the case of CuO to explore the proposed reaction in more detail. CuO was chosen because of its lower optimum temperature and extended period of high conversion.

Figure 6.2 show the effect of different NH₃ feed concentrations at the optimum temperature of 825 °C. Note the duration of Figure 6.2(b) is much longer than the other experiments. The following observations can be made from this series of experiments:-

- the peak conversion is achieved within 500 s in all three cases
- the peak conversion (rather than concentration) reduces as the feed concentration of NH₃ is increased
- long durations are required before NH₃ breakthrough, despite the higher feed concentrations

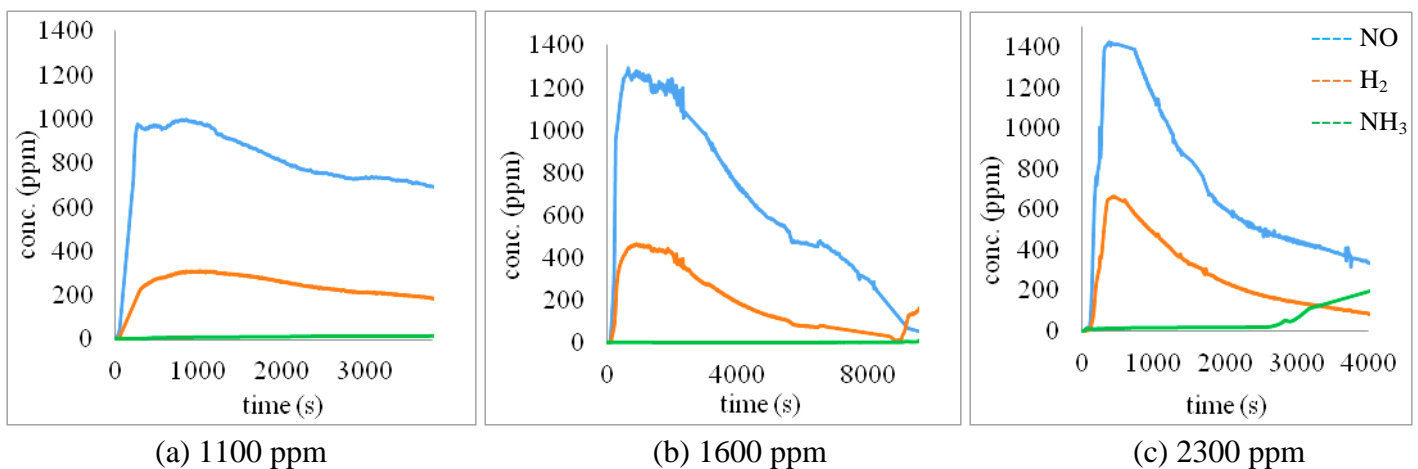


Figure 6.2 Effect of ammonia concentration

(Operating conditions: 15 g CuO (100-120 micron), 825 °C, 2100 ml/min N₂)

Figure 6.3 shows the effect of the reaction temperature for a higher feed concentration of 2300 ppm. The feed with higher concentration of ammonia is selected to study effect of temperature so as to observe breakthrough of ammonia within one hour of experiment. The experiments performed at 810 °C and 840 °C are reported in Appendix C. The following observations can be made from Figure 6.3:-

- the fast initial response appears to be independent of temperature

- after the peak, the decline in the NO concentration at the lowest temperature appears to be linear with time and is different to the higher temperature profiles
- the time when the NH₃ breakthrough occurs appears to be independent of temperature
- the maximum conversion appears to increase with increasing temperature only to a certain temperature beyond which conversion decreases

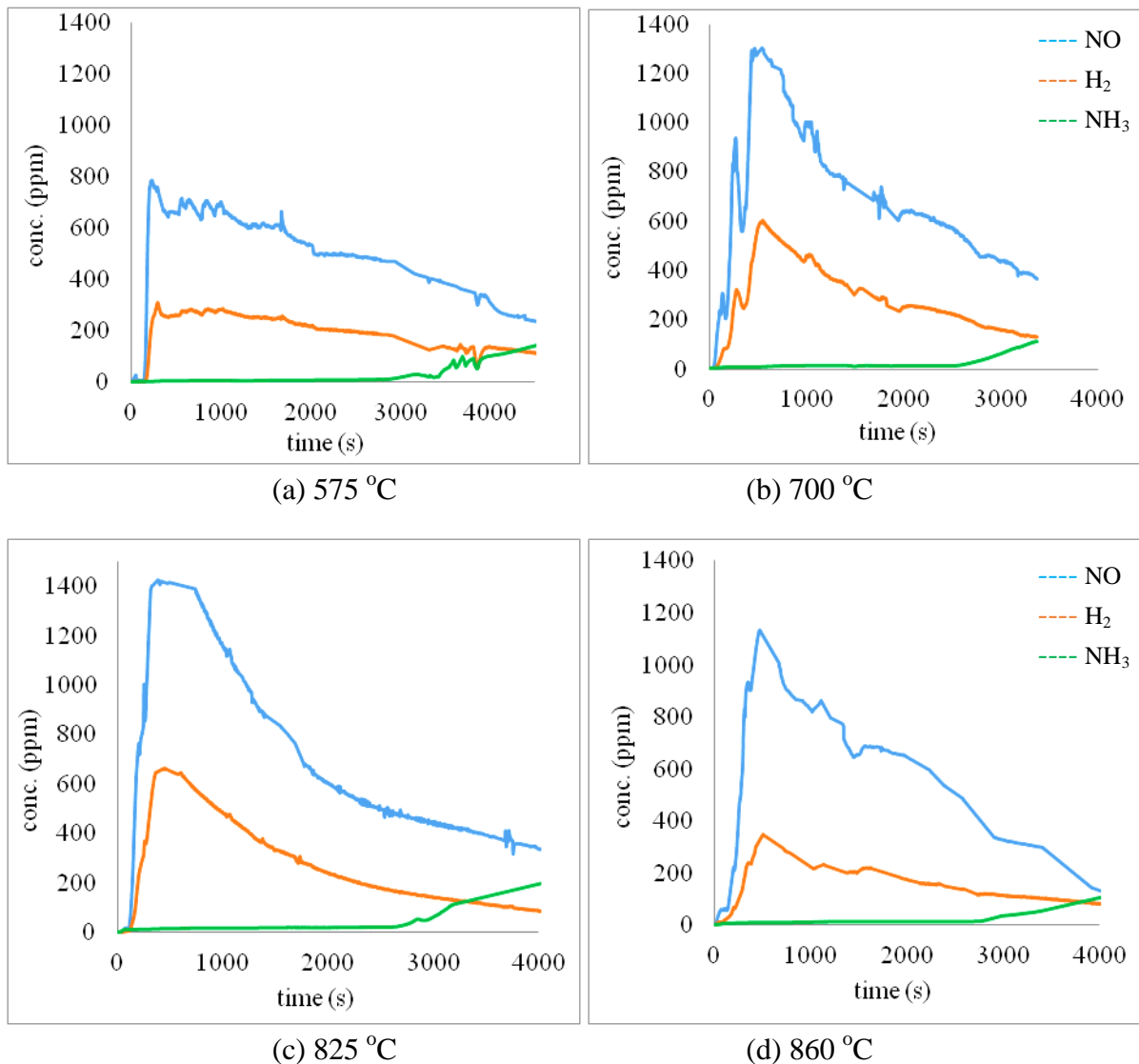
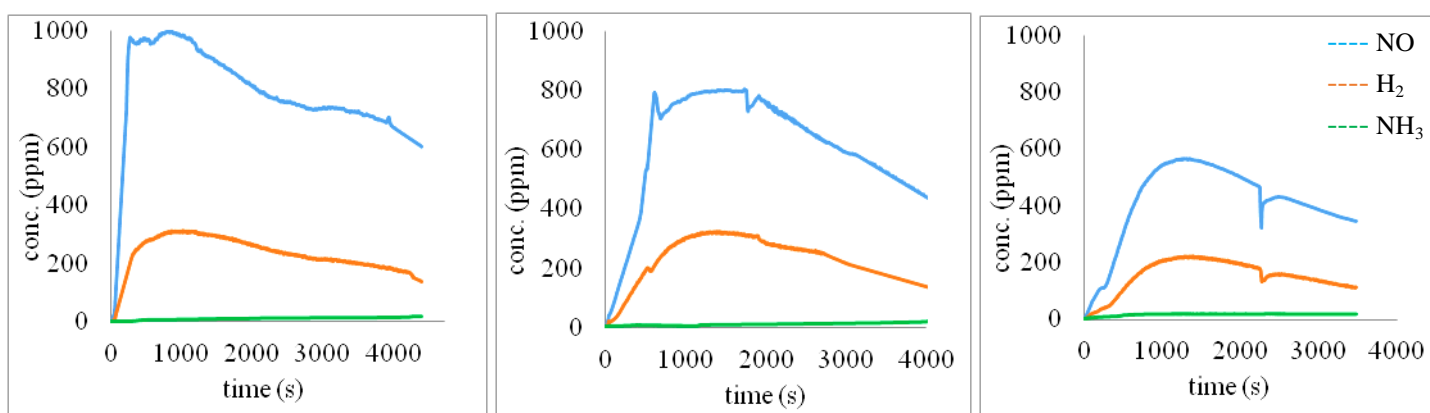


Figure 6.3 Effect of temperature (Operating conditions: 15 g CuO (100-120 micron), 2300 ppm NH₃ (4.8 ml/min NH₃ and 2100 ml/min N₂))

Figure 6.4 shows the influence of the copper oxide particle size on the reaction conversions at the optimum temperature and feed concentration and for the same mass of CuO. The particle size is determined in a range based on the particles collected between two particular mesh screens. The following observations are made:-

- the initial response is slower as the particle size is reduced
- the maximum conversion reduces as the particle size is reduced
- x (the ratio of H_2 to NO) increases as the particle size is reduced

When the copper oxide was inspected at the end of each experiment, a portion of it appeared in an agglomerated state. Agglomeration means that although the copper oxide may have been loaded with a particular particle size, this particle size probably increased during the experiment. In the following discussion section, an attempt will be made to separate the reaction hydrodynamics from a proposed underlying reaction mechanism.



(a) 100-120 micron (b) 40-60 micron (c) 1-10 micron
 Figure 6.4 Effect of particle size (Operating conditions: 15 g CuO, 825 °C, 1100 ppm NH₃ (2.3 ml/min NH₃ and 2100 ml/min N₂))

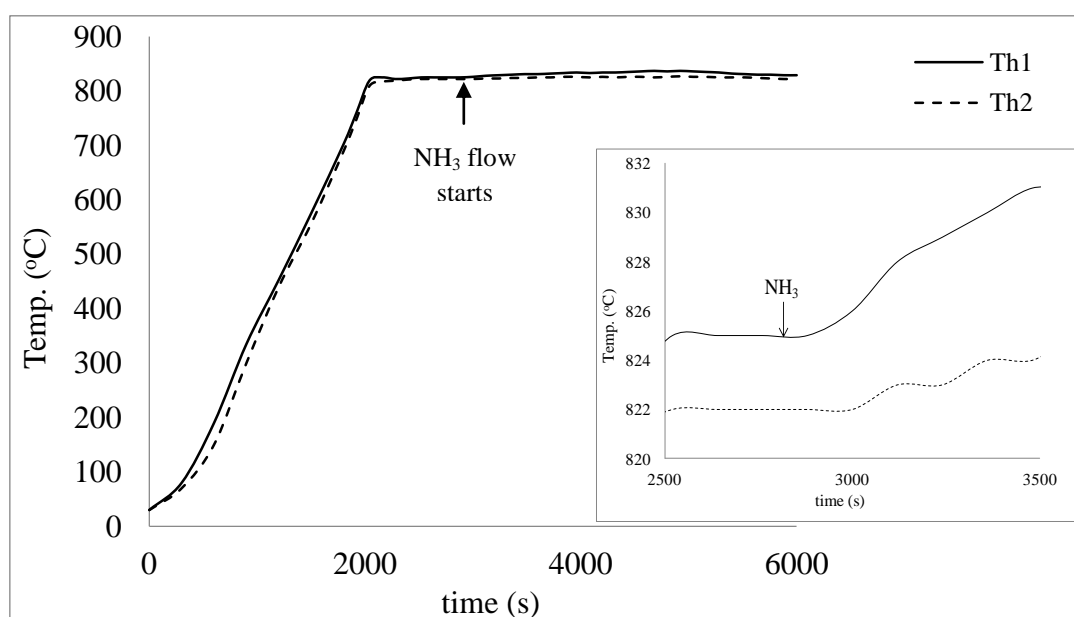


Figure 6.5 Temperature measurements (Operating conditions: 15 g CuO, 825 °C, 1100 ppm NH₃ (2.3 ml/min NH₃ and 2100 ml/min N₂))

Figure 6.5 shows the variation in temperatures recorded by two thermocouples, Th1 dipped in metal oxide powder and Th2 placed in the centre of the fluidising zone. The furnace temperature is set at 825 °C and NH₃ flow is started when the steady set temperature is attained. At steady state, Th1 read 827 °C and Th2 read 823 °C for set furnace temperature of 825 °C. As soon as NH₃ flow starts, both the thermocouples measured slightly higher temperatures proving the existence of some exothermic reactions occurring inside the reactor.

6.2 Discussion

Heterogeneous reactions are characterised by surface adsorption and diffusion limited steps. The reduction reaction of CuO is reported to be auto-catalytic and takes place at the copper-copper oxide interface where copper acts as a catalyst (Wang & Yeh 1983). Under heat treatment CuO easily loses part of oxygen in the lattice to form the paramelaconites CuO_{1-α}, in particular, Cu₄O₃ which is a mixed oxide (Cu₂O.2CuO) crystal with body-centered tetragonal lattice containing both Cu^I and Cu^{II} ions (Evarestov & Veryazov 1990). From the equilibrium composition calculations using HSC (Outotec 2015) for CuO-O₂ system, it was found that CuO starts to lose its oxygen at temperatures above 600 °C, as shown in Figure 6.6. The liberation of oxygen could be expected to occur at lower temperatures in reducing atmospheres, such as Figure 6.3(a) at 575 °C. 15 g of metal oxide with average particle size of 110 micron on the distributor plate with 4 cm diameter is enough to cover the entire cross-section area through which the feed gas entered the reactor. The 10 cm long enclosed cylindrical chamber between the two distributor plates provides sufficient area for fluidising particles to mix with gas efficiently. During the peak conversions, almost entire ammonia appears to get converted to NO and H₂. The yield of NO and H₂ drops down gradually with time but NH₃ still seem to get adsorbed on CuO and react to form different species. For fixed batch of CuO and continuously entering NH₃, the decrease in conversion can be owed to the decrease in the activity of metal oxide due to depletion of lattice oxygen from its surface.

The short incubation period in most of the experiments before formation of NO can be attributed to the activation of metal oxide adsorption sites and the formation of copper nuclei that would act as catalyst for further reaction. The studies on catalytic oxidation of ammonia by oxides such as MnO₂, Co₃O₄, CuO and Fe₂O₃ report N₂ to be the predominant product at low temperatures and NO as dominant product at higher temperatures (Amores et al. 1997).

Adsorption of NH_3 onto the surface is expected to be relatively fast based on van der Waals attraction between the ammonia and the polar MO surface (Skúlason et al. 2012). Based on the theory of complex formation, adsorption of a species on transition metal oxides increases the coordination number (number of atoms or ligands directly bonded to the metal atom) whereas desorption reduces it (Kiselev & Krylov 1989). Dowden and Wells (1961) proposed the chemisorption of molecules on cations (transition metals) to be accompanied by the exothermic effect of crystal-field stabilization. The major factors that need to be considered in explaining the catalytic activity and heat of adsorption (Q) are the electron transitions, the polarizing action of the cation, and the crystal field stabilising energy (CFSE) (Kiselev & Krylov 1989). However, these factors are not studied in the scope of the present work and would be dealt with in future detailed experimental investigations.

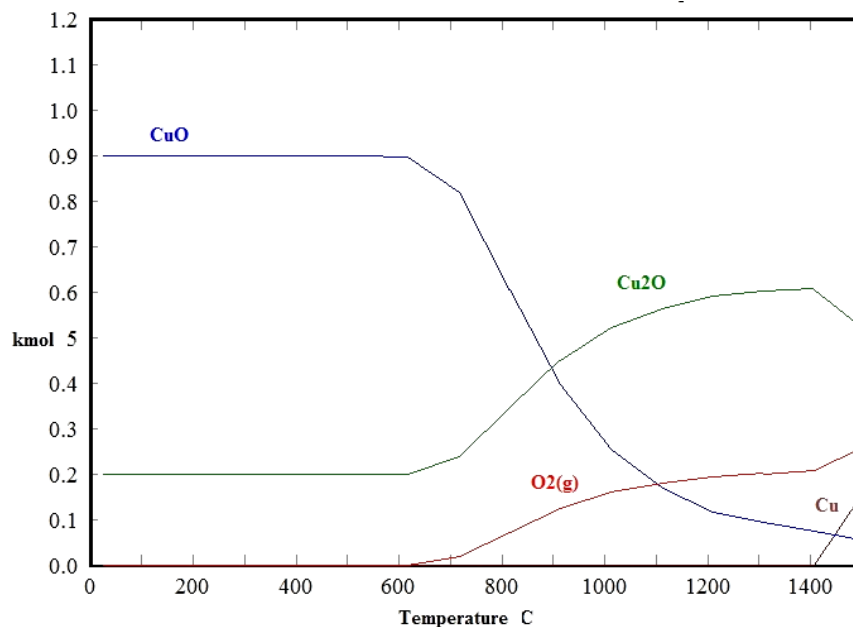


Figure 6.6 HSC results for equilibrium composition of oxides of copper
(Feed parameters: 1 kmol CuO, 0.1 kmol Cu₂O, 0.1 kmol Cu, 1000 kmol N₂)

In the present study, it is postulated that ammonia would adsorb on the metal oxide surface, and react with the oxygen available from the lattice of the metal oxide, before desorption of the product gases from the surface. The adsorption – desorption rates need not be the same and gas-metal oxide complexes would form. Figure 6.7 shows the proposed mechanism for the reaction of ammonia and CuO, where NH_3 is first adsorbed on the surface of CuO and Cu₂O and then reacts with lattice oxygen to form intermediate complex species that later desorbs into products such as NO, N₂, H₂ and H₂O. Kosaki et al. (1982) reported a similar

mechanism for the reaction of NH_3 with metal oxide-Pt/ Al_2O_3 . NH_3 adsorbs on the metal oxide forming ammonia-metal oxide complex releasing some heat in the process. This is facilitated by the presence of a lone pair of electrons on the nitrogen atom of NH_3 . The presence of lattice oxygen enables the reaction to form NO , but if oxygen is not available, the arrival of a second NH_3 molecule allows the formation of N_2 .

The balanced equations for possible reactions taking place in the reactor are written as follows:

Adsorption

- (a) $\text{CuO}_{(s)} + \text{NH}_{3(g)} \rightarrow [(\text{CuO}).\text{NH}_3] + Q_a$
 (b) $\text{Cu}_2\text{O}_{(s)} + \text{NH}_{3(g)} \rightarrow [(\text{Cu}_2\text{O}).\text{NH}_3] + Q_b$
 (c) $\text{Cu}_{(s)} + \text{NH}_{3(g)} \rightarrow [\text{Cu}.\text{NH}_3] + Q_c$

Desorption

- (d1) $[(\text{CuO})_{18}.\text{NH}_3]_4 + Q_{d1} \rightarrow 9 \text{Cu}_2\text{O}_{(s)} + 4 \text{NO}_{(g)} + \text{H}_{2(g)} + 5 \text{H}_2\text{O}_{(g)}$
 (d2) $[(\text{CuO})_{18}.\text{NH}_3]_4 + 2 \text{NH}_3 \rightarrow 9 \text{Cu}_2\text{O}_{(s)} + 3 \text{N}_{2(g)} + 9 \text{H}_2\text{O}_{(g)} + Q_{d2}$
 (e1) $[(\text{Cu}_2\text{O})_9.\text{NH}_3]_4 + Q_{e1} \rightarrow 18 \text{Cu}_{(s)} + 4 \text{NO}_{(g)} + \text{H}_{2(g)} + 5 \text{H}_2\text{O}_{(g)}$
 (e2) $[(\text{Cu}_2\text{O})_9.\text{NH}_3]_4 + 2 \text{NH}_3 \rightarrow 18 \text{Cu}_{(s)} + 3 \text{N}_{2(g)} + 9 \text{H}_2\text{O}_{(g)} + Q_{e2}$

Additional Reaction

- (f) $1.5 \text{NO}_{(g)} + \text{NH}_{3(g)} \rightarrow 1.25 \text{N}_{2(g)} + 1.5 \text{H}_2\text{O}_{(g)} + Q_f$

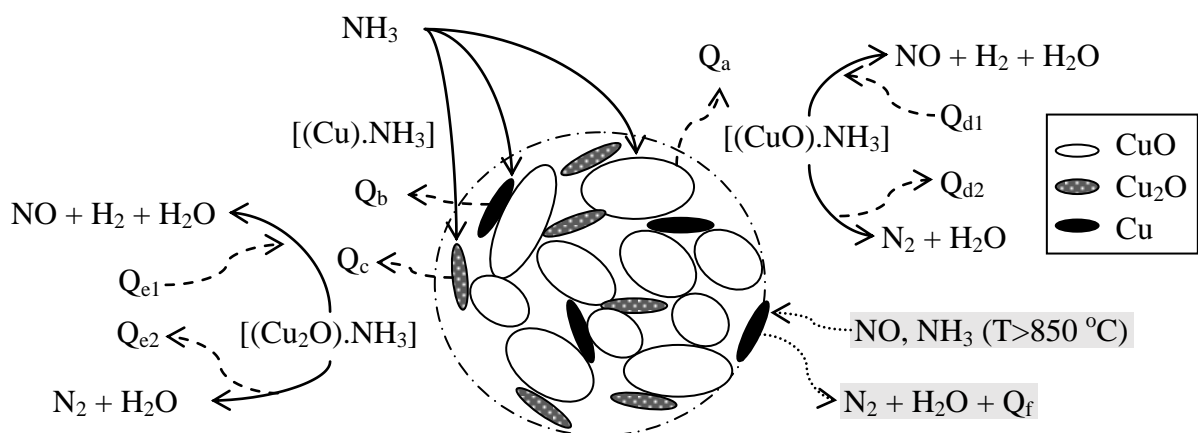


Figure 6.7 Proposed reaction mechanism for ammonia and CuO

Table 6.1 gives the HSC Chemistry results for desorption reactions at 25 °C and 825 °C. The temperature of 825 °C is selected based on the experimental results obtained for the case of CuO. The exothermic nature of reactions d2, e2 and f justifies the temperature rise by 10 to 20 °C observed during experiments inside the reactor. The N₂ forming desorption steps (d2 or e2) are both spontaneous above room temperatures and their exothermicity and spontaneity increase with increasing temperature. For the reaction f between NO and NH₃, its spontaneity and exothermicity both stays almost constant over a wide range of temperature. Although the reaction of NO and NH₃ is thermodynamically spontaneous over a wide range of temperatures, it is kinetically inhibited. This reaction has been studied extensively where NH₃ is used as a reagent to reduce NO_x emissions (Chmielarz et al. 2005; Zhao et al. 2008). The catalytic process operates over a wide range of temperatures from as low as 100 °C. However, the non-catalytic process requires temperatures above 900 °C (Duo et al. 1992). This may in fact set the temperature limit for CuO. Given that any of the surface reactions can happen simultaneously at different reaction sites, this explains why the temperature inside the reactor is maintained at 825 °C, and in some cases increases as the experiment progresses. The temperature measurements reported in Figure 6.5 supports the possibility of exothermic desorption reactions d2 and e2 forming N₂ and H₂O.

Table 6.1 HSC Chemistry results for desorption and additional reactions

No.	Reaction Set	T _o		T _r (°C)	T _r		T = 825 °C	
		ΔH _o (kJ)	ΔG _o (kJ)		ΔH (kJ)	ΔG (kJ)	ΔH (kJ)	ΔG (kJ)
d1	4.5 CuO _(s) + NH _{3(g)} → 2.25 Cu ₂ O _(s) + NO _(g) + 0.25 H _{2(g)} + 1.25 H ₂ O _(g)	162	72	445	153	-50	143	-157
d2	3 CuO _(s) + NH _{3(g)} → 1.5 Cu ₂ O _(s) + 0.5 N _{2(g)} + 1.5 H ₂ O _(g)	-97	-156	--	--	--	-111	-305
e1	2.25 Cu ₂ O _(s) + NH _{3(g)} → 4.5 Cu _(s) + NO _(g) + 0.25 H _{2(g)} + 1.25 H ₂ O _(g)	213	145	890	205	-50	206	-36
e2	1.5 Cu ₂ O _(s) + NH _{3(g)} → 3 Cu _(s) + 0.5 N _{2(g)} + 1.5 H ₂ O _(g)	-63	-107	--	--	--	-69	-224
f	1.5 NO _(g) + NH _{3(g)} → 1.25 N _{2(g)} + 1.5 H ₂ O _(g)	-452	-456	--	--	--	-452	-468

The fact that there is no rise in the concentration of H₂ after the decrease in NO yield indicates that the dissociation of NH₃ is not occurring to any significant extent. The profiles reported in Figure 6.8 show the H₂/NO ratio for different metal oxide cases of their highest

conversion experiments. The ratio H_2/NO appears to reach maximum at peak conversions following which it gradually decreases and stays constant for a considerable period of time as the metal oxide is getting consumed. Figure 6.7 shows the proposed mechanism where the steps d1 and d2 (or e1 and e2) are assumed to occur simultaneously at different reaction sites. Therefore, at 825 °C providing there is lattice oxygen available, then desorption pathways d1 and e1 are the most favourable, but if the oxygen is not available, then the desorption pathways of d2 and e2 occur. d2 and e2 being second order with respect to NH_3 , are more limited kinetically than d1 and e1, but as shown in Table 6.2 are favoured thermodynamically. It is necessary to consider the proposed mechanism in the light of the experimental results presented in Figures 6.2-6.4.

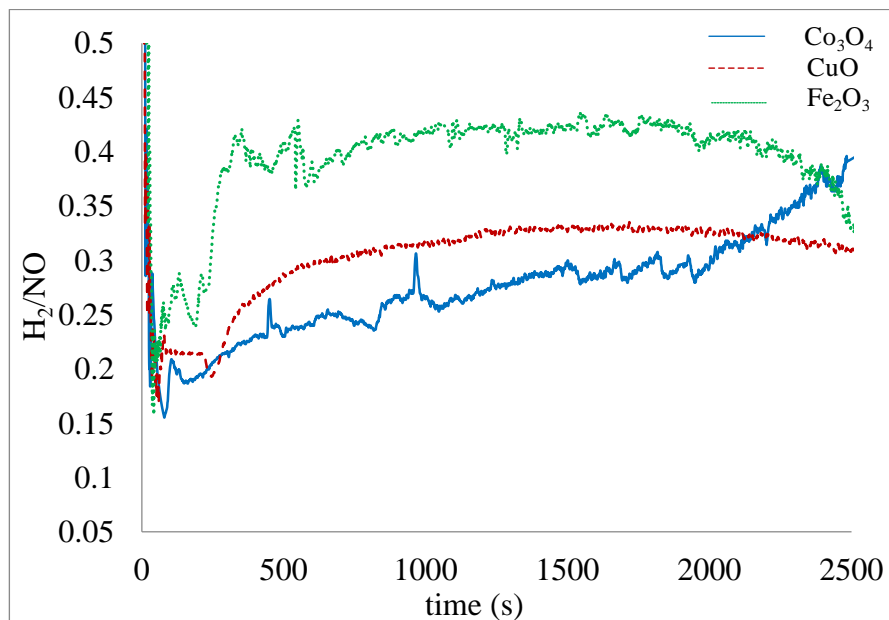


Figure 6.8 H_2/NO for different metal oxides

Figure 6.2 shows decreasing conversion to NO on increasing NH_3 feed. This can be explained by the increased desorption rate for the N_2 forming steps, d2 and e2 on increasing NH_3 concentration, whereas desorption steps d1 and e1 are dependent on the supply of heat Q_{d1} and Q_{e1} , but independent of NH_3 . Initially this energy can come from within the particle itself, but after an initial high conversion period, the energy is likely to be supplied by reactions d2 and e2 or by radiation from the furnace walls. In addition, the availability of the metal oxide surface for ammonia adsorption would decrease with increasing NH_3 concentration with other operating parameters remaining unchanged.

Figure 6.3 shows increasing conversion to NO with increasing reaction temperature. Again this is consistent with the competition between desorption steps, d1 and d2 and e1 and e2. As the temperature is increased, reactions d1 and e1 become increasingly spontaneous and thermodynamically favoured as oxygen is able to be more easily liberated from the metal oxide lattice. Also their endothermic heats of reactions reduce in magnitude and therefore the reaction temperatures can be sustained for longer time without being supplemented by the energy from the N₂ forming steps or from radiation (where the radiative flux is proportional to temperature to the fourth power). The N₂ forming desorption steps are less dependent on temperature and therefore compete more strongly at lower temperatures. As reported in literature on NH₃ oxidation (Il'chenko 1976), formation of NO is favoured at higher temperatures (above 400 °C), and N₂O and N₂ at lower temperatures (below 400 °C).

Figure 6.4 shows that larger particles are preferred to smaller ones. This result is counter intuitive as the smaller particles would have a much larger reaction surface area and would be expected to react more quickly and probably provide the greatest conversion. In fact, quite the opposite occurs and the fastest reaction and best conversion is achieved by the large particles. The smaller CuO particles tend to agglomerate faster at high temperatures than larger particles (Sullivan et al. 2012) thereby reducing the sites for adsorption of ammonia and hence the conversion. In addition, considering the design of reactor used in experiments, the smaller particles may block the distributor plate voids obstructing the gas-solid mixing. An experiment was performed for 200 micron particle size and it was found that the conversion actually dropped. This suggests the need to find an optimum particle size for high conversions. The agglomerated particles often formed bigger lumps and cakes thereby limiting the amount of metal oxide available for reaction with ammonia. Often it has been observed that the lump of CuO which appeared reddish brown on the surface had black CuO within. The same behaviour has been observed in case of Co₃O₄ and Fe₂O₃. This limited the characterisation study of the metal oxide particles.

6.2.1 N₂O formation

Considering the impact of greenhouse gas emissions in conventional nitric acid plant, it is important to check for N₂O emissions, if any, in the proposed process. The previous sections reported the feasibility of the reaction between ammonia and metal oxide to form NO and H₂

with more detailed results for the case of CuO. Table 6.2 shows the possible reactions between ammonia and copper oxide forming N₂ and N₂O.

Table 6.2 Possible reactions between ammonia and copper oxide forming N₂O

No.	Reaction	ΔH_0 (kJ)	ΔG_0 (kJ)	T_e (°C)	T_r (°C)	ΔH_r (kJ)	ΔG (kJ)
1.	$4 \text{ CuO}_{(s)} + 2 \text{ NH}_{3(g)} \rightarrow 4 \text{ Cu}_{(s)} + \text{ N}_2\text{O}_{(g)} + 3 \text{ H}_2\text{O}_{(g)}$	77.2	-30.83	-	825	53.07	-306.7
2.	$3 \text{ CuO}_{(s)} + 2 \text{ NH}_{3(g)} \rightarrow 3 \text{ Cu}_{(s)} + \text{ N}_{2(g)} + 3 \text{ H}_2\text{O}_{(g)}$	-161.6	-264.1	-	825	-181.3	-529.3
3.	$8 \text{ CuO}_{(s)} + 2 \text{ NH}_{3(g)} \rightarrow 4 \text{ Cu}_2\text{O}_{(s)} + \text{ N}_2\text{O}_{(g)} + 3 \text{ H}_2\text{O}_{(g)}$	32.0	-95.88	-	825	-3.1	-414.7
4.	$6 \text{ CuO}_{(s)} + 2 \text{ NH}_{3(g)} \rightarrow 3 \text{ Cu}_2\text{O}_{(s)} + \text{ N}_{2(g)} + 3 \text{ H}_2\text{O}_{(g)}$	-195.5	-312.9	-	825	-223.5	-610.3
5.	$5 \text{ CuO}_{(s)} + 2 \text{ NH}_{3(g)} \rightarrow 3 \text{ Cu}_{(s)} + \text{ Cu}_2\text{O}_{(s)} + \text{ N}_2\text{O}_{(g)} + 3 \text{ H}_2\text{O}_{(g)}$	65.97	-47.09	-	825	39.03	-333.7
6.	$4 \text{ CuO}_{(s)} + 2 \text{ NH}_{3(g)} \rightarrow 2 \text{ Cu}_{(s)} + \text{ Cu}_2\text{O}_{(s)} + \text{ N}_{2(g)} + 3 \text{ H}_2\text{O}_{(g)}$	-172.9	-280.4	-	825	-195.4	-556.3

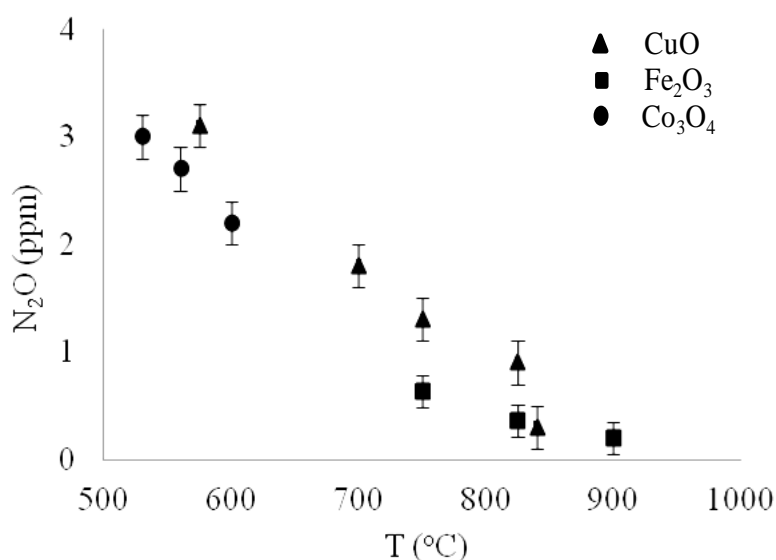


Figure 6.9 N₂O analysis results for Co₃O₄, CuO and Fe₂O₃

Reactions 1, 3 and 5 are the possible reactions that would lead to the formation of N₂O and H₂O, and Reactions 2, 4 and 6 would result in formation of N₂ and H₂O. The reactions forming N₂ are more spontaneous than those forming N₂O. The N₂ forming reactions are exothermic and the N₂O forming reactions are endothermic. The slight higher temperature obtained inside the reactor can be attributed to the exothermic nature of side reaction forming

N₂. In addition, the experimental results confirm that there is hardly any N₂O formation in the system for any of the metal oxides. Figure 6.9 represent the results for N₂O analysis of the samples collected during peak NO conversions for different metal oxides. Formation of N₂O is favoured at lower temperatures and hence Co₃O₄ results show the highest *i.e.* 3 ppm N₂O for 1100 ppm feed NH₃ whereas CuO and Fe₂O₃ cases have nearly 1 ppm N₂O for the same NH₃ feed.

The sharp rise in the NO and H₂ yield at the onset of experimental readings justifies the presence of activated metal oxide in each case. The change in the amount of metal oxide for highest NO conversion experiments is calculated to be around 0.9 g, 0.8 g and 1.0 g for Co₃O₄, Fe₂O₃ and CuO respectively (Table 6.3). The total NO formed in each case is calculated from area under the curve up to 2500 s. The measurements are expected to be within the error range of about 10-20 % as there is a possibility of some metal oxide getting reoxidised by ambient air during reactor cooling or during the removal from the reactor. Table 6.3 indicates that nearly 29.5 %, 32.5 % and 41.3 % of depleted oxygen has contributed towards the formation of NO and H₂O by reactions d1 & e1 in case of Co₃O₄, Fe₂O₃ and CuO respectively. If the NH₃ which is not consumed to form NO is used by desorption steps d2 and e2, then the total O₂ depletion percentage would be 51.6, 56.9 and 68.9 % respectively for Co₃O₄, Fe₂O₃ and CuO. This provides further evidence that the reaction steps d2 and e2 are also important and consume a significant portion of the lattice oxygen. Based on proposed reaction mechanism, it is expected that the remaining oxygen stays in the intermediate complex which could not decompose to form gaseous products.

Table 6.3 Calculations for change in weight of metal oxides

Metal oxide	Experiment time (s)	Change in weight (g)	Total NO (ppm)	% of depleted O ₂ towards NO & H ₂ O		Total depleted O ₂ (%)
				d1&e1	d2&e2	
Co ₃ O ₄	2500	0.9±0.1	1500000	29.5	22.1	51.6
Fe ₂ O ₃	2500	0.8±0.2	1470000	32.5	24.4	56.9
CuO	2500	1.0±0.2	2075000	41.3	27.5	68.9

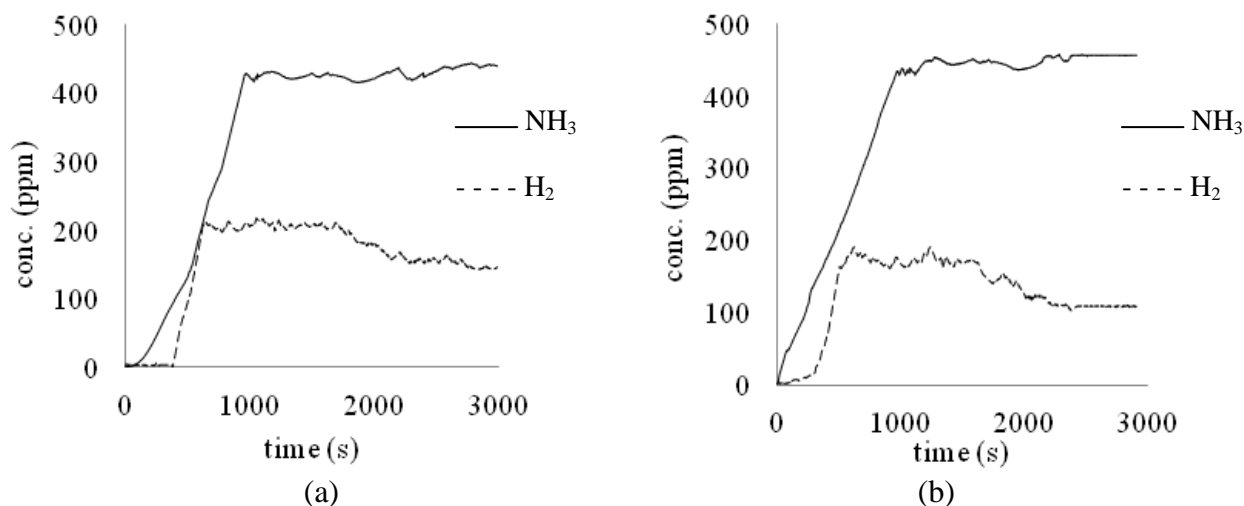


Figure 6.10 Experimental results for decomposition of NH₃ (a) Al₂O₃: 1 ml/min NH₃, 2 l/min N₂, T = 825 °C (b) Empty Reactor: 1 ml/min NH₃, 2 l/min N₂, T = 825 °C

Figure 6.10 shows the results for decomposition of NH₃ into N₂ and H₂ in presence of inert metal oxide Al₂O₃ and in a reactor with no metal oxide at 825 °C. The decomposition of NH₃ obtained without any metal oxide at 825 °C was about 8 to 9 % which is in agreement with the results reported in the literature (White & Melville 1888). For Al₂O₃, the percentage varied from 9 to 11 % which indicates the slight catalytic effect of the metal oxide. In addition, there is no significant increase in the NH₃ concentration when the NO concentration starts declining. Based on the N₂O measurements, the possibility of side reaction forming N₂O is negligible. The desorption reactions forming either NO or N₂ seem to be the most likely competing reactions, where the latter decreases the NO conversion. The other studies also confirm the reaction between NH₃ and NO forming N₂ and/or N₂O as part of the reaction of activated metal oxide with NH₃ (Kosaki et al. 1979; 1982).

6.3 Experiments with Reactor 4

The gas-solid reactions involving metal oxides at high temperatures in fluidised reactor often encounter problems such as agglomeration and sintering. These problems related to aggregation of metal oxide particles can be resolved by vibrating the reactor (Wank et al. 2004), using sound waves (Zhu et al. 2004), or by micro nozzles (Quevedo et al. 2010). Hence, an additional set of experiments were performed using a modified reactor (Reactor 4) with tapered hole sloping towards the centre of bottom distributor plate. The reactor was subjected to shaking and vibration using rubber hammer at equal intervals of time to avoid

agglomeration of metal oxide particles. Figure 5.2(c) in Chapter 5 shows the effect of tapping the Reactor 4 at room temperature for 15 g Fe_2O_3 and 2100 ml/min of N_2 flowrate. When tapped, the fixed bed of particles is transformed to spouted bed for a period of time and then settles down allowing almost entire gas to flow through the hole in distributor plate. The tapping at regular interval ensures that the gas solid mixing is continuous and efficient. The series of experiments similar to Reactor 1 are performed with different metal oxides using Reactor 4. The trend of the results obtained in these additional experiments is similar to that in earlier experiments. However, the fluctuations are visible in the measurements because of the manual tapping of the reactor.

6.3.1 Results and Discussion

The results reported in Figure 6.11 for highest obtained NH_3 to NO conversions for four different metal oxides confirms the possibility of reaction of NH_3 with different metal oxides at suitable operating conditions. The ammonia is found to react with metal oxides Co_3O_4 , CuO , Fe_2O_3 , and Mn_3O_4 at 530 °C, 825 °C, 830 °C, and 900 °C and giving about 97 %, 78 %, 80 %, and 56 % conversion to NO respectively. There is no rise in the concentration of H_2 after decrease in NO conversion implying that the dissociation of NH_3 is not to a significant extent in a short residence time of 0.4 s. This indicates that the metal oxide is the limiting species which must interact with gases efficiently so as to react to a maximum extent. This suggests the importance of the hydrodynamics of the reactor and hence emphasizes the need for entrained flow reactor for such solid gas reactions. The particle size of metal oxides used in these experiments is in the range of 100 – 120 micron for CuO , Fe_2O_3 and Mn_3O_4 but 50 micron for Co_3O_4 . It was difficult to obtain larger particle size for Co_3O_4 due to its sintering at much lower temperatures compared to other metal oxides. Co_3O_4 in powdered form appeared to be moist and softer than other metal oxides. During experiment, it was observed that Co_3O_4 powder forms granules of about 0.5 mm diameter. This formation of granules and the difference in particle size might be the reason for lesser effect of tapping in case of Co_3O_4 . The gas samples are collected for N_2O analysis during the period of maximum conversion to NO in each of the metal oxide cases. The gas chromatograph results report that the maximum amount of N_2O formed in case of best NO conversions obtained for Fe_2O_3 , Co_3O_4 , Mn_3O_4 and CuO are 0.3, 3.1, 0.3, and 0.6 ppm respectively. The effect of various parameters such as temperature, NH_3 concentration, fixed and spouted bed, and particle size

on the yield of NO is also studied with respect to three different metal oxides, viz. Co_3O_4 , Fe_2O_3 and CuO .

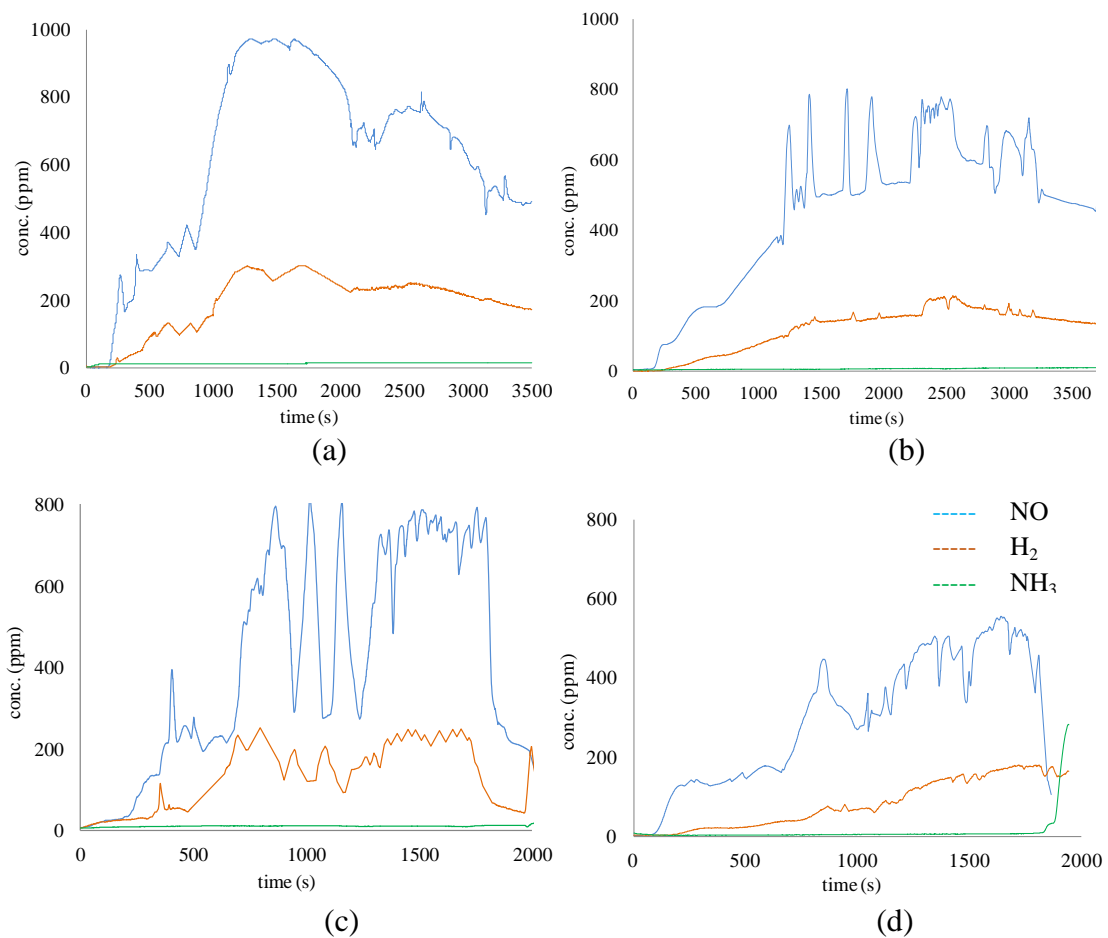


Figure 6.11 Highest NO conversion results (Reactor 2) (a) Co_3O_4 (b) CuO (c) Fe_2O_3 (d) Mn_3O_4 (Operating conditions: 1000 ppm NH_3 (2.1 ml/min NH_3 and 2100 ml/min N_2))

Figure 6.12(a) and (b) represents the experimental results obtained for Co_3O_4 along with the major operating conditions in caption. The conversion to NO increased with the increase in temperature from 515 °C to 530 °C but then started decreasing with further rise in temperature thus implying 530 °C as the most desired operating temperature (Figure 6.12(a)). The temperature check experiments are performed for Co_3O_4 between 450 °C to 650 °C, however, the NH_3 to NO conversion vary by about 20 % between the temperatures of 500 °C – 560 °C as shown in Figure 6.12. The conversion to NO increased from 35 % at 515 °C to 55 % at 530 °C and then decreased gradually to 40 % at 560 °C. For fixed amount of Co_3O_4 the NO yield decreased with the increase in concentration of NH_3 going in the feed (Figure 6.12(b)).

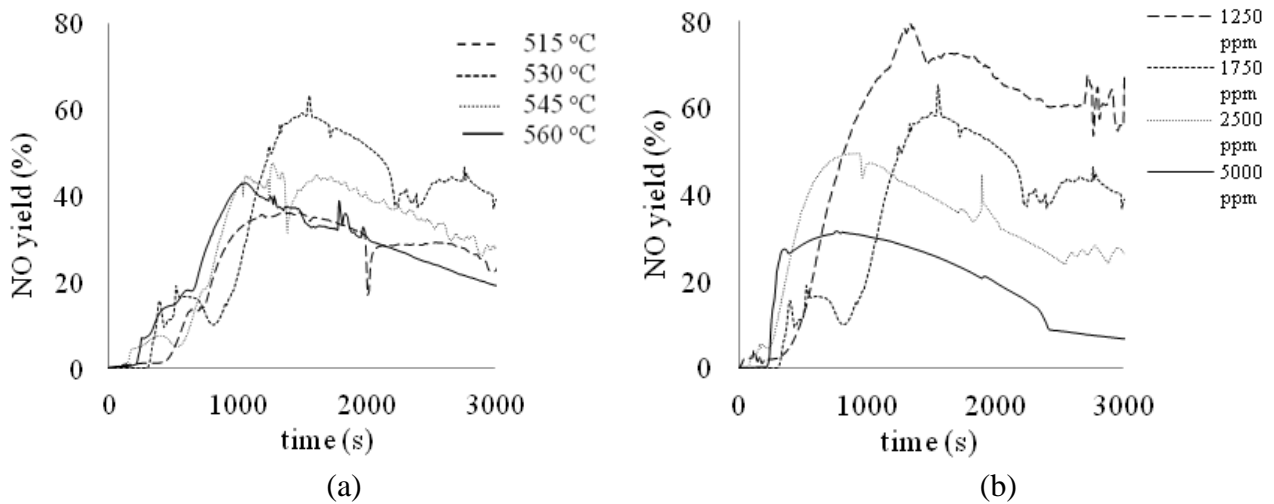


Figure 6.12 Experimental results for Co₃O₄ (a) Effect of temperature on NO yield: 3.5 ml/min NH₃, 2100 ml/min N₂ (b) Effect of NH₃ concentration on NO yield: 2100 ml/min N₂, T = 530 °C

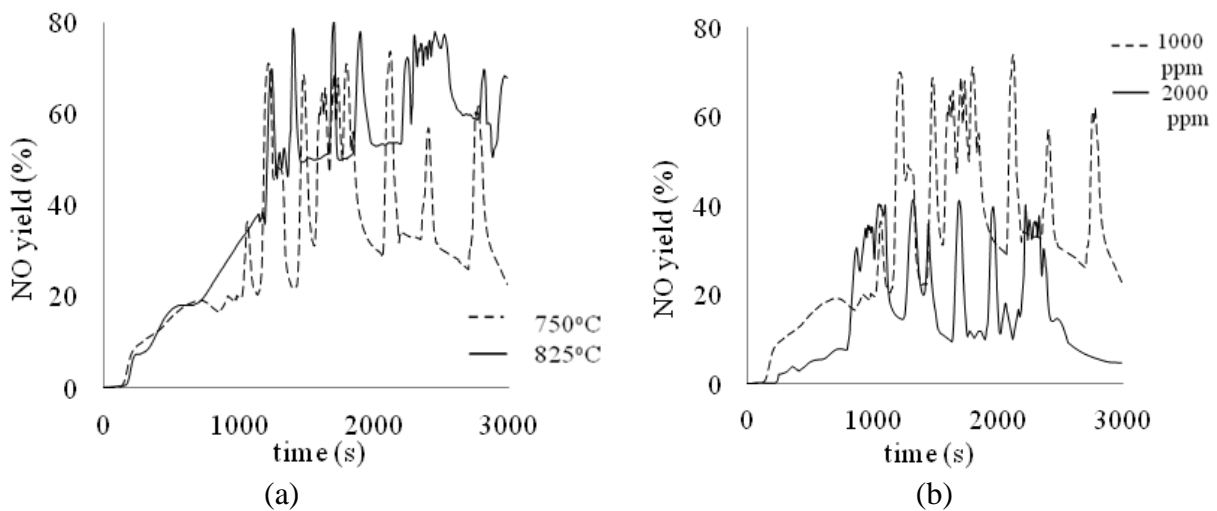


Figure 6.13 Experimental results for CuO (a) Effect of temperature on NO yield: 2.100 ml/min NH₃, 2100 ml/min N₂ (b) Effect of NH₃ concentration on NO yield: 2100 ml/min N₂, T = 750 °C

Figure 6.13(a) represents the effect of temperature on NO yield for CuO and though the highest conversion is obtained at 825 °C, there is not a significant difference in the yield of NO from 750 °C to 825 °C and hence the further experiments for CuO are performed at 750 °C. From Figure 6.13 (b) it is seen that the NO yield dropped down from 80 % to 40 % when the NH₃ concentration is increased from 1000 ppm to 2000 ppm for same quantity of metal oxide.

Figure 6.14(a) represents the effect of temperature on NO yield for Fe₂O₃ and the NO yield appeared to increase from 800 °C to 825 °C but then decreased from 850 °C to 950 °C thereby giving highest conversion at 825 °C. Figure 6.14(b) shows that the NO yield

dropped down from 80 % to 30 % when the NH_3 concentration is increased from 1000 ppm to 4000 ppm for same quantity of Fe_2O_3 .

Figure 6.15(a) and (b) represents the effect of particle size on NO yield in case of CuO and Fe_2O_3 respectively. In case of CuO, the NO yield increased slightly with the increase in particle size whereas in case of Fe_2O_3 , the NO yield increased by 10 % with the increase in particle size. The explanation for each of these observations is already given in Section 6.2 of this chapter.

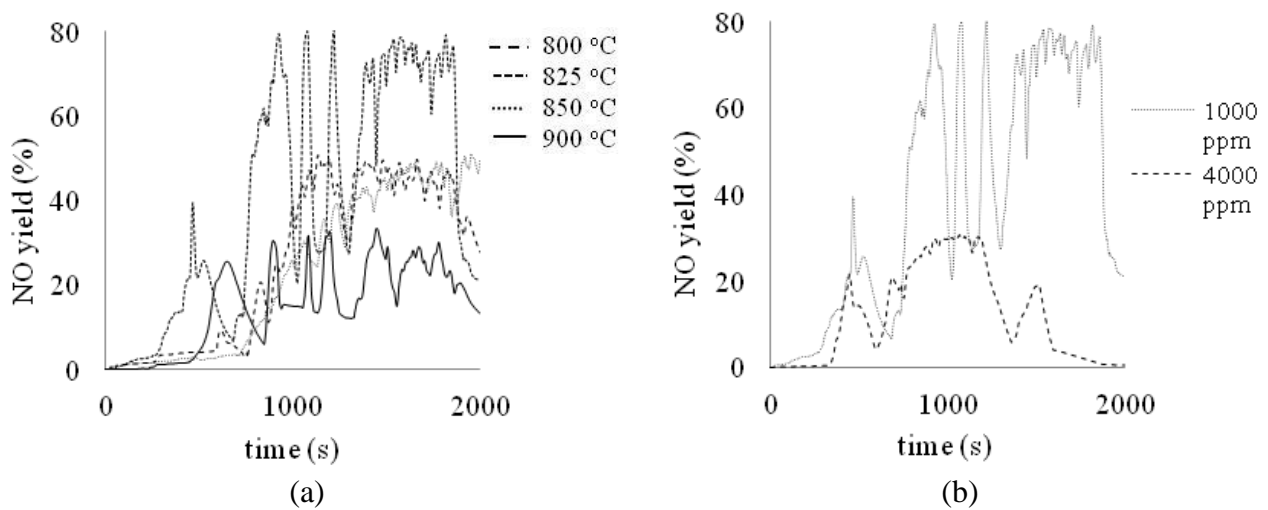


Figure 6.14 Experimental results for Fe_2O_3 (a) Effect of temperature on NO yield: 2.1 ml/min NH_3 , 2100 ml/min N_2 (b) Effect of NH_3 concentration on NO yield: 2100 l/min N_2 , $T = 830^\circ\text{C}$

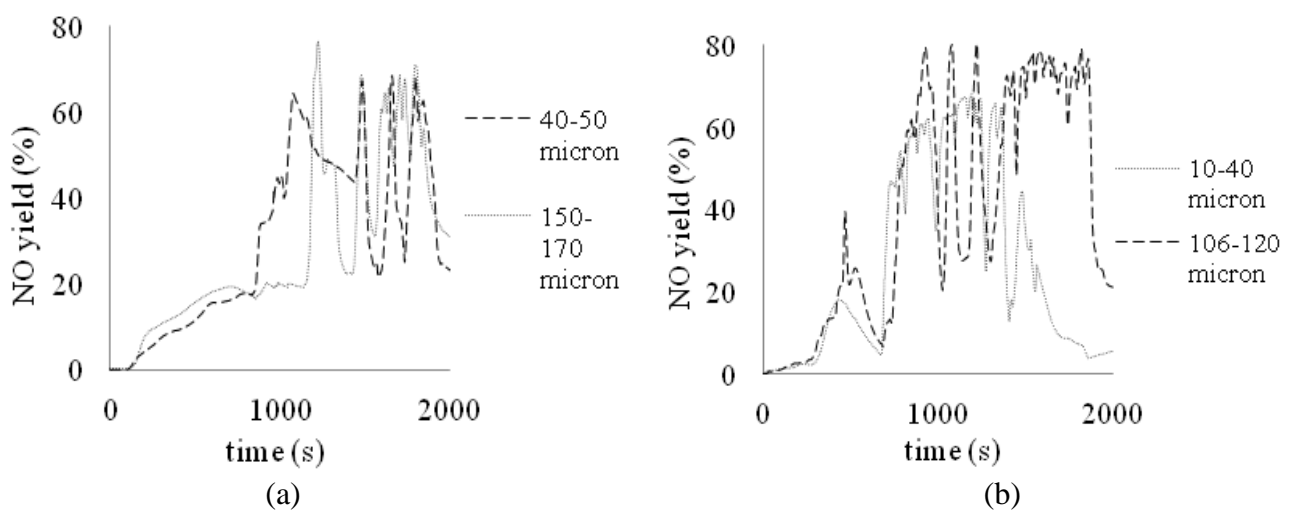


Figure 6.15 Experimental results for effect of particle size on NO yield (a) CuO: 2.1 ml/min NH_3 , 2100 ml/min N_2 , $T = 750^\circ\text{C}$ (b) Fe_2O_3 : 2.1 ml/min NH_3 , 2100 ml/min N_2 , $T = 830^\circ\text{C}$

6.4 Conclusions

The chemical looping approach is applied to the production of nitric oxide and hydrogen from the reaction between ammonia and metal oxide. The experiments for the proposed reaction between ammonia and metal oxide are carried out for different metal oxides. The high conversions of about 85 to 90 % are obtained for different metal oxides proving the reaction feasibility. A reaction mechanism has been proposed based on an adsorption-desorption mechanism with two competing desorption steps. These assumed desorption steps are representing two parallel reactions dependent on the temperature and the extent of oxygen available for reaction on a specific metal oxide species. At high temperatures, or where the particle temperature can be maintained, and when lattice oxygen is available, then the NO desorption step is strongly favoured with high conversions achieved. At lower temperatures or when the lattice oxygen has been depleted, then the N₂ forming desorption step occurs more readily and in a batch system where the oxygen is not replenished, this step will eventually dominate. However, the present experimental study is restricted to low concentrations of NH₃ fed to the reactor. The major challenges are to obtain high NO conversions for higher NH₃ concentrations and separation of NO from H₂ produced in the reduction step. Pd membranes exist for separation of hydrogen from other gases but are expensive and have got operational problems. Hence, research is needed to find out the appropriate process to separate NO from H₂. This has not been included in the scope of present study. The next step is to design and simulate the process flowsheet and perform the thermodynamic analysis of the entire flowsheet. The proposed process need to be compared with the conventional SMR process on energy and exergy basis so as to check the profitability of the proposed process. The same has been reported in the next chapter.

CHAPTER 7

THERMODYNAMIC ANALYSIS

This chapter discusses the thermodynamic analysis of the proposed chemical looping based processes in comparison to that of the conventional SMR process. The flowsheets for all the processes are simulated in Aspen Plus version 7.3 to obtain material and energy balances in addition to the stream data required for process integration.

7.1 Introduction

The path to sustainability depends competitively on the efficient utilization of resources and energy along with global economy and environmental impact. Energy is defined as the capacity to perform work and its analysis is conventionally used to evaluate the performance of a process on the basis of the first law of thermodynamics. In contrast, the exergy balance is based on the second law of thermodynamics which accounts for energy degradation or exergy loss due to irreversibilities in real processes (Kotas 1995). Exergy analysis is the study of the various exergy losses and it reveals ways of reducing or eliminating the sources of existing inefficiencies (Hajjaji et al. 2012). Thermodynamic analysis has been widely accepted as one of the methods for the comparison of alternative processes for a given purpose (Taheri et al. 2014). The last couple of decades have seen a wide application of thermodynamic analysis, in particular, exergy analysis in energy systems and chemical processes. For instance, there are many studies reporting energy and exergy analysis of hydrogen production by steam methane reforming (SMR) (Simpson & Lutz 2007; Boyano et al. 2011) and quite a few studies that compared different hydrogen (H₂) production processes on the basis of energy and exergy efficiencies (Koroneos & Rovas 2012; Koroneos et al. 2003). This is because the efficiency and technology of hydrogen production is improving over time, but the process still remains energy intensive and expensive compared to conventional fuels.

For any material, heat, or work stream, exergy is a property governed by temperature, pressure and composition of that stream with respect to a reference state (Szargut et al. 2005). In the case of a work stream and electricity, the exergy is equal to its energy

irrespective of the reference state, and for a material stream, the exergy is equal to the work that could be produced by bringing the stream in thermo-mechanical and chemical equilibrium with the reference state. The thermal exergy is due to the temperature difference between the stream and the reference state, mechanical exergy is due to the pressure or concentration difference, and chemical exergy is the minimum amount of work required to form a substance from the constituents in the reference environment (Dincer & Rosen 2013). It is possible for a single stream to possess one or more forms of exergy. The reference state or the environmental state (T_0, P_0) is usually the dividing state in the processes used to determine physical and chemical exergy. The system attains equilibrium with the surroundings at the reference state. The positive and negative value of exergy obtained for above ambient and below ambient conditions explains the physical significance of having a dividing state between the system and surroundings. The different possible forms of exergy, in particular, physical (thermo-mechanical) and chemical exergy are defined in the literature (Khaleduzzaman et al. 2014; Tsatsaronis & Cziesla 2004). For a real system, the total exergy input is always higher than its exergy output as a certain amount of exergy is irreversibly destroyed within the system or released to the environment as heat losses and smokestack effluents (Bejan 2002). Figure 7.1 shows the energy and exergy balance for a common real system. Since all real processes involve exergy destruction and losses, exergy efficiency (η_{Ex}) is defined as the ratio of the exergy of desired products ($E_{x_{prod}}$) to the total input exergy ($E_{x_{in}}$).

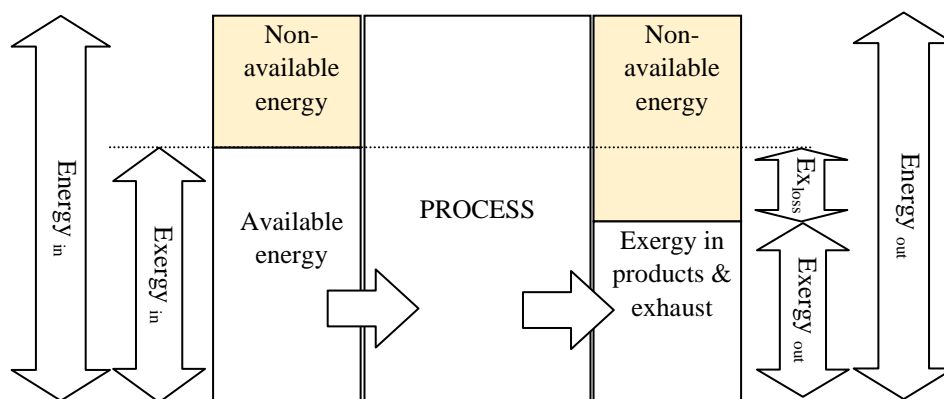


Figure 7.1 Energy and exergy balance for a system

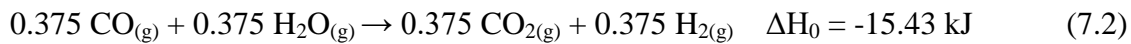
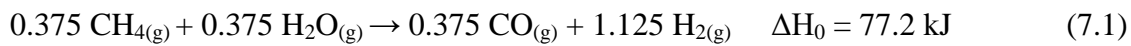
In chemical process plants producing hydrogen, ammonia, nitric acid, etc. there is a potential to recover waste or excess heat by process heat exchange or by generating utilities (Kirova-Yordanova 2011). In the case of chemical reactors, it is difficult to

reduce the exergy losses arising due to the difference in chemical exergies of the reactants and products in a reactor. However, a complete exergetic analysis of the heat exchanger network and the utilities consumed could help to identify sources of exergy loss and possible improvements. A recent method proposed to estimate exergy destruction in a heat exchanger requires stream data of the exchanger's inputs and outputs, thereby eliminating the need of difficult mathematical calculations (Paniagua et al. 2013). In cases where excess fuel is burnt to supply heat, the exergy efficiency of the process can be improved either by reducing the fuel or by generating a hot utility. In cases where the minimum amount of fuel is burnt to supply heat, the options such as preheating the combustion air can be considered to reduce the fuel content further. Some studies have applied pinch analysis for improvement of heat exchanger network (HEN) and then performed exergy analysis for the modified process (Modarresi et al. 2012). The Intended Exergy Yield was proposed by Sorin & Paris (1999) as a new thermodynamic criteria for process improvement and applied the combined exergy distribution load method and pinch analysis for the case study of hydrogen production by SMR. There are similar studies that employed both pinch analysis and exergy analysis to improve the process performance (Ataei 2011; Hanak et al. 2014). In the present chapter, the thermodynamic analysis is performed for three different processes of SMR, chemical looping using hydrolysis (CLHYD), and chemical looping using air oxidation (CLAO). Though the experimental study focussed mainly on CuO, regeneration of CuO by hydrolysis is not feasible in single step and usually requires an electrolytic step. Hence, the case of $\text{Fe}_2\text{O}_3/\text{Fe}_3\text{O}_4$ is selected for thermodynamic analysis on account of the data available for regeneration of Fe_3O_4 and the experimental results obtained in the present study. The objective is to compare the proposed chemical looping based processes to the base case of SMR on a thermodynamic basis. These energy and exergy analyses provide a better understanding of the entire process and also help to improve the processes further.

7.2 Process Simulation

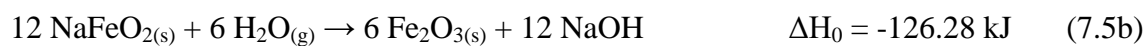
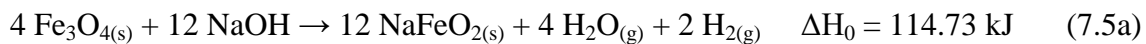
Figure 7.2(a), (b) and (c), respectively represents the main process reactions with their standard heats of reaction occurring in each of the processes, namely, SMR, CLHYD and CLAO for 1 mole/s of NO production. The reactions in the case of the chemical looping based processes are based on the $\text{Fe}_2\text{O}_3/\text{Fe}_3\text{O}_4$ cycle. The reactions are stoichiometrically

balanced so as to produce 1 mole/s of NO. Equations 7.5a and 7.5b represent the reactions occurring in two regenerators operating at 100 °C and 130 °C respectively. Equation 7.6 shows the regeneration of oxidised metal oxide by air oxidation liberating a large amount of heat. The reactions 7.8a and 7.8b are in accordance with the experimental results obtained for the case of Fe₂O₃ and the mechanism described in Chapter 6. However, the reaction 7.8b which produces N₂ rather than NO is mildly endothermic at 830 °C unlike the CuO case which is exothermic. Figure 7.3(a), (b) and (c), respectively represents the schematic block diagrams of the major units in each of the three processes. The dashed line represents the boundary of the system considered for the thermodynamic analysis. The steam methane reforming for NO production and the two processes of chemical looping based NO and H₂ production are simulated under steady state conditions using the flowsheeting simulator Aspen Plus 7.3 (Aspentech 2011).

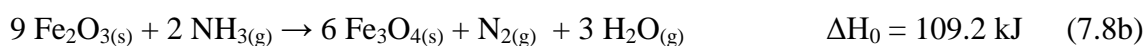
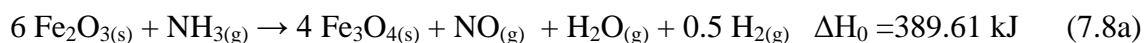


(a)

Regeneration (Hydrolysis)



Regeneration (Air Oxidation)



(b)

Figure 7.2 Reactions in each process for NO production (a) SMR (b) CLHYD & CLAO

The SMR process shown in Figure B.1 (Appendix B) is divided into three blocks, namely, the hydrogen block, ammonia synthesis block and the NO production block. The chemical looping based processes are also divided into three blocks, namely, ammonia synthesis, NO production and metal oxide regeneration block. In the case of CLHYD (Figure B.2), the regeneration block produces H_2 from water that can be used for NH_3 synthesis whereas in the case of CLAO (Figure B.3), the metal oxide is oxidised by air. The thermodynamic data and phase behaviour predictions of the material streams are obtained using the Soave–Redlich–Kwong equation of state (Aspentech 2011), with a component list restricted to Fe_2O_3 , Fe_3O_4 , NaOH, NaFeO₂, CH_4 , O_2 , N_2 , H_2O , CO, NH_3 , NO, H_2 and CO_2 .

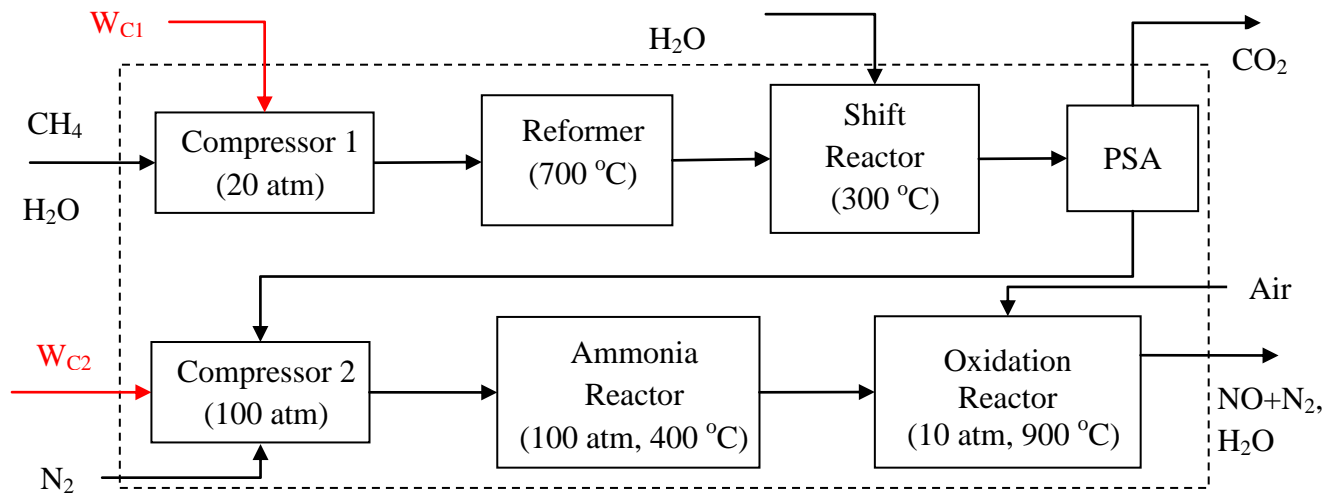
In Figure 7.3, for CL based processes, Separators 1 and 2 are gas-solid separators and Separator 3 is a condenser for separating out NH_3 and H_2O from product gas stream. H_2 and NO purification are performed by a membrane separation module that was modelled with the Aspen PlusTM module Component Separator as an isothermal Palladium (Pd) membrane. Membrane based separation techniques offer benefits such as ease of operation, low energy consumption, lower carbon footprint though relatively expensive for hydrogen separation (He & Hägg 2012). Hydrogen transport through Pd membrane includes dissociative adsorption of H_2 onto the metal surface, diffusion of atomic H through the bulk metal, and associative desorption of H_2 from the metal surface (Adhikari & Fernando 2006). The reforming and the ammonia reactors are modeled using the library model RGibbs which calculates the chemical and phase equilibria by minimizing the Gibbs free energy of all the species expected to participate in the equilibrium (Aspentech 2011). In both high temperature and low temperature water gas shift reactors, methane is considered as an inert and only CO gets converted to CO_2 (Hajjaji et al. 2012). The furnace required to supply heat to the reformer was modeled using the library model Rstoic (Aspentech 2011). The process heat exchangers are simulated as simple heaters and coolers using the HeatX model.

In chemical looping based processes, the conversion of NH_3 to NO is considered as 80 % whereas about 19 % of NH_3 is assumed to react with metal oxide to give N_2 and H_2O based on the experimental results. In experimental study, for 1100 ppm NH_3 as feed, only 10 to 30 ppm NH_3 left unconverted from the reactor. The nitrogen is used as carrier gas for NH_3 in experiments and hence, in flowsheet modelling N_2 is assumed to be in excess as twice the flowrate of NH_3 . The unknown parameters are approximated using data available

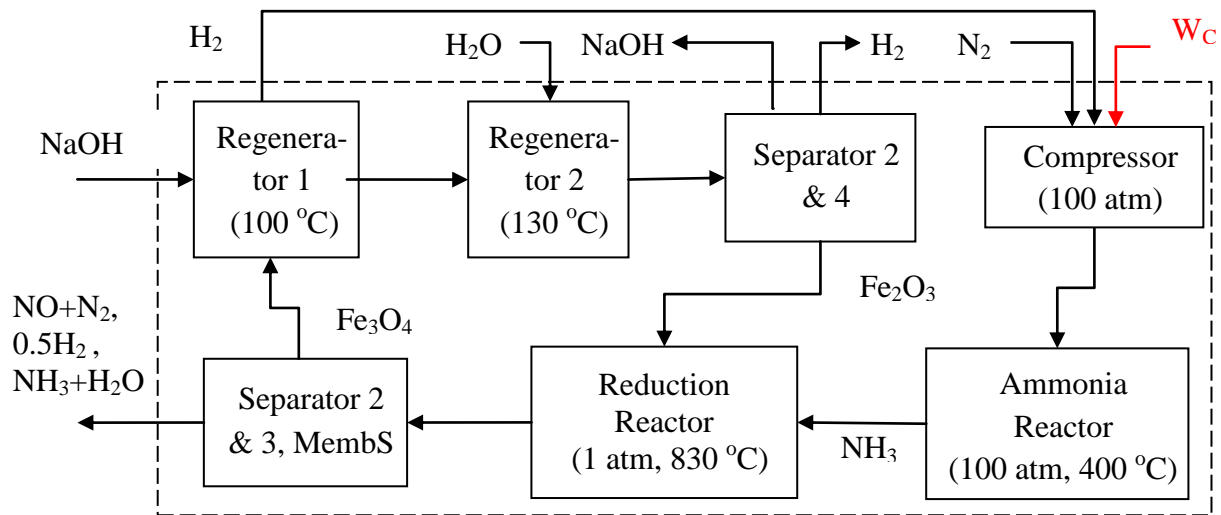
in the literature for specific metal oxides employed in water splitting applications (Charvin et al. 2007). The Aspen Plus simulated flowsheets report the material and energy balances that are required for thermodynamic and economic analysis of the processes. These flowsheets are important as they allow a sensitivity analysis to be conducted with respect to any of the less certain parameters. The Aspen Plus simulated flowsheets with detailed stream summary for steam methane reforming (SMR), chemical looping using hydrolysis (CLHYD), and chemical looping using Air Oxidation (CLAO) are reported in the Appendix B. The flowsheet and data for the base case of SMR is taken from the previous exergy analysis studies which used Aspen Plus simulation (Simpson & Lutz 2007; Hajjaji et al. 2012). The heat required in CLHYD process is assumed to be supplied by burning methane with air in 1:10 molar ratio. Table 7.1 represents the major operating parameters and the assumptions for the components in each process. All the heating and cooling required in each process is assumed to be supplied by external utilities.

Table 7.1 Major operating parameters and assumptions for simulated processes

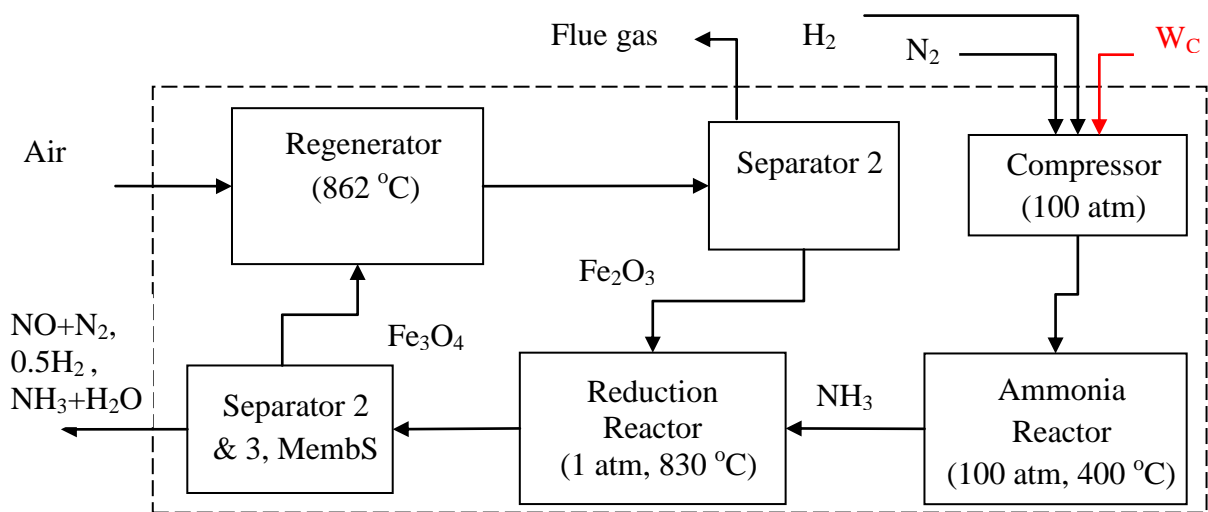
Reference state	$P_0 : 1 \text{ atm}$ $T_0 : 25 \text{ }^\circ\text{C}$
SMR process (Simpson & Lutz 2007)	Natural gas feed : 100 % pure CH_4 Steam/Carbon Ratio (Reformer) : 3.2 Air/Fuel Ratio (Combustor) : 10:1 Air/ NH_3 Ratio (NO Reactor) : 10:1
Conversions and P,T	NO Reactor (SMR) : 95 % (10 atm, 900 $^\circ\text{C}$) Reduction Reactor (CLHYD) : 80 % (1 atm, 830 $^\circ\text{C}$) Regenerator 1 (CLHYD) : 100 % (1 atm, 100 $^\circ\text{C}$)(Charvin, Abanades, Lemort, et al. 2007) Regenerator 2 (CLHYD) : 100 % (1 atm, 130 $^\circ\text{C}$)(Charvin, Abanades, Lemort, et al. 2007) Reduction Reactor (CLAO) : 80 % (1 atm, 830 $^\circ\text{C}$) Regenerator (CLAO) : 100 % (1 atm, 862 $^\circ\text{C}$)
Efficiency	Compressor : 80 % Pump : 90 % Split : 100 %
HEN	$\Delta T : 20 \text{ }^\circ\text{C}$
Pressure drop	Compressors : 0.1 atm between each stage Heaters and Coolers : 0 Reactors : 0



(a)



(b)



(c)

Figure 7.3 Schematic block diagram for NO production (a) SMR (b) CLHYD (c) CLAO

7.3 Methodology

The energy analysis is carried out through pinch analysis by targeting minimum hot and cold utilities required in the process. The energy flows that are taken into account include the heating and cooling duties and the heats of reactions that take place throughout the process. The exergy of a stream of matter is defined by Kotas (1995) as the maximum amount of work obtainable when the stream is brought from its initial state to the dead state by (reversible) processes during which the stream may interact only with the environment. On neglecting the potential and kinetic energy components, the other major components of exergy transfer are the ones associated with heat interaction, work, and mass flow.

The exergy associated with heat transfer Ex_H is given by

$$Ex_H = Q(1 - (T_0/T)) \quad (7.9)$$

where T_0 is the reference temperature and Q is the heat transfer occurring at temperature T . Hence, for a stream going to ambient conditions, the Equation 7.9 represents the exergy loss during heat transfer.

The exergy associated with exchange of work Ex_w is given by

$$Ex_w = W \quad (7.10)$$

The exergy associated with mass flow Ex_M is given by

$$Ex_M = Ex_P + Ex_C + Ex_{mix} \quad (7.11)$$

where Ex_P and Ex_C are the physical and chemical exergies respectively. The physical exergy is calculated by

$$Ex_P = (H - H_0) - T_0(S - S_0) \quad (7.12)$$

where H , S , and T represent the enthalpy, entropy and temperature respectively, and subscript 0 represents the reference environment condition (Bejan 1988). In the case of chemical reactors involving transfer of heat, the exergy associated with heat transfer is also added to the physical and chemical exergies of the streams involved. The exergy losses in compressors and mixing are mainly due to the changes in entropy of the streams and are given by

$$\Delta Ex = \Delta H - T_0 \Delta S \quad (7.13)$$

For streams mixing at constant temperature and undergoing no change in chemical composition, the term ΔH is zero.

The exergy destruction Ex_D is the difference between the total amount of exergy entering and leaving the system.

$$Ex_D = Ex_{in} - Ex_{out} \quad (7.14)$$

The streams leaving the system consist of desired products, side products, exhaust and waste. However, for efficiency calculation, the exergy content of desired and useful products is considered. The exergy efficiency of a system is defined as the ratio of exergy of the final desired output or product to the total exergy delivered into the system.

$$\eta_{Ex} = \frac{Ex_{prod}}{Ex_{in}} \quad (7.15)$$

The stream data is obtained from the Aspen Plus simulated flowsheet and the modified problem table algorithm (MPTA) is applied to perform energy analysis for a specific delta T (Bandyopadhyay & Sahu 2010). The step-by-step methodology for energy and exergy analysis employed in this work is as follows:

- Simulate a process under steady state conditions using Aspen Plus
- Generate stream data from the flowsheet and find minimum heating and cooling utilities
- Calculate the amount of heat that can be recovered as useful exergy (e.g. steam)
- Calculate the exergy loss for heat exchanger network (HEN)
- Calculate the exergies of all the components, and work entering and leaving the overall process
- Calculate the exergy losses and exergetic efficiency for overall process
- Calculate the exergy losses for individual components of process flowsheet and match the summation with the value from above step

7.4 Results

Table 7.2 shows the stream data extracted from the converged flowsheet for each of the three processes. The minimum temperature difference (ΔT_{min}) is selected as 20 °C for all the three processes. Figures 7.4, 7.5 and 7.6 show the Grand Composite Curves (GCC) obtained for SMR, CLHYD and CLAO respectively. The GCC can determine the surplus and deficit of

heat duty in each temperature interval as well as the total external hot and cold utility requirement (Bandyopadhyay & Sahu 2010). All the three processes are threshold processes, in that neither requires any hot utility. However, in case of CLHYD, the heat required for reduction reactor is assumed to be supplied by burning fresh methane. All three cases show a large potential to generate steam at different pressures. The high pressure (HP) steam is assumed to be generated at 100 atm, 310 °C and the low pressure (LP) steam is assumed to be generated at 4 atm, 140 °C. The exergy of the steam generated is calculated using Carnot factor at that temperature and is considered as the useful product exergy. The chemical exergies of the different components is considered at reference state of 1 atm, 25 °C, and are listed in Table 7.3. The work done by the compressors and pumps is also a part of the exergy entering into the process. Table 7.4 shows the total exergy analysis calculations for SMR, CLHYD, and CLAO processes with 1 mole/s NO production as the basis.

The exergy values for different streams above ambient temperature are calculated using the enthalpy and entropy values reported by Aspen Plus. The streams below ambient conditions are not considered for thermodynamic analysis in the present study. Each process requires a similar amount of ammonia and as the below ambient process is only related to the condensation of ammonia in the ammonia synthesis loop, the exergy requirements are assumed to be similar and cancel out on a comparative basis. The exergy calculated from Aspen data takes into account the losses in physical and chemical exergy simultaneously. The exergy losses associated with transfer of heat are accounted by using Equation (7.1). The exergetic efficiencies of the SMR, CLHYD and CLAO processes are found out to be 15.7 %, 48.1 % and 40.8 % respectively not including steam generation. Including steam generation, the overall exergetic efficiencies of the SMR, CLHYD and CLAO processes increased to 37 %, 63 % and 66.5 %, respectively.

Table 7.2 Stream data for SMR, CLHYD and CLAO processes

<i>Stream data for SMR</i>							
Blocks	Heat load (kW)	T _{in} (°C)	T _{out} (°C)	Blocks	Heat load (kW)	T _{in} (°C)	T _{out} (°C)
COOLER4	388	900	35	HEATER6	28.95	15	180
COOLER2	117.3	1009.2	50	HEATER1	95.59	25	400
COOLER5	84.44	400	35	HEATER5	65.56	130	400
COOLER3	19.2	450	35	HEATER2	53.98	382.1	700
NOREACTOR	240.4	900	899.5	HEATER3	20.77	330.6	450
NH3REACTOR	55.39	400	399.5	HEATER8	217.7	327.6	900
SHIFTRACTR	10.64	300	299.5	HEATER4	62.8	140	350
COOLER1	70.47	700	300	REFORMER	89.49	700	700.5

<i>Stream data for CLHYD</i>							
Blocks	Heat load (kW)	T _{in} (°C)	T _{out} (°C)	Blocks	Heat load (kW)	T _{in} (°C)	T _{out} (°C)
COOLER5	283	400	100	COOLER1	546	830	400
CLRCOMB	622.1	2098.5	50	HEATER1	53.67	130	400
COOLER4	76.38	400	32.1	HEATER2	884	116.4	830
COOLER7	109.5	400	35	PREHEATE	35.54	25	200
COOLER6	5.411	400	35	HEATER6	68	98.8	130
AMMR	66.63	400	399.5	HEATER3	91.52	25	100
COOLER3	6.424	128	35	HEATER4	124.7	25	105
COOLER2	121.8	128	35	MAINREAC	359.8	830	830.5

<i>Stream data for CLAO</i>							
Blocks	Heat load (kW)	T _{in} (°C)	T _{out} (°C)	Blocks	Heat load (kW)	T _{in} (°C)	T _{out} (°C)
NH3REACT	66.48	400	399.5	COOLER1	73.69	830	400
REGENRTR	461.5	862	861.5	MAINREAC	358.7	829.9	830
COOLER7	109.2	400	35	HEATER1	120.9	25	700
COOLER3	116.4	862	50	HEATER2	52.2	130	400
COOLER2	74.68	400	35	HEATER3	51.77	30.7	485
COOLER6	5.389	400	35	HEATER5	1.139	15	40

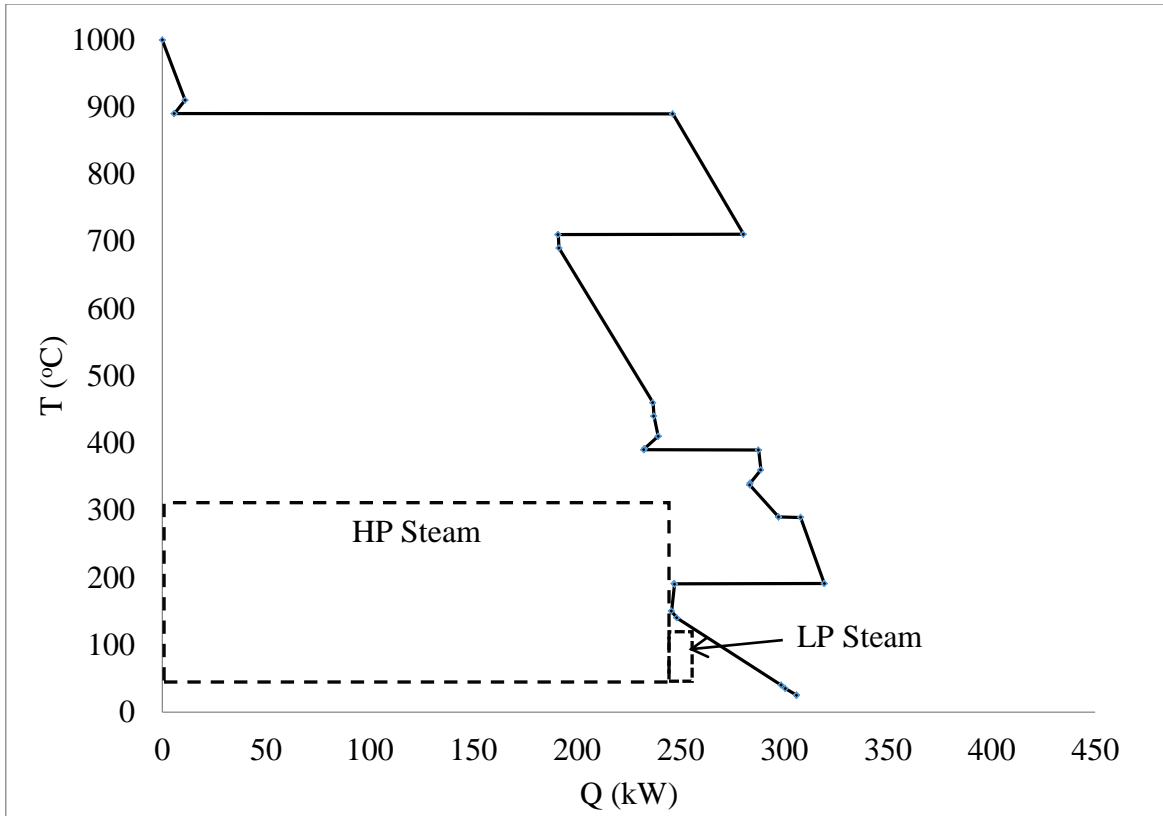


Figure 7.4 Grand Composite Curve for SMR based process

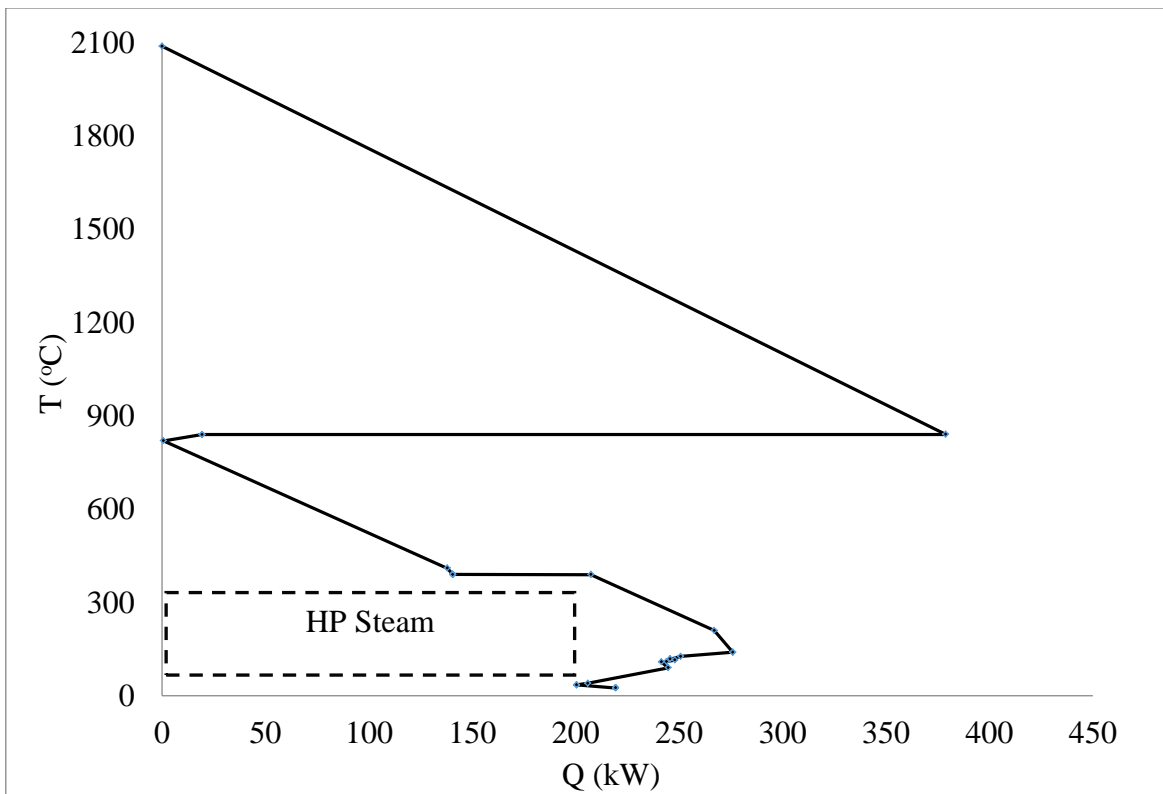


Figure 7.5 Grand Composite Curve for CLHYD process ($\text{Fe}_2\text{O}_3/\text{Fe}_3\text{O}_4$)

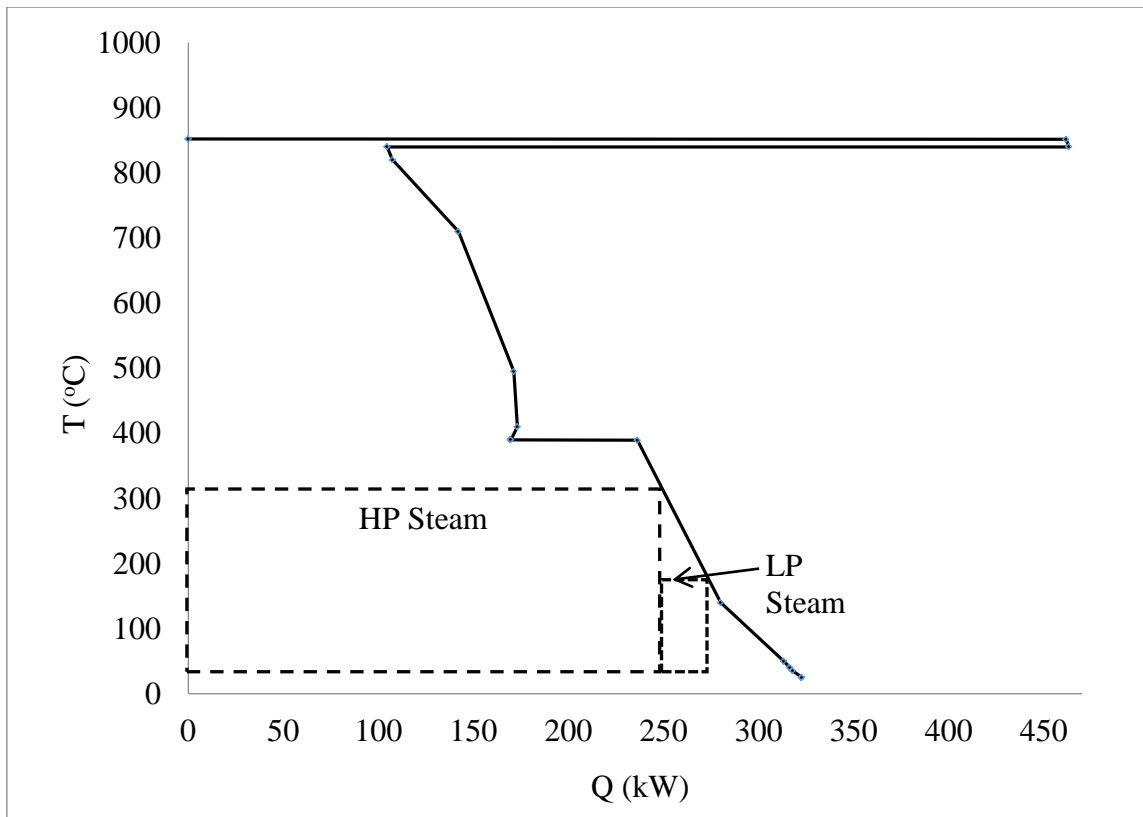


Figure 7.6 Grand Composite Curve for CLAO process ($\text{Fe}_2\text{O}_3/\text{Fe}_3\text{O}_4$)

Table 7.3 Chemical exergy values for chemical species at 25°C

Species	Exergy (kJ/mol)	Species	Exergy (kJ/mol)
CH_4	831.66	N_2	0.72
Air	0	O_2	3.97
NO	88.97	NO_2	55.83
H_2	236.10	N_2O	106.96
$\text{H}_2\text{O}_{(l)}$	0.77	NH_3	338.2
$\text{H}_2\text{O}_{(g)}$	9.34	Fe_2O_3	17.24
CO	275	Fe_3O_4	122.82
CO_2	27.9	NaOH	76.9

Table 7.4 Exergy efficiency calculations for overall processes

Process	SMR		CLHYD		CLAO	
			(Fe ₂ O ₃ /Fe ₃ O ₄)		(Fe ₂ O ₃ /Fe ₃ O ₄)	
Components	Ex _{in}	Ex _{out}	Ex _{in}	Ex _{out}	Ex _{in}	Ex _{out}
CH ₄	415.83		598.80			
Air	0		0		0	
NO		88.98		88.98		88.98
H ₂				229.98	448.61	119.21
H ₂ O (l)	1.22	1.95	1.93	2.21		1.05
CO		13.61				
CO ₂		12.58		20.09		
N ₂	0.40	6.13	1.90	5.45	1.90	4.83
O ₂		3.20		0.13		0.13
H ₂ exh		18.64		19.52		3.38
NO ₂		0.52				
N ₂ O		0.06				
NH ₃		0.36		3.98		3.97
Work (kW)	147.63		59.80		59.80	
	Ex _{in}	Ex _{prod}	Ex _{in}	Ex _{prod}	Ex _{in}	Ex _{prod}
Total (kW)	565.08	88.98	662.42	318.96	510.31	208.19
Ex loss (kW)		476.10		343.46		302.11
Steam generation						
	η _C	Ex _{out}	η _C	Ex _{out}	η _C	Ex _{out}
HP Steam (kW)	0.49	119.74	0.49	97.75	0.49	124.62
LP Steam (kW)	0.28	1.39			0.28	6.68
Ex efficiency (%)	15.74		48.15		40.80	
Ex efficiency (including steam) (%)	36.93		62.91		66.53	

7.5 Discussion

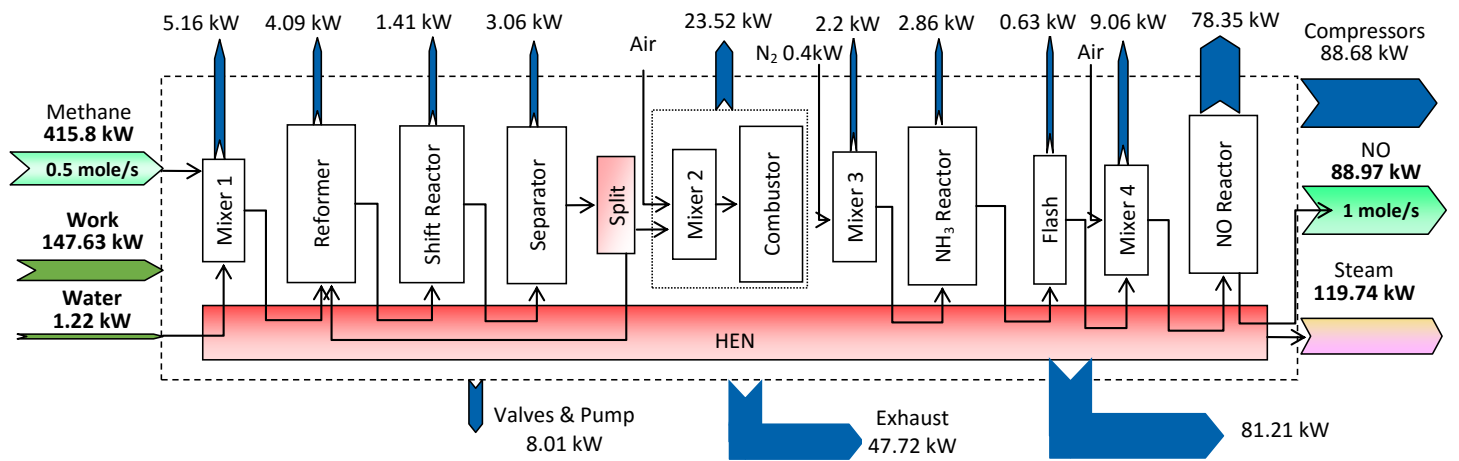
From the GCC shown in Figures 7.4 to 7.6, it is observed that the area between the process GCC and the steam utility reflects the most significant amount of the HEN exergy losses. Figure 7.7 shows the exergy input, output and losses from the major components in each process. The heat exchanger network (HEN) block collectively represents the heaters, coolers and heat exchangers in the flowsheet for each process. The summation of exergy losses from individual components is verified to match the total exergy loss for overall process reported in Table 7.4 with the error less than $\pm 1\%$. Figure 7.8 represents the percentage contribution of different process components towards the total exergy loss after steam generation. The detail calculation for each block and the HEN is reported in Appendix B for all three processes. In the case of the SMR process, the major exergy destruction occurs in the NO reactor due to the highly exothermic oxidation of ammonia at high temperatures of $900\text{ }^{\circ}\text{C}$, HEN and compressors. The losses in the HEN could be reduced by a substantial amount by utilising the waste heat to generate high pressure (HP) and low pressure (LP) steam. The reforming section including the reformer, mixers and combustor incurs the losses of about 32.68 kW. The NO reactor requires an ammonia to air ratio of 1:10 at 10 atm pressure which increases the compressor work and hence the losses in the specific compressor. The exhaust stream mainly consists of the flue gases such as CO, CO₂ and water exiting from the combustor and the gases left after separating NO. In conventional nitric acid plants, the heat is recovered from the flue gases before discharging into the atmosphere using a tail gas expander.

In the CLHYD process for Fe₂O₃/Fe₃O₄ cycle, the major chemical inputs are Fe₂O₃, NaOH, water and air. Out of these, the metal oxide and NaOH are regenerated and hence can be reused. The endothermic reaction between ammonia and Fe₂O₃ at $830\text{ }^{\circ}\text{C}$ requires about 359.8 kW of heat which needs to be supplied externally. CH₄ is assumed to supply required heat to the process resulting in major exergy input to the process. The salient feature of CLHYD process is its self-sufficiency in terms of H₂ required for NH₃ production with the possibility of generating surplus H₂. This increases the exergy efficiency of the process to 48.15 % in comparison to 15.74 % for SMR process without considering steam generation. The two regenerators operate at atmospheric pressure and closer temperatures (regenerator 1 at $130\text{ }^{\circ}\text{C}$ and regenerator 2 at $100\text{ }^{\circ}\text{C}$) and hence incur lower exergy losses. HEN encounters highest exergy loss of about 34 % followed by exhaust and compressors. The exergy of about

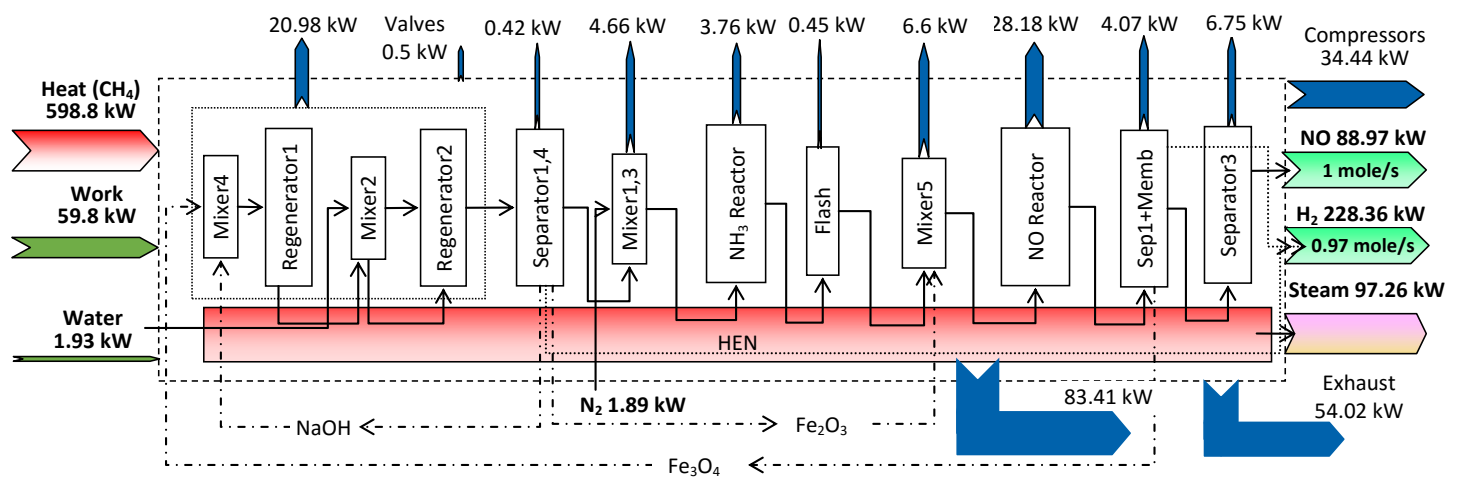
54.02 kW is lost in the exhaust stream due to the flue gases leaving from combustor. As reported in Figure 7.7, the HEN exergy loss is highest for SMR and CLHYD and is significantly lower for CLAO – consistent with GCC. The HEN exergy loss of the first two was similar to the exergy of the NO product, so reducing the HEN exergy loss would increase the efficiency of the process further.

In the case of the CLAO process, the heat for reduction reaction is supplied by the single regenerator operating at a temperature of 862 °C exothermically. But the process requires H₂ to be supplied as feed, as it is not self-sufficient in terms of H₂ required for NH₃ production. The exergy losses in different blocks of CLAO are similar to that in CLHYD except for the HEN. The HEN exergy losses in CLAO are lower than in SMR and CLHYD due to the oxidation reactor providing heat for the reduction reactor. The steam generation potential for this process is higher than that for CLHYD. The exergy efficiency without considering steam generation is 40.8 % which is much lower than CLHYD process, but considering the steam generation potential the process exergy efficiency increases to 66.53 %. The exhaust exergy losses are much lower in CLAO process as no fossil fuel is burnt to supply the heat unlike SMR and CLHYD. For all three processes, separators, splitters and flash operations are the components with the least exergy losses. The NO product stream mixed with N₂ is assumed to be obtained at 35 °C in all three cases for exergy calculations.

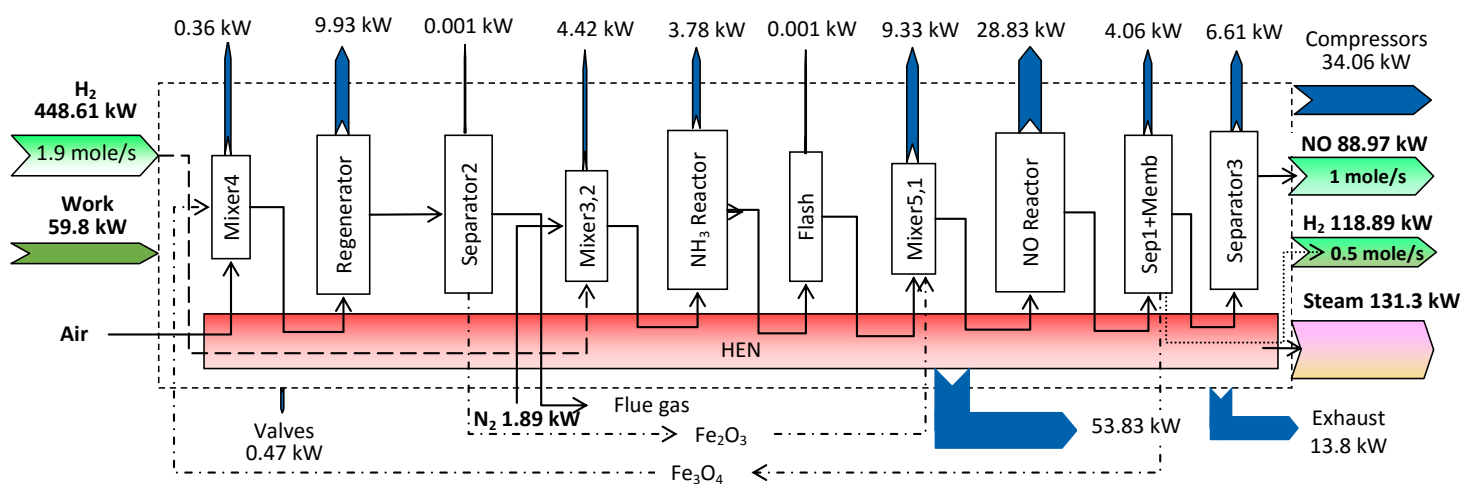
From the results, the chemical looping based processes are exergetically more efficient than the SMR process for the production of NO. The exergy efficiency is calculated considering NO, H₂ and steam as desired or useful products. The CLAO offers the advantage of a lower temperature difference between oxidation and reduction reactors whereas CLHYD offers the advantage of producing surplus hydrogen having chemical exergy of 236.11 kJ/mol. Furthermore, the Fe₂O₃/Fe₃O₄ cycle considered in CLHYD process is a 3-step cycle resulting in the additional reactor and utilities. It is expected that the 2-step hydrolysis based cycles would be preferred on account of the reduced number of reactors and process units. Hence, it would be important to make a decision between exergy recoveries either by steam generation as in case of CLAO or by H₂ production as in case of CLHYD for a fixed amount of NO production.



(a) SMR process



(b) CLHYD process



(c) CLAO process

Figure 7.7 Exergy input, output and losses from the major components in each process

For $\text{Fe}_2\text{O}_3/\text{Fe}_3\text{O}_4$ cycle, the thermodynamic analysis results indicate CLAO as a better alternative to be looked upon for the NO production in nitric acid plant over CLHYD. This can be mainly attributed to the heat requirement of about 359 kW in reduction reactor which is supplied by burning CH_4 externally in CLHYD case and is supplied by regenerator in case of CLAO process. However, the net heat requirement of reduction reactor would be lower for other metal oxides as the reaction 7.8b for metal oxide cycles such as CuO/Cu , $\text{Co}_3\text{O}_4/\text{CoO}$, NiO/Ni , etc. is considerably exothermic. This would increase the efficiency of CL based processes further by reducing the exergy losses in the HEN and by avoiding the exhaust generated due to burning of fossil fuel.

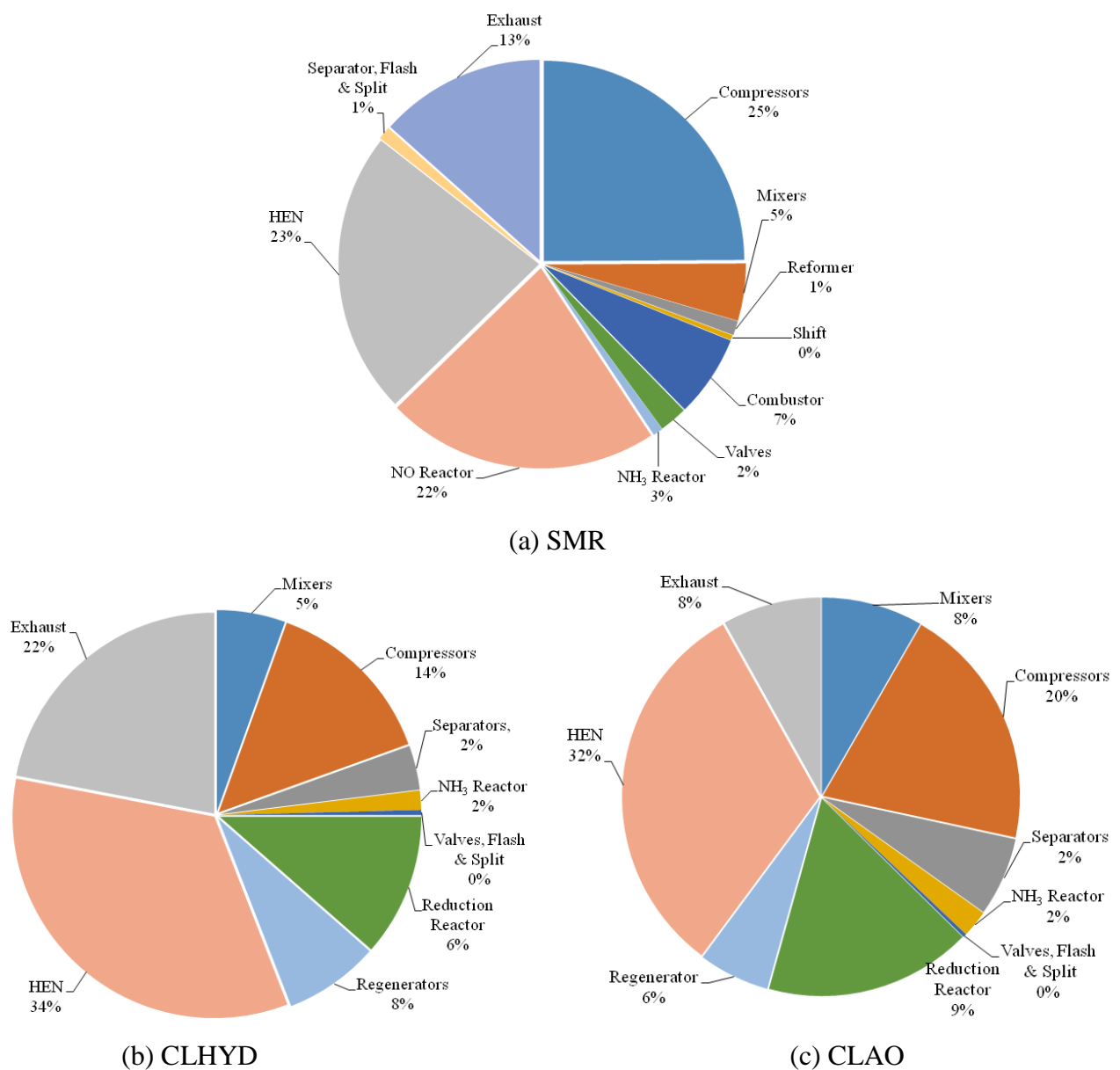


Figure 7.8 Percentage contributions of individual process components towards total process exergy loss

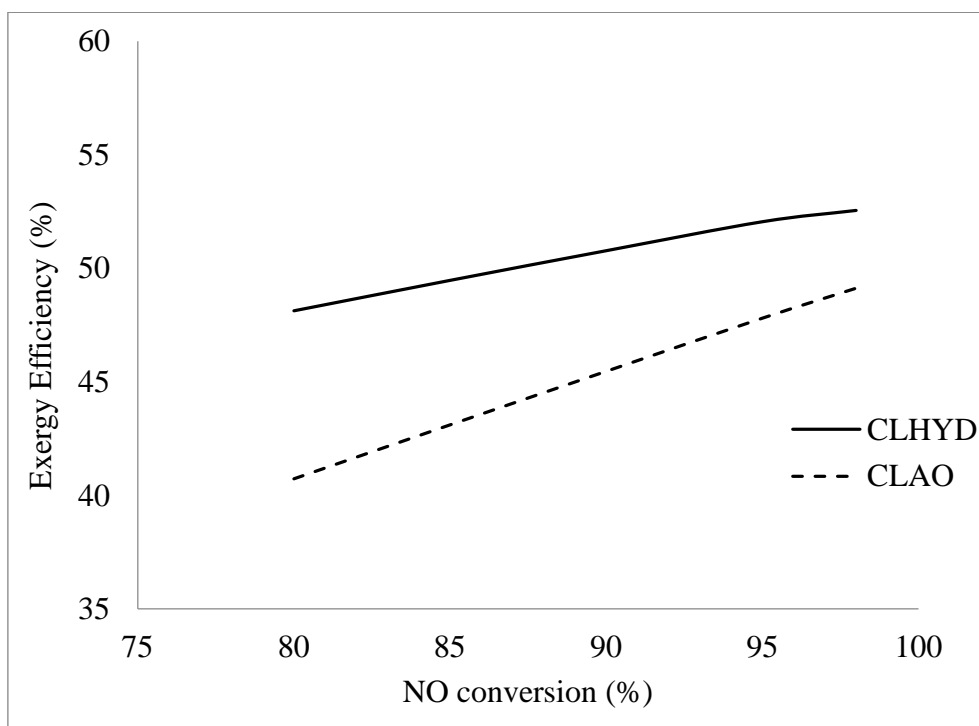


Figure 7.9 Effect of NO conversion on exergy efficiency of CL based processes

Figure 7.9 shows the effect of NO conversion in the reduction reactor on exergy efficiency of CL based processes without considering the steam as a desired product. It is observed that in both cases, with the increase in reaction conversion to NO, the exergy efficiency of overall process increases. The higher conversion requires additional heat to be supplied to the reduction reactor which would bring down the efficiency slightly. However, the net exergy efficiency increases more in case of CLAO due to lower exergy losses in HEN and exhaust than CLHYD as CH_4 is used to supply heat in CLHYD.

Finally these results point to some interesting integration opportunities which have not been explored as part of this thesis. The first is the possibility of using solar thermal energy in the CLHYD main reactor. The required temperature for this reactor of 830°C is very compatible with solar thermal energy through a parabolic dish or solar tower system. The use of solar energy would remove completely the use of a fossil fuel from this chemical looping system. The exergy of this option would increase significantly.

The second option is to include the SMR reformer within the CLAO system and use the heat generated by the metal oxide regeneration reactor to drive the reforming reactor. Although

CH₄ will be consumed to generate this hydrogen, the exergy loss from the CLAO oxidation reaction would be saved. The third option is similar and is a hybrid of the two chemical looping schemes, where the excess energy from the CLAO reactor is used to run the CLHYD reactor.

7.5 Conclusions

From the thermodynamic analysis, it is found that the CL based processes are more efficient for the production of NO compared to SMR based process. The hydrogen produced in CLAO can be used for partial production of ammonia and CLHYD process offers the advantage of producing surplus hydrogen thereby making the process more environmentally benign. However, there is a need to supply external heat for the reduction reaction at 830 °C (for Fe₂O₃/Fe₃O₄ case) in CLHYD process. This amount of heat would vary depending on the metal oxide used as the N₂ forming step is expected to bring down the heat requirement of the reduction reactor. CLAO process has an efficient HEN as the temperature difference between oxidation and reduction reactors is lower unlike CLHYD. For the case of Fe₂O₃/Fe₃O₄, CLAO is found to be most efficient followed by CLHYD and SMR. These calculations are based on the conversions obtained from experimental results for a particular metal oxide which were restricted to lower concentrations of ammonia. The sensitivity analysis result for the effect of reaction conversion on exergy efficiency showed that the efficiency increases with the increase in the conversion to NO and H₂ though at the expense of the supply of additional heat. The increase in heat requirement would add to thermal exergy input but the amount of chemical exergy gained in the form of products NO and H₂ is of higher value than the thermal exergy required. These thermodynamic analysis results suggest the possibility to have process modifications so as to make each of them more exergy efficient and environmentally benign.

CHAPTER 8

CONCLUSIONS AND FUTURE WORK

The proposed chemical looping based process for nitric oxide and hydrogen production is studied thermodynamically and experimentally, and is shown to be environmentally more benign and exergetically more efficient than the conventional SMR based process.

8.1 Main Contributions

- The Ostwald's process is the only commercial process to produce nitric oxide whereas there are numerous processes for hydrogen production. Hydrogen is required as a feedstock for ammonia production and hence NO production. A cost-benefit analysis of eight different hydrogen producing technologies is performed with different qualitative and quantitative criteria using the multi-criteria decision making tool known as the Analytic Hierarchy Process. Using this decision making tool, water splitting by the chemical looping approach was shown to be one of the best technologies for balancing economic performance and environmental impact.
- The application of chemical looping is extended to the production of NO and H₂ from ammonia and metal oxide based on thermochemical cycles. Nitric oxide and hydrogen are produced by reduction of metal oxide by ammonia, and the metal oxide is regenerated by oxidation thus completing the cycle. Based on the method of regeneration of the metal oxide, two chemical looping based processes are proposed; chemical looping using hydrolysis (CLHYD) and chemical looping using air oxidation (CLAO).
- The thermodynamic and experimental feasibility of the proposed chemical looping based process is carried out for different metal oxides. A reaction mechanism is proposed based on the theory of heterogeneous gas-solid reactions. The detailed experimental study of Copper Oxide is used to test this hypothesis.
- The proposed processes are simulated in Aspen Plus and are compared with the SMR approach for NO production on the basis of energy and exergy analysis. The chemical looping processes are found to be exergetically more efficient and environmentally more benign than

the SMR process. The thermodynamic analysis emphasise the possibility to have process modifications so as to make each of the process more exergy efficient and cleaner.

8.2 Future work

A new process was proposed for the production of nitric oxide and hydrogen by chemical looping. This new process is investigated using a semi-batch experimental study. This was followed by a thermodynamic comparison to the SMR based process. However, there is still scope for doing more experiments over a greater range of conditions including further development of the reactor. The possible directions of future work are as follows:

- *Appropriate set-up and reactor design*

The experiments in the present work are carried out in a set-up originally built for chemical looping combustion study in batch mode. The conversions are expected to improve further with a continuous flow reactor.

- *Metal oxide properties and mixtures*

Combining metal oxides as individual powders or as an amalgam might give a further improvement in conversion. It is recommended to undertake more experimental parameter studies on particle size, temperatures, gas velocities, the mass of metal oxides, modes of mixing, etc.

- *Reaction mechanism and kinetics*

The temperature programmed reduction (TPR) experiments are used to find the most efficient reduction conditions in the field of heterogeneous catalysis. These experiments can help in confirming the reaction mechanism and kinetics. Surface spectroscopy can also confirm the reduced phases of the metal oxide.

- *Process optimization*

The involvement of high temperature reduction and oxidation steps in the process provides a wider scope for applying the concepts of process integration and thereby optimize the process thermodynamically and economically.

APPENDIX A

PAIRWISE COMPARISON MATRICES FOR CHAPTER 3

The eight hydrogen production technologies are compared for five criteria individually resulting in five 8×8 pair wise comparison matrices whose priority vectors give the scores of each technology for each criterion. The weights of each attribute are calculated using an eigenvector method and are checked for their consistency. The pair wise comparison matrix for criterion of energy efficiency is shown in Table 3.5 of Chapter 3. The matrices for rest of the four criteria, namely, GHG emissions, Scalability, Raw material and utilities consumption, and Waste disposal and non GHG emissions are reported in following tables (Table A.1 to Table A.4). These values for each technology are synthesised with the criteria weights for two cases to give the final scores in Table 3.6 and Table 3.7.

Table A.1 GHG emissions

	SMR	CG	POX	BG	PV-EL	W-EL	H-EL	WS-CL	Priority Vector
SMR	1	1/2	2	1/5	1/4	1/8	1/7	1/6	0.0276
CG	2	1	3	1/4	1/3	1/7	1/6	1/5	0.0391
POX	1/2	1/3	1	1/6	1/5	1/9	1/8	1/7	0.0203
BG	5	6	4	1	2	1/4	1/3	1/2	0.1102
PV-EL	4	3	5	1/2	1	1/5	1/4	1/3	0.0765
W-EL	8	7	9	4	5	1	2	3	0.3328
H-EL	7	6	8	3	4	1/2	1	2	0.2330
WS-CL	6	5	7	2	3	1/3	1/2	1	0.1605
$\lambda_{\max} = 8.36$			C.I. = 0.05				C.R. = 0.04		

Table A.2 Scalability

	SMR	CG	POX	BG	PV-EL	W-EL	H-EL	WS-CL	Priority Vector
SMR	1	4	2	9	5	7	6	3	0.3284
CG	1/4	1	1/3	6	2	4	3	1/2	0.1093
POX	1/2	3	1	8	4	6	5	2	0.2311
BG	1/9	1/6	1/8	1	1/5	1/3	1/4	1/2	0.0258
PV-EL	1/5	1/2	1/4	5	1	3	2	1/3	0.0743
W-EL	1/7	1/4	1/6	3	1/3	1	1/2	1/5	0.0355
H-EL	1/6	1/3	1/5	4	1/2	2	1	1/4	0.0508
WS-CL	1/3	2	1/2	2	3	5	4	1	0.1449
$\lambda_{\max} = 8.40$			C.I. = 0.06				C.R. = 0.04		

Table A.3 Raw material and utilities consumption

	SMR	CG	POX	BG	PV-EL	W-EL	H-EL	WS-CL	Priority Vector
SMR	1	2	3	1/2	1/3	1/4	1/5	1/6	0.0477
CG	1/2	1	2	1/3	1/4	1/5	1/6	1/7	0.0327
POX	1/3	1/2	1	1/4	1/5	1/6	1/7	1/8	0.0236
BG	2	3	4	1	1/2	1/3	1/4	1/5	0.0709
PV-EL	3	4	5	2	1	1/2	1/3	1/4	0.1059
W-EL	4	5	6	3	2	1	1/2	1/3	0.1572
H-EL	5	6	7	4	3	2	1	1/2	0.2307
WS-CL	6	7	8	5	4	3	2	1	0.3313
$\lambda_{\max} = 8.29$			C.I. = 0.04				C.R. = 0.03		

Table A.4 Waste disposal and non GHG emissions

	SMR	CG	POX	BG	PV-EL	W-EL	H-EL	WS-CL	Priority Vector
SMR	1	1/3	1/2	3	1/4	1/5	1/5	1/7	0.0356
CG	3	1	2	5	1/2	1/3	1/3	1/5	0.0757
POX	2	1/2	1	4	1/3	1/4	1/4	1/6	0.0511
BG	1/3	1/5	1/4	1	1/6	1/7	1/7	1/9	0.0202
PV-EL	4	2	3	6	1	1/2	1/2	1/4	0.1135
W-EL	5	3	4	7	2	1	1	1/3	0.1736
H-EL	5	3	4	7	2	1	1	1/3	0.1736
WS-CL	7	5	6	9	4	3	3	1	0.3568
$\lambda_{\max} = 8.32$			C.I. = 0.05				C.R. = 0.033		

APPENDIX B

FLWSHEET DATA AND CALCULATIONS FOR CHAPTER 7

Following are the equations used to calculate the exergy loss for different process components in all three processes. The exergy destroyed for a material stream is calculated by

$$\Delta(\text{Ex}_P + \text{Ex}_C) = \Delta H - T_0 \Delta S \quad (\text{B.1})$$

where ΔH is the change in enthalpy (kW) and ΔS is change in entropy (kW/molK) calculated using stream data obtained from Aspen Plus simulation results.

The exergy loss associated with the heat stream with respect to ambient conditions is calculated by

$$\text{Ex}_Q = Q(1 - T_0/T) \quad (\text{B.2})$$

For heat exchanger network (HEN), the exergy factor (ϵ) is calculated by

$$\epsilon = T - (T_0 * \ln(T/T_0)) \quad (\text{B.3})$$

The corresponding exergy in the eighth column of the table for HEN exergy loss calculations is given by

$$\text{Exergy Ex} = mC_p(\Delta\epsilon) \quad (\text{B.4})$$

The flowchart in Figure B.1 represents the methodology proposed to calculate the exergy loss for a HEN having all the streams above ambient temperature. The exergy factor (ϵ) is calculated for the temperatures arranged in descending order with respect to reference temperature T_0 . The exergy for each interval is calculated using exergy factors and the cumulative heat capacity flows ($\sum mC_{pint}$). The value in the last row and column gives the exergy loss for a HEN. This methodology offers the advantage of measuring the exergy loss without a need to draw composite curves and measure the area under curves.

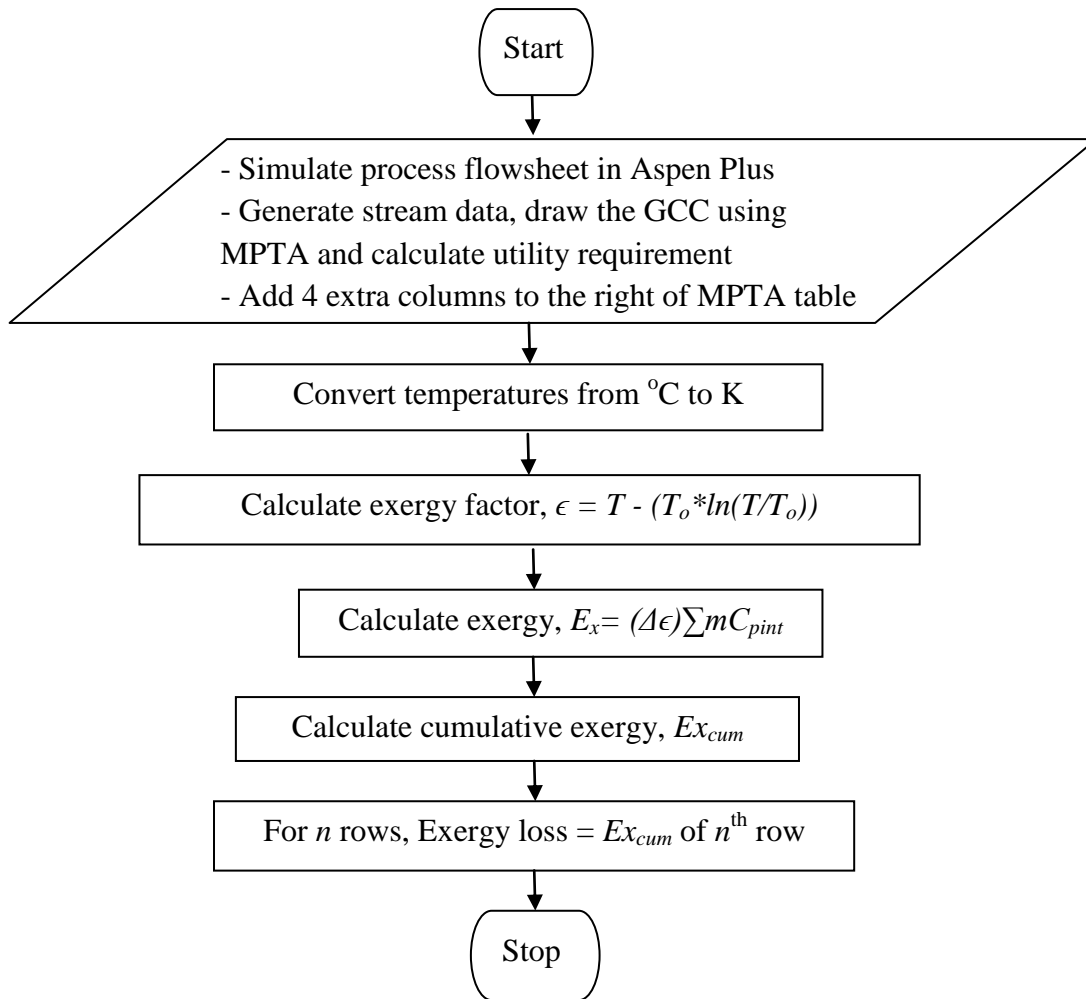


Figure B.1 Flowchart for exergy loss calculation of HEN

Figure B.2 represent the Aspen Plus simulated flowsheet for steam methane reforming (SMR) based process to produce nitric oxide (NO). The Soave–Redlich–Kwong equation of state is used for simulation with component list as CH₄, O₂, N₂, H₂O, NH₃, NO, H₂, CO and CO₂. The flowsheet is divided into three blocks, namely, hydrogen, ammonia and nitric oxide block. Table B.1 reports the stream summary of the simulated flowsheet. The enthalpy and entropy values from this table are used to determine exergy losses for each process component. Table B.2 reports the overall exergy loss for SMR based process which is about 476.11 kW. Table B.3 reports the exergy loss of individual process components considering HEN as separate block accounting for all the heaters and coolers in the process. Table B.4 reports the exergy losses calculate for HEN using MPTA based approach. The summation of these losses comes out to be 475.75 kW which is in agreement with the previous value within error of ±1 %. These calculations are represented in Figure 7.7 of Chapter 7 in the main text.

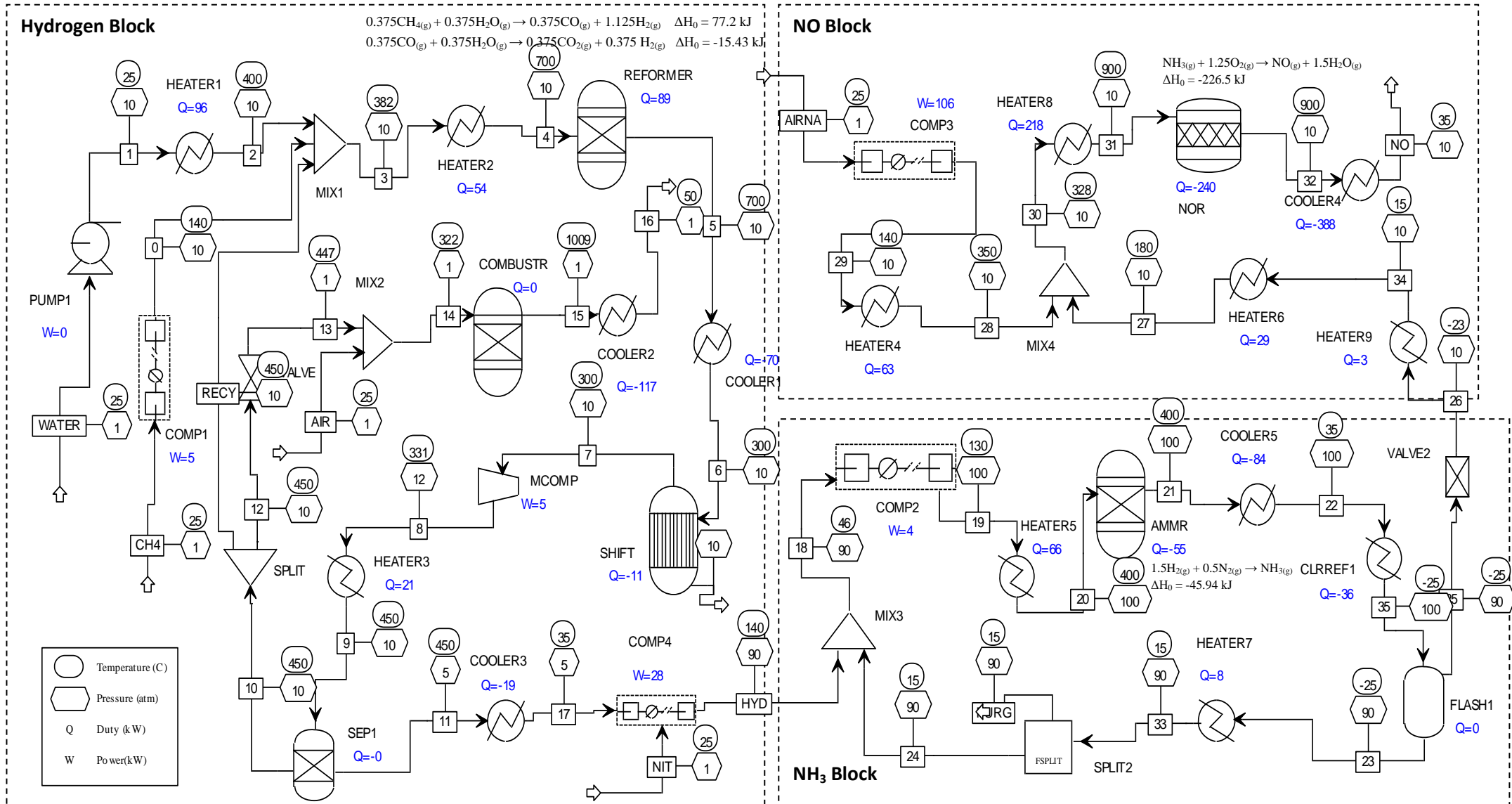


Figure B.2 Aspen Plus simulation flowsheet for SMR case

Table B.1 Aspen Plus stream summary for SMR case

Substream: MIXED	0	1	2	3	4	5	6	7	8	9	10	11	12	13	14	15	16	17	18	19	20	21	
Mole Flow mol/sec																							
N2	0.000	0.000	0.000	0.000	0.000	0.000	0.000	0.000	0.000	0.000	0.000	0.000	0.000	0.000	0.574	0.574	0.574	0.000	4.188	4.188	4.188	3.666	
O2	0.000	0.000	0.000	0.000	0.000	0.000	0.000	0.000	0.000	0.000	0.000	0.000	0.000	0.000	0.153	0.000	0.000	0.000	0.000	0.000	0.000	0.000	
NH3	0.000	0.000	0.000	0.000	0.000	0.000	0.000	0.000	0.000	0.000	0.000	0.000	0.000	0.000	0.000	0.000	0.000	0.000	0.150	0.150	0.150	1.194	
CH4	0.500	0.000	0.000	0.604	0.604	0.186	0.186	0.186	0.186	0.186	0.186	0.000	0.082	0.082	0.082	0.000	0.000	0.000	0.000	0.000	0.000	0.000	
H2O	0.000	1.590	1.590	2.562	2.562	2.011	2.011	1.736	1.736	1.736	1.736	0.000	0.764	0.764	0.787	0.968	0.968	0.000	0.000	0.000	0.000	0.000	
CO	0.000	0.000	0.000	0.013	0.013	0.297	0.297	0.023	0.023	0.023	0.023	0.000	0.010	0.010	0.010	0.050	0.050	0.000	0.000	0.000	0.000	0.000	
CO2	0.000	0.000	0.000	0.519	0.519	0.653	0.653	0.927	0.927	0.927	0.927	0.000	0.408	0.408	0.408	0.451	0.451	0.000	0.000	0.000	0.000	0.000	
NO	0.000	0.000	0.000	0.000	0.000	0.000	0.000	0.000	0.000	0.000	0.000	0.000	0.000	0.000	0.000	0.000	0.000	0.000	0.000	0.000	0.000	0.000	
H2	0.000	0.000	0.000	0.102	0.102	1.490	1.490	1.764	1.764	1.764	0.182	1.582	0.080	0.080	0.080	0.064	0.064	1.582	3.647	3.647	3.647	2.081	
NO2	0.000	0.000	0.000	0.000	0.000	0.000	0.000	0.000	0.000	0.000	0.000	0.000	0.000	0.000	0.000	0.000	0.000	0.000	0.000	0.000	0.000	0.000	
N2O	0.000	0.000	0.000	0.000	0.000	0.000	0.000	0.000	0.000	0.000	0.000	0.000	0.000	0.000	0.000	0.000	0.000	0.000	0.000	0.000	0.000	0.000	
Total Flow mol/sec	0.500	1.590	1.590	3.801	3.801	4.637	4.637	4.637	4.637	4.637	3.055	1.582	1.344	1.344	2.094	2.106	2.106	1.582	7.984	7.984	7.984	6.940	
Temperature C	140	25.03	400	382.09	700	700	300	300	330.61	450	450	450	450	447.34	321.64	1009.19	50	35	46.41	130	400	400	
Pressure atm	10	10	10	10	10	10	10	10	12	10	10	5	10	1	1	1	1	10	90	99.9	100	100	
Enthalpy kW	-35.099	-459.553	-363.963	-819.908	-765.927	-676.439	-746.908	-757.551	-752.415	-731.642	-751.500	19.678	-330.660	-330.660	-336.706	-336.706	-453.998	0.475	-2.522	17.970	83.534	28.141	
Entropy kJ/mol-K	-0.087	-0.171	-0.035	-0.024	-0.007	0.017	-0.003	-0.006	-0.005	0.003	-0.005	0.013	-0.005	0.014	0.017	0.047	-0.058	-0.018	-0.031	-0.025	-0.010	-0.022	

Substream:	22	23	24	25	26	27	28	29	30	31	32	33	34	35	AIR	AIRNA	CH4	HYD	NIT	NO	PURG	RECY	WATER
Mole Flow mol/sec																							
N2	3.666	3.664	3.638	0.002	0.002	0.002	7.900	7.900	7.902	7.902	7.918	3.663	0.002	3.666	0.574	7.900	0.000	0.550	0.550	7.918	0.026	0.000	0.000
O2	0.000	0.000	0.000	0.000	0.000	0.000	2.100	2.100	2.100	2.100	0.807	0.000	0.000	0.000	0.153	2.100	0.000	0.000	0.000	0.807	0.000	0.000	0.000
NH3	1.194	0.151	0.150	1.043	1.043	1.043	0.000	0.000	1.043	1.043	0.000	0.151	1.043	1.194	0.000	0.000	0.000	0.000	0.000	0.000	0.001	0.000	0.000
CH4	0.000	0.000	0.000	0.000	0.000	0.000	0.000	0.000	0.000	0.000	0.000	0.000	0.000	0.000	0.000	0.000	0.500	0.000	0.000	0.000	0.000	0.104	0.000
H2O	0.000	0.000	0.000	0.000	0.000	0.000	0.000	0.000	0.000	0.000	1.565	0.000	0.000	0.000	0.023	0.000	0.000	0.000	0.000	1.565	0.000	0.972	1.590
CO	0.000	0.000	0.000	0.000	0.000	0.000	0.000	0.000	0.000	0.000	0.000	0.000	0.000	0.000	0.000	0.000	0.000	0.000	0.000	0.000	0.013	0.000	0.000
CO2	0.000	0.000	0.000	0.000	0.000	0.000	0.000	0.000	0.000	0.000	0.000	0.000	0.000	0.000	0.000	0.000	0.000	0.000	0.000	0.000	0.000	0.519	0.000
NO	0.000	0.000	0.000	0.000	0.000	0.000	0.000	0.000	0.000	0.000	1.001	0.000	0.000	0.000	0.000	0.000	0.000	0.000	0.000	1.001	0.000	0.000	0.000
H2	2.081	2.080	2.065	0.001	0.001	0.001	0.000	0.000	0.001	0.001	0.001	2.080	0.001	2.081	0.000	0.000	0.000	1.582	0.000	0.001	0.015	0.102	0.000
NO2	0.000	0.000	0.000	0.000	0.000	0.000	0.000	0.000	0.000	0.000	0.009	0.000	0.000	0.000	0.000	0.000	0.000	0.000	0.000	0.009	0.000	0.000	0.000
N2O	0.000	0.000	0.000	0.000	0.000	0.000	0.000	0.000	0.000	0.000	0.001	0.000	0.000	0.000	0.000	0.000	0.000	0.000	0.000	0.001	0.000	0.000	0.000
Total Flow n	6.940	5.894	5.852	1.046	1.046	1.046	10.000	10.000	11.046	11.046	11.302	5.894	1.046	6.940	0.750	10.000	0.500	2.132	0.550	11.302	0.041	1.711	1.590
Temperature	35	-25	15.01	-25	-22.94	180	350	130	327.64	900	900	15	15	-25	25	25	25	140	25	35	15.01	450	25
Pressure at	100	90	90	90	10	10	10	6.9	10	10	10	90	10	100	1	1	1	90	1	10	90	10	1
Enthalpy kW	-56.296	-17.641	-9.909	-74.420	-74.420	-42.020	96.830	33.460	54.810	272.505	32.092	-9.978	-70.973	-92.411	-6.046	-0.067	-37.268	7.386	-0.003	-355.942	-0.070	-420.845	-459.584
Entropy kJ/r	-0.048	-0.041	-0.036	-0.204	-0.203	-0.102	0.007	-0.005	-0.001	0.022	0.027	-0.036	-0.191	-0.066	0.003	0.004	-0.081	-0.023	0.000	-0.033	-0.036	-0.005	-0.171

Table B.2 Overall Exergy Loss for SMR based process

Exergy in	kW
CH ₄	415.83
Work	147.63
Water	1.224
Nitrogen	0.396
	565.08
Exergy out	kW
NO	88.98
Exergy Loss (kW)	476.11

Table B.3 Individual Component Exergy Loss for SMR based process

Blocks	Input---Output	$\Delta(E_{x_{ph}} + E_{x_{ch}})$	Ex_Q	Total Ex loss (kW)
Comp1	CH4---0	-3.19		3.19
Mixer1	0,2,Recy---3	5.16		5.16
Reformer	4---5	-57.97	62.07	4.10
Shift	6---7	6.52	-5.11	1.42
Mcomp	7---8	-4.63		4.63
Valve	12---13	7.66		7.66
Mixer2	Air,13---14	4.87		4.87
Combustor	14---15	18.66		18.66
Comp4	17,NIT---HYD	-13.12		13.12
Mixer3	HYD,24---18	2.19		2.19
Comp2	18---19	-5.68		5.68
AmmReac	20---21	33.72	-30.86	2.87
Flash	22---23,25	-0.63		0.63
Valve2	25---26	0.34		0.34
Mixer4	27,28---30	9.07		9.07
Comp3	AirNA---29	-62.07		62.07
NO reactor	31---32	257.66	-179.30	78.36
Split2	33---24,purge	0.00		0.00
Separator	9---10,11	-3.07		3.07
Split	10---Rec,12	0.01		0.01
Exhaust		47.72		47.72
HEN		200.95		200.95
TOTAL Ex loss (kW)				475.75

Table B.4 HEN Exergy Loss for SMR based process

T(°C)	mC _p	mC _{pint}	Q _{int}	Q _{cas}	T (K)	Exergy Factor	Exergy	Cumulative Ex (kW)
999.20	0.12	0.12	0.00	0.00	1272.35	839.72	0.00	0.00
910.00	-0.38	-0.26	10.91	10.91	1183.15	772.19	8.26	8.26
890.00	0.45	0.19	-5.16	5.75	1163.15	757.28	-3.85	4.41
890.00	480.80	480.99	0.00	5.75	1163.15	757.28	0.00	4.41
889.50	-480.80	0.19	240.50	246.24	1162.65	756.91	178.83	183.24
710.50	-178.98	-178.79	34.10	280.35	983.65	627.75	24.61	207.85
710.00	178.98	0.19	-89.39	190.95	983.15	627.41	-62.29	145.56
710.00	-0.17	0.02	0.00	190.95	983.15	627.41	0.00	145.56
690.00	0.18	0.20	0.41	191.36	963.15	613.53	0.29	145.84
460.00	-0.17	0.02	45.28	236.65	733.15	464.89	29.27	175.11
440.00	0.05	0.07	0.46	237.11	713.15	453.14	0.27	175.38
410.00	-0.19	-0.12	2.08	239.18	683.15	435.95	1.19	176.57
410.00	-0.24	-0.36	0.00	239.18	683.15	435.95	0.00	176.57
392.10	0.17	-0.19	-6.52	232.66	665.25	425.97	-3.64	172.93
390.00	0.23	0.04	-0.41	232.25	663.15	424.81	-0.23	172.71
390.00	110.78	110.82	0.00	232.25	663.15	424.81	0.00	172.71
389.50	-110.78	0.04	55.41	287.66	662.65	424.53	30.49	203.19
360.00	-0.30	-0.26	1.08	288.74	633.15	408.61	0.58	203.78
340.60	0.17	-0.09	-5.09	283.65	613.75	398.49	-2.66	201.12
337.60	0.38	0.29	-0.27	283.38	610.75	396.95	-0.14	200.98
290.00	21.28	21.57	13.89	297.28	563.15	373.55	6.83	207.81
290.00	-0.18	21.40	0.00	297.28	563.15	373.55	0.00	207.81
289.50	-21.28	0.12	10.70	307.97	562.65	373.31	5.03	212.85
190.98	0.19	0.31	11.40	319.37	464.13	332.18	4.76	217.60
190.98	-724.15	-723.84	0.00	319.37	464.13	332.18	0.00	217.60
190.88	724.15	0.31	-72.38	246.99	464.03	332.15	-25.88	191.72
190.88	-0.17	0.14	0.00	246.99	464.03	332.15	0.00	191.72
190.00	-0.18	-0.04	0.12	247.11	463.15	331.83	0.04	191.77
150.00	0.30	0.26	-1.51	245.60	423.15	318.77	-0.49	191.28
140.00	0.24	0.50	2.61	248.21	413.15	315.90	0.75	192.03
40.00	-0.12	0.38	50.42	298.63	313.15	298.52	8.76	200.78
35.00	0.17	0.55	1.91	300.54	308.15	298.32	0.08	200.86
25.00	0.18	0.73	5.51	306.05	298.15	298.16	0.09	200.95
25.00	-0.45	0.28	0.00	306.05	298.15	298.16	0.00	200.95
25.00	-0.23	0.05	0.00	306.05	298.15	298.16	0.00	200.95
25.00	-0.05	0.00	0.00	306.05	298.15	298.16	0.00	200.95

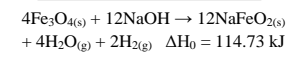
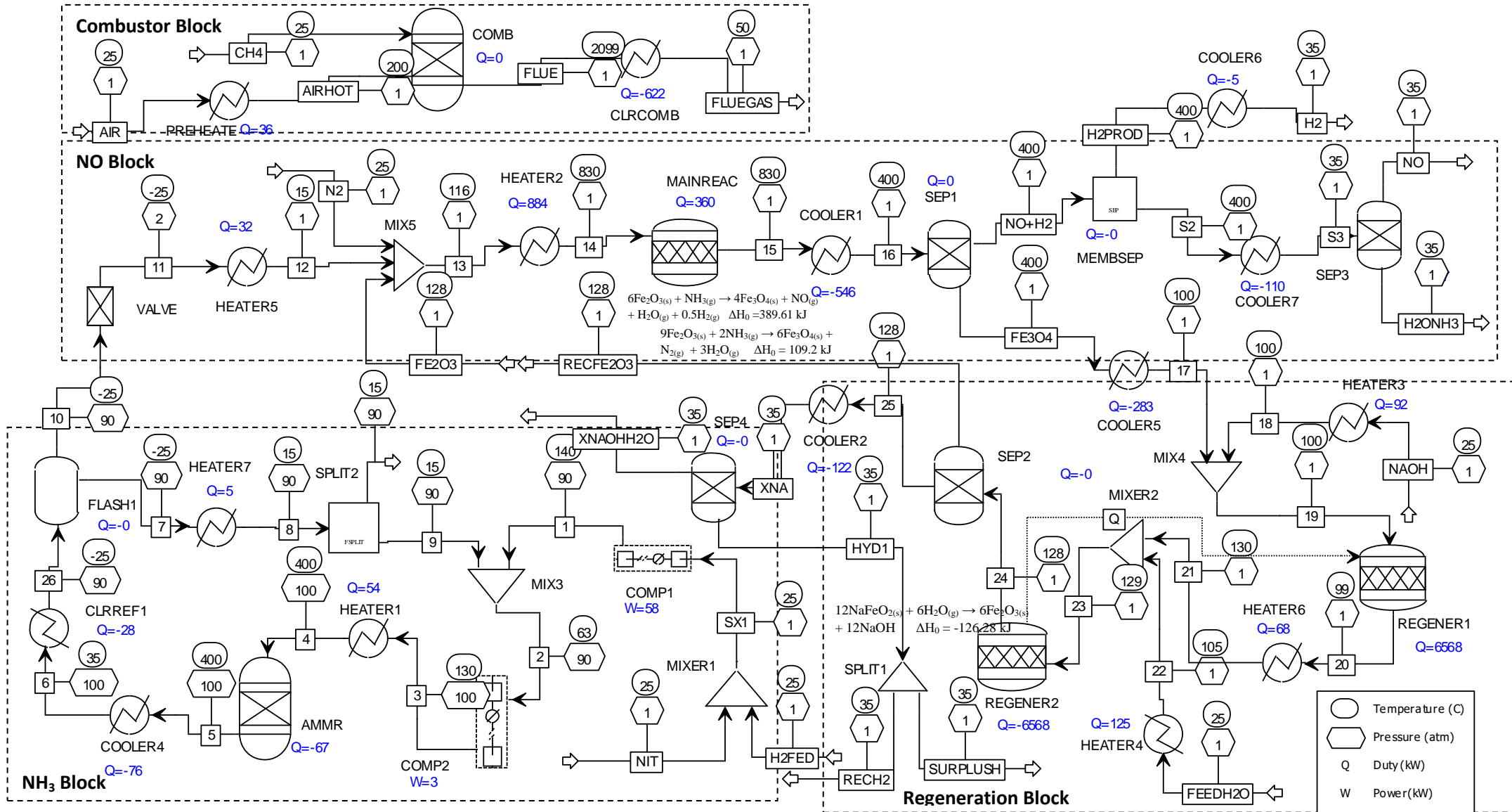


Figure B.3 Aspen Plus simulation flowsheet for CLHYD case

Table B.6 Overall Exergy Loss for CLHYD process

Exergy in	kW
CH ₄ (for heat)	598.8
Work	59.8
Water	1.93
Nitrogen	1.894
	662.42
Exergy out	kW
NO	88.98
H ₂	229.98
Exergy Loss (kW)	343.47

Table B.7 Individual Component Exergy Loss for CLHYD process

Blocks	Input---Output	$\Delta(\text{Ex}_{\text{ph}} + \text{Ex}_{\text{ch}})$	Ex _Q	Total Ex loss (kW)
Mixer1	NIT,H2feed---SX1	3.54		3.54
Comp1	SX1---1	-30.06		30.06
Mixer3	1,9---2	1.12		1.12
Comp2	2---3	-4.39		4.39
NH3 reactor	4---5	40.93	-37.12	3.82
Flash	6---7,10	-0.44		0.44
Valve	10---11	0.46		0.46
Mixer5	12,N2,Fe2O3---13	6.63		6.63
Reduction reactor	14---15	-234.37	262.55	28.18
Separator1	16---NOH2,Fe3O4	0.00		0.00
MEMBSEP	NO+H2---H2PROD,S2	-4.07		4.07
Separator3	S3---H2ONH3,NO	-0.15	-6.6	6.75
Mixer4	17,18---19	0.00		0.00
Regenerators	19---20 & 23---24	18.79		18.79
Mixer2	21,22---23	2.19		2.19
Separator2	24---25,RecFE2O3	0.00		0.00
Sepeartor4	XNA---HYD1,XNAOHH2O	0.037		0.037
Split	HYD2--- RECH2,SURPLUSH	0.00		0.08
Exhaust				54.02
HEN				181.16
TOTAL Ex loss (kW)				343.62

Figure B.3 represent the Aspen Plus simulated flowsheet for CLHYD process to produce NO and H₂. The Soave–Redlich–Kwong equation of state is used for simulation with component list restricted to Fe₂O₃, Fe₃O₄, NaOH, NaFeO₂, O₂, N₂, H₂O, NH₃, NO, CH₄, CO₂ and H₂. The flowsheet is divided into three sections, namely, ammonia block, nitric oxide block and

regeneration block having two regenerators. Table B.5 reports the stream summary of the simulated flowsheet. Table B.6 reports the overall exergy loss for CLHYD process which is about 343.4 kW. Table B.7 reports the exergy loss of individual process components whose summation comes out to be 343.62 kW. Table B.8 reports the exergy losses calculated for HEN.

Table B.8 HEN Exergy Loss for CLHYD process

T(°C)	mC _p	mC _{pint}	Q _{int}	Q _{cas}	T (K)	Exergy Factor	Exergy	Cumulative Ex (kW)
2088.5	0.30	0.30	0.00	0.00	2361.65	1744.61	0.00	0.00
840.5	-719.60	-719.30	379.00	379.00	1113.65	720.74	310.93	310.93
840	719.60	0.30	-359.65	19.35	1113.15	720.38	-263.34	47.60
840	-1.24	-0.94	0.00	19.35	1113.15	720.38	0.00	47.60
820	1.27	0.33	-18.70	0.65	1093.15	705.78	-13.65	33.95
410	-0.20	0.14	137.21	137.86	683.15	435.95	90.30	124.25
390	0.94	1.08	2.72	140.58	663.15	424.81	1.51	125.77
390	0.21	1.29	0.00	140.58	663.15	424.81	0.00	125.77
390	0.30	1.59	0.00	140.58	663.15	424.81	0.00	125.77
390	0.01	1.60	0.00	140.58	663.15	424.81	0.00	125.77
390	133.26	134.86	0.00	140.58	663.15	424.81	0.00	125.77
390	-1.27	133.59	0.00	140.58	663.15	424.81	0.00	125.77
389.5	-133.26	0.33	66.80	207.38	662.65	424.53	36.75	162.52
210	-0.20	0.13	59.57	266.95	483.15	339.23	28.31	190.83
140	0.20	0.33	9.02	275.97	413.15	315.90	3.01	193.84
140	-2.18	-1.85	0.00	275.97	413.15	315.90	0.00	193.84
126.4	1.24	-0.61	-25.19	250.78	399.55	312.28	-6.70	187.13
118	0.07	-0.54	-5.15	245.63	391.15	310.21	-1.27	185.87
118	1.31	0.77	0.00	245.63	391.15	310.21	0.00	185.87
115	-1.56	-0.79	2.30	247.93	388.15	309.51	0.54	186.41
110	-1.22	-2.01	-3.97	243.96	383.15	308.37	-0.90	185.51
108.8	2.18	0.17	-2.42	241.54	381.95	308.11	-0.53	184.97
90	-0.94	-0.78	3.12	244.67	363.15	304.36	0.62	185.60
40	-0.30	-1.08	-38.86	205.81	313.15	298.52	-4.53	181.06
35	0.20	-0.88	-5.40	200.40	308.15	298.32	-0.22	180.85
35	1.22	0.34	0.00	200.40	308.15	298.32	0.00	180.85
35	1.56	1.90	0.00	200.40	308.15	298.32	0.00	180.85
25	-0.30	1.60	19.01	219.41	298.15	298.16	0.31	181.16
25	-0.01	1.59	0.00	219.41	298.15	298.16	0.00	181.16
25	-0.07	1.52	0.00	219.41	298.15	298.16	0.00	181.16
25	-1.31	0.21	0.00	219.41	298.15	298.16	0.00	181.16
25	-0.21	0.00	0.00	219.41	298.15	298.16	0.00	181.16

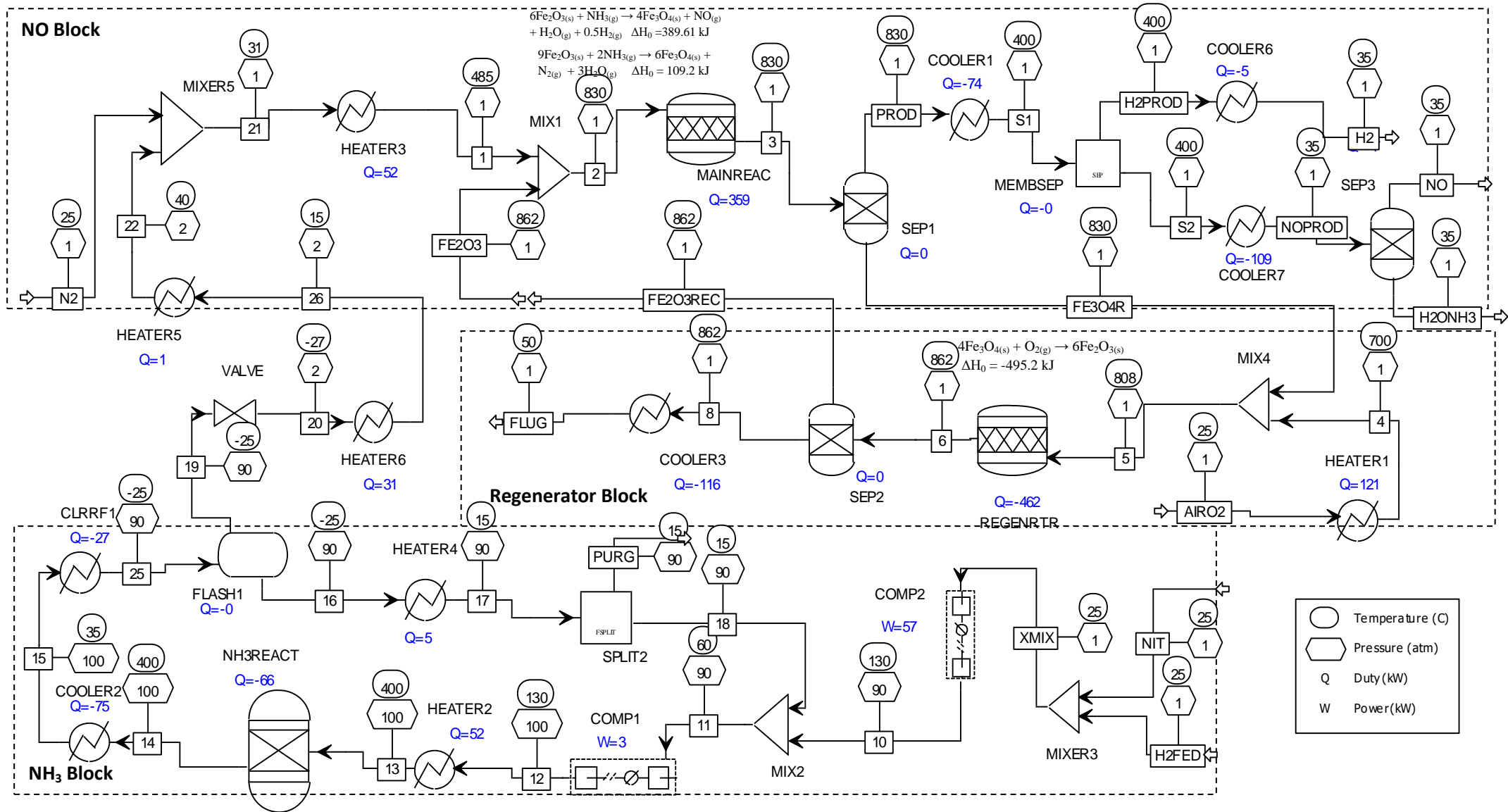


Figure B.4 Aspen Plus simulation flowsheet for CLAO case

Table B.9 Aspen Plus stream summary for CLAO process

Substream: MIXED	1	2	3	4	5	6	8	10	11	12	13	14	15	16	17	18	19	20	21	22
Mole Flow mol/sec																				
H2	0.002	0.002	0.505	0.000	0.000	0.000	0.000	1.900	4.745	4.745	4.745	2.861	2.861	2.859	2.859	2.845	0.002	0.002	0.002	0.002
N2	2.001	2.001	2.120	4.582	4.582	4.582	4.582	0.634	1.633	1.633	1.633	1.005	1.005	1.004	1.004	0.999	0.001	0.001	2.001	0.001
O2	0.000	0.000	0.000	1.218	1.218	0.033	0.033	0.000	0.000	0.000	0.000	0.000	0.000	0.000	0.000	0.000	0.000	0.000	0.000	0.000
H3N	1.255	1.255	0.011	0.000	0.000	0.000	0.000	0.000	0.087	0.087	0.087	1.343	1.343	0.087	0.087	0.087	1.255	1.255	1.255	1.255
H2O	0.000	0.000	1.363	0.000	0.000	0.000	0.000	0.000	0.000	0.000	0.000	0.000	0.000	0.000	0.000	0.000	0.000	0.000	0.000	0.000
NO	0.000	0.000	1.006	0.000	0.000	0.000	0.000	0.000	0.000	0.000	0.000	0.000	0.000	0.000	0.000	0.000	0.000	0.000	0.000	0.000
Total Flow mol/sec	3.259	3.259	5.006	5.800	5.800	4.615	4.615	2.534	6.465	6.465	6.465	5.209	5.209	3.951	3.951	3.931	1.259	1.259	3.259	1.259
Temperature C	485.00	829.89	830.00	700.00	808.40	862.00	862.00	130.00	59.66	130.00	400.00	400.00	35.00	-25.00	15.00	15.00	-25.00	-27.26	30.68	40.00
Pressure atm	1.00	1.10	1.00	1.00	1.00	1.00	1.00	89.90	90.00	99.90	100.00	100.00	100.00	90.00	90.00	90.00	90.00	1.50	1.00	2.00
Enthalpy kW	-5.328	40.622	-107.036	120.845	141.782	119.748	119.748	8.030	2.915	16.601	68.805	2.325	-72.351	-9.946	-5.141	-5.115	-89.568	-89.568	-57.095	-57.082
Entropy kJ/mol-K	0.000	0.014	0.043	0.040	0.044	0.041	0.041	-0.024	-0.031	-0.026	-0.010	-0.029	-0.062	-0.040	-0.035	-0.035	-0.204	-0.203	-0.032	-0.103
Substream: CISOLID																				
FE3O4	0.000	0.000	4.738	0.000	4.738	0.000	0.000	0.000	0.000	0.000	0.000	0.000	0.000	0.000	0.000	0.000	0.000	0.000	0.000	0.000
FE2O3	0.000	7.200	0.093	0.000	0.093	7.200	0.000	0.000	0.000	0.000	0.000	0.000	0.000	0.000	0.000	0.000	0.000	0.000	0.000	0.000
Total Flow mol/sec	0.000	7.200	4.831	0.000	4.831	7.200	0.000	0.000	0.000	0.000	0.000	0.000	0.000	0.000	0.000	0.000	0.000	0.000	0.000	0.000
Temperature C		829.89	830.00		808.40	862.00														
Pressure atm	1.00	1.10	1.00	1.00	1.00	1.00	1.00	89.90	90.00	99.90	100.00		100.00	90.00	90.00	90.00	90.00	90.00	1.50	1.00
Enthalpy kW		-5068.268	-4561.903		-4582.840	-5022.317														
Entropy kJ/mol-K		-0.090	-0.081	0.000	-0.085	-0.084	0.000	0.000	0.000	0.000	0.000	0.000	0.000	0.000	0.000	0.000	0.000	0.000	0.000	0.000
MIXED	25	26	AIRO2	FE2O3	FE2O3REC	FE3O4R	FLUG	H2	H2FED	H2ONH3	H2PROD	N2	NIT	NO	NOPROD	PROD	PURG	S1	S2	XMIX
Mole Flow mol/sec																				
H2	2.861	0.002	0.000	0.000	0.000	0.000	0.000	0.505	1.900	0.000	0.505	0.000	0.000	0.000	0.000	0.505	0.014	0.505	0.000	1.900
N2	1.005	0.001	4.582	0.000	0.000	0.000	4.582	0.000	0.000	0.000	0.000	2.000	0.634	2.120	2.120	2.120	0.005	2.120	2.120	0.634
O2	0.000	0.000	1.218	0.000	0.000	0.000	0.033	0.000	0.000	0.000	0.000	0.000	0.000	0.000	0.000	0.000	0.000	0.000	0.000	0.000
H3N	1.343	1.255	0.000	0.000	0.000	0.000	0.000	0.000	0.000	0.011	0.000	0.000	0.000	0.000	0.011	0.011	0.000	0.011	0.011	0.000
H2O	0.000	0.000	0.000	0.000	0.000	0.000	0.000	0.000	0.000	1.363	0.000	0.000	0.000	0.000	1.363	1.363	0.000	1.363	1.363	0.000
NO	0.000	0.000	0.000	0.000	0.000	0.000	0.000	0.000	0.000	0.005	0.000	0.000	0.000	1.001	1.006	1.006	0.000	1.006	1.006	0.000
Total Flow r	5.209	1.259	5.800	0.000	0.000	0.000	4.615	0.505	1.900	1.380	0.505	2.000	0.634	3.121	4.501	5.006	0.020	5.006	4.501	2.534
Temperature C	-25.00	15.00	25.00				50.00	35.00	25.00	35.00	400.00	25.00	25.00	35.00	35.00	830.00	15.00	400.00	400.00	24.96
Pressure atm	90.00	2.00	1.00	1.00	1.00	1.00	1.00	1.00	1.00	1.00	1.00	1.00	1.00	1.00	1.00	1.00	90.00	1.00	1.00	1.00
Enthalpy kW	-99.504	-58.221	-0.039				3.339	0.146	0.002	-393.353	5.535	-0.012	-0.004	91.201	-295.483	-107.036	-0.026	-180.731	-186.269	-0.002
Entropy kJ/r	-0.080	-0.106	0.004	0.000	0.000	0.000	0.003	0.001	0.000	-0.168	0.024	0.000	0.000	0.010	-0.039	0.043	-0.035	0.026	0.023	0.005
Substream: CISOLID																				
FE3O4	0.000	0.000	0.000	0.000	0.000	4.738	0.000	0.000	0.000	0.000	0.000	0.000	0.000	0.000	0.000	0.000	0.000	0.000	0.000	0.000
FE2O3	0.000	0.000	0.000	7.200	7.200	0.093	0.000	0.000	0.000	0.000	0.000	0.000	0.000	0.000	0.000	0.000	0.000	0.000	0.000	0.000
Total Flow r	0.000	0.000	0.000	7.200	7.200	4.831	0.000	0.000	0.000	0.000	0.000	0.000	0.000	0.000	0.000	0.000	0.000	0.000	0.000	0.000
Temperature C				862.00	862.00	830.00														
Pressure atm		2.00	1.00	1.00	1.00	1.00	1.00	1.00	1.00	1.00	1.00	1.00	1.00	1.00	1.00	1.00	90.00	1.00	1.00	1.00
Enthalpy kW				-5022.317	-5022.317	-4561.903														
Entropy kJ/r	0.000	0.000	0.000	-0.084	-0.084	-0.081	0.000	0.000	0.000	0.000	0.000	0.000	0.000	0.000	0.000	0.000	0.000	0.000	0.000	0.000

Table B.10 Overall Exergy Loss for CLAO process

Exergy in	kW
H ₂	448.61
Work	59.8
Nitrogen	1.89
	510.29
Exergy out	kW
NO	88.98
H ₂	119.21
Exergy Loss (kW)	302.12

Table B.11 Individual Component Exergy Loss for CLAO process

Blocks	Input---Output	$\Delta(E_{x_{ph}} + E_{x_{ch}})$	Ex _Q	Total Ex loss (kW)
Mixer3	Nit,H2fed--Xmix	3.53		3.53
Comp2	Xmix---10	-29.74		29.74
Mixer2	10,18--11	0.89		0.89
Comp1	11---12	-4.32		4.32
NH3 reactor	13---14	40.82	-37.03	3.78
Flash	25---16,19	0.01		0.01
Valve	19---20	0.48		0.48
Mixer5	N2,22---21	7.50		7.50
Mixer1	1,Fe2O3--2	1.83		1.83
Main reactor	2----3	-232.92	261.75	28.83
Seperator1	3---Prrod,Fe3O4R	0.00		0.00
Split	17----18,purge	0.00		0.00
Seperator3	NOPROD--NO,NH3H2O	-0.16	-6.75	6.91
Mixer4	Fe3O4R,4--5	0.37		0.37
Regenerator	5--6	385.11	-375.18	9.93
Seperator2	6---8,Fe2O3Rec	0.00		0.00
MembSep	S1----S2, H2Prod	-4.06		4.06
Exhaust				13.80
HEN		185.06		185.14
TOTAL Ex loss (kW)				301.05

Figure B.4 represent the Aspen Plus simulated flowsheet for CLAO process to produce NO and H₂. The Soave–Redlich–Kwong equation of state is used for simulation with component list restricted to Fe₂O₃, Fe₃O₄, O₂, N₂, H₂O, NH₃, NO and H₂. The flowsheet is divided into three sections, namely, ammonia block, nitric oxide block and regeneration block. Table B.9

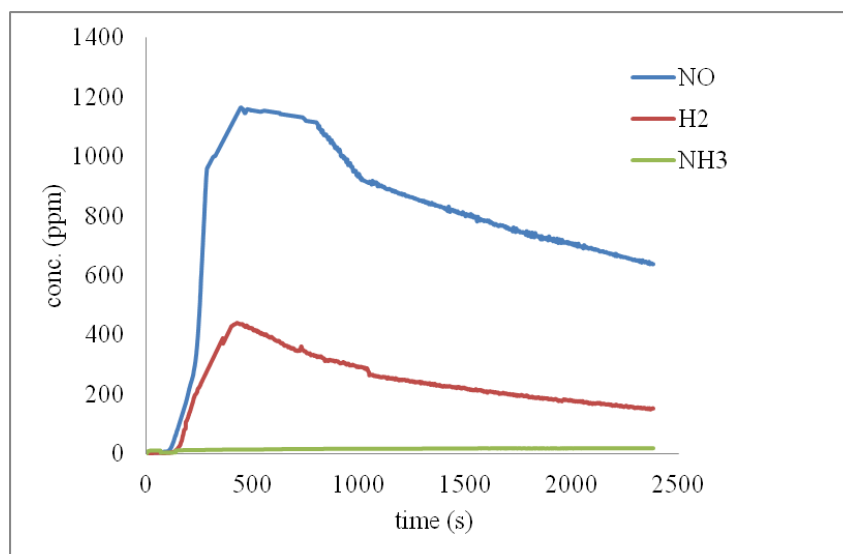
reports the stream summary of the simulated flowsheet. Table B.10 reports the overall exergy loss for CLAO process which is about 302.12 kW. Table B.11 reports the exergy loss of individual process components whose summation comes out to be 301.05 kW. Table B.12 reports the exergy losses calculated for HEN.

Table B.12 HEN Exergy Loss for CLAO process

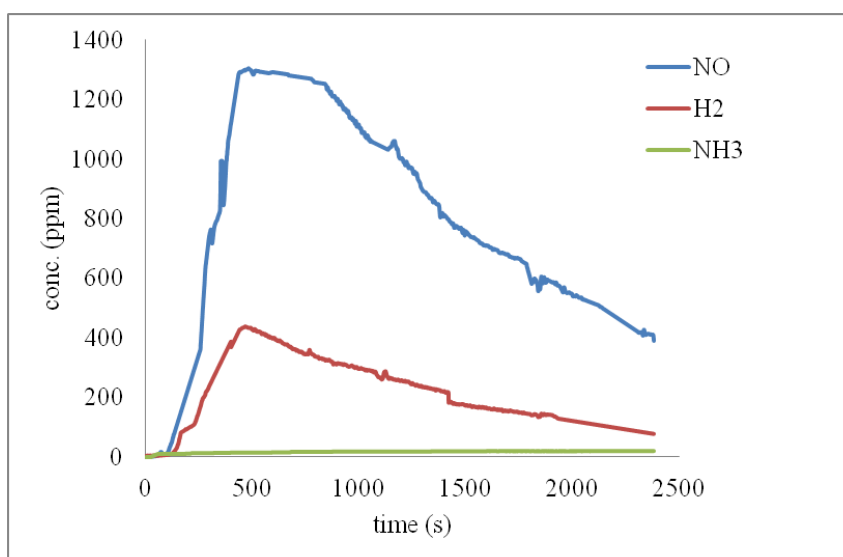
T(°C)	mC _p	mC _{pint}	Q _{int}	Q _{cas}	T (K)	Exergy Factor	Exergy	Cumulative Ex (kW)
852	923.0	923.00	0.00	0.00	1125.15	729.18	0.00	0.00
852	0.14	923.14	0.00	0.00	1125.15	729.18	0.00	0.00
851.5	-923.0	0.14	461.57	461.57	1124.65	728.81	339.23	339.23
840	-3587.0	-3586.86	1.65	463.22	1113.15	720.38	1.21	340.44
839.9	3587.0	0.14	-358.69	104.53	1113.05	720.30	-262.61	77.83
820	0.17	0.31	2.85	107.39	1093.15	705.78	2.08	79.91
710	-0.18	0.14	34.62	142.01	983.15	627.41	24.67	104.58
495	-0.11	0.02	29.16	171.16	768.15	485.98	19.18	123.76
410	-0.19	-0.17	1.84	173.00	683.15	435.95	1.08	124.84
390	132.96	132.79	-3.43	169.57	663.15	424.81	-1.91	122.93
390	0.30	133.09	0.00	169.57	663.15	424.81	0.00	122.93
390	0.20	133.29	0.00	169.57	663.15	424.81	0.00	122.93
390	0.01	133.31	0.00	169.57	663.15	424.81	0.00	122.93
390	-0.17	133.14	0.00	169.57	663.15	424.81	0.00	122.93
389.5	-132.96	0.18	66.57	236.14	662.65	424.53	36.63	159.56
140	0.19	0.37	43.79	279.92	413.15	315.90	19.07	178.62
50	-0.05	0.32	33.19	313.12	323.15	299.15	6.18	184.80
40.7	0.11	0.44	3.01	316.12	313.85	298.56	0.19	184.99
40	-0.14	0.29	0.31	316.43	313.15	298.52	0.01	185.01
35	0.18	0.47	1.47	317.90	308.15	298.32	0.06	185.06
25	0.05	0.52	4.73	322.63	298.15	298.16	0.08	185.14
25	-0.30	0.22	0.00	322.63	298.15	298.16	0.00	185.14
25	-0.20	0.01	0.00	322.63	298.15	298.16	0.00	185.14
25	-0.01	0.00	0.00	322.63	298.15	298.16	0.00	185.14

APPENDIX C

ADDITIONAL EXPERIMENTAL RESULTS



(a) 810 °C



(b) 840 °C

Figure C.1 Effect of temperature (Operating conditions: 15 g CuO (100-120 micron), 2300 ppm NH₃ (4.8 ml/min NH₃ and 2100 ml/min N₂))

REFERENCES

- Abanades, S., Charvin, P., Flamant, G. & Neveu, P., 2006. Screening of water-splitting thermochemical cycles potentially attractive for hydrogen production by concentrated solar energy. *Energy*, 31(14), pp.2805–2822.
- Adanez, J., Abad, A., Garcia-labiano, F., Gayan, P. & de Diego, L.F., 2012. Progress in chemical-looping combustion and reforming technologies. *Progress in Energy and Combustion Science*, 38(2), pp.215–282.
- Adhikari, S. & Fernando, S., 2006. Hydrogen Membrane Separation Techniques. *Industrial & Engineering Chemistry Research*, 45, pp.875–881.
- Afgan, N.H. & Carvalho, M.G., 2002. Multi-criteria assessment of new and renewable energy power plants. *Energy*, 27, pp.739–755.
- Alonso, J.A. & Lamata, M., 2006. Consistency in the analytic hierarchy process: a new approach. *International Journal of Uncertainty, Fuzziness and Knowledge-Based Systems*, 14(4), pp.445–459.
- Amores, J.M.G., Sanchez, E.V., Ramis, G. & Busca, G., 1997. An FT-IR study of ammonia adsorption and oxidation over anatase-supported metal oxides. *Applied Catalysis B: Environmental*, 13(1), pp.45–58.
- Armaroli, N. & Balzani, V., 2011. The hydrogen issue. *ChemSusChem*, 4(1), pp.21–36.
- Aspentech, 2011. Aspen Plus: Getting started building and running a process model. Available at: http://support.aspentech.com/Public/Documents/Engineering/Aspen%20Plus/V7.3/AspenPlusUserModelsV7_3-Ref.pdf
- Ataei, A., 2011. Application of combined pinch and exergy analysis in retrofit of an olefin plant for energy conservation. *Scientific research and Essays*, 6(12), pp.2437–2446.
- Ataei, A. & Yoo, C., 2010. Combined pinch and exergy analysis for energy efficiency optimization in a steam power plant. *International Journal of the Physical Sciences*, 5(July), pp.1110–1123.
- Bamberger, C.E. & Richardson, D.M., 2000. Hydrogen production from water by thermochemical cycles. *Cryogenics*, (April 1976), pp.197–208.
- Bandyopadhyay, S. & Sahu, G.C., 2010. Modified problem table algorithm for energy targeting. *Industrial & Engineering Chemistry Research*, 49, pp.11557–11563.
- Bartels, J.R., Pate, M.B. & Olson, N.K., 2010. An economic survey of hydrogen production from conventional and alternative energy sources. *International Journal of Hydrogen Energy*, 35(16), pp.8371–8384.
- Bejan, A., 1988. *Advanced Engineering Thermodynamics*, USA: John Wiley & Sons.
- Bejan, A., 2002. Fundamentals of exergy analysis, entropy generation minimization, and the generation of flow architecture. *International Journal of Energy Research*, 26(7), pp.545–565.
- Birkeland-Eyde Process. *Wikipedia*. Available at: http://en.wikipedia.org/wiki/Birkeland-Eyde_process.

- Boyano, A., Blanco-Marigorta, A.M., Morosuk, T. & Tsatsaronis, G., 2011. Exergoenvironmental analysis of a steam methane reforming process for hydrogen production. *Energy*, 36(4), pp.2202–2214.
- Cetinkaya, E., Dincer, I. & Naterer G.F., 2011. Life cycle assessment of various hydrogen production methods. *International Journal of Hydrogen Energy*, 37(3), pp.2071–2080.
- Charvin, P., Abanades, S., Lemort, F. & Flamant G., 2008. Analysis of solar chemical processes for hydrogen production from water splitting thermochemical cycles. *Energy Conversion and Management*, 49(6), pp.1547–1556.
- Charvin, P., Abanades, S., Lemort, F. & Flamant G., 2007. Hydrogen production by three-step solar thermochemical cycles using hydroxides and metal oxide systems. *Energy & Fuels*, 21(5), pp.2919–2928.
- Charvin, P., Abanades, S., Lemort, F. & Flamant G., 2007. Two-step water splitting thermochemical cycle based on iron oxide redox pair for solar hydrogen production. *Energy*, 32(7), pp.1124–1133.
- Chatzimouratidis, A.I. & Pilavachi, P.A., 2007. Objective and subjective evaluation of power plants and their non-radioactive emissions using the analytic hierarchy process. *Energy Policy*, 35, pp.4027–4038.
- Chemical Economics Handbook, Nitric Acid. Available at: <https://www.ihs.com/products/nitric-acid-chemical-economics-handbook.html> [Accessed November 18, 2015].
- Chemical Engineering Online. Available at: <http://www.chemengonline.com/pci-home> [Accessed November 18, 2015]
- Chen, C.S., Murad, F., Smith, K., Seitz, W., Merrell, W.J. & Balaban, A.T., 2014. Extended production of nitric oxide from microencapsulated chemical reactants. U.S. Patent No. 20140056957, 27 February 2014.
- Chmielarz, L. Kuśtrowski, P., Dziembaj, R., Cool, P. & Vansant, E., 2006. Catalytic performance of various mesoporous silicas modified with copper or iron oxides introduced by different ways in the selective reduction of NO by ammonia. *Applied Catalysis B: Environmental*, 62(3-4), pp.369–380.
- Chmielarz, L., Kuśtrowski, P., Rafalska-Łasocha, A. & Dziembaj, R., 2005. Selective oxidation of ammonia to nitrogen on transition metal containing mixed metal oxides. *Applied Catalysis B: Environmental*, 58(3-4), pp.235–244.
- Chui, F., Elkamel, A. & Fowler M., 2005. Analytic Hierarchy Process and Life Cycle Analysis for the assessment of hydrogen production pathways. In *Proceedings International Hydrogen Energy Congress and Exhibition*. pp. 13–15.
- Connor, H., 1967. The manufacture of nitric acid : The role of platinum alloy gauzes in the ammonia oxidation process. *Platinum Metals Rev.*, 11(1), pp.2–9.
- Cormos, C.C., 2011. Hydrogen production from fossil fuels with carbon capture and storage based on chemical looping systems. *International Journal of Hydrogen Energy*, 36(10), pp.5960–5971.
- Darvell, L.I., Heiskanen, K., Jones, J.M., Ross, B., Simell, P. & Williams, A., 2003. An investigation of alumina-supported catalysts for the selective catalytic oxidation of ammonia in biomass gasification. *Catalysis Today*, 81(4), pp.681–692.

- Dincer, I. & Rosen, M., 2013. *Exergy: Energy, Environment And Sustainable Development* 2nd ed., Oxford: Elsevier Ltd.
- Dowden, D. & Wells, D., 1961. A Crystal field interpretation of some activity patterns. In *Actes 2e Congr. Int. Catalyse ed Technip*. Paris.
- Dufour, J., Serrano, D.P., Galvez, J.L., Gonzalez, A., Soria, E. & Fierro, J.L., 2011. Life cycle assessment of alternatives for hydrogen production from renewable and fossil sources. *International Journal of Hydrogen Energy*, 7, pp.1173–1183.
- Duo, W., Dam-Johansen, K. & Ostergaard K., 1992. Kinetics of the gas-phase reaction between nitric oxide, ammonia and oxygen. *The Canadian Journal of Chemical Engineering*, 70, pp.1014–1020.
- Echegaray, F., Velloso, A. & Wagner, M., 2000. Method and production of nitric acid. U.S. Patent No. 6165435, 26 December 2000.
- Edrisi, A., Mansoori, Z. & Dabir B., 2014. Using three chemical looping reactors in ammonia production process - A novel plant configuration for a green production. *International Journal of Hydrogen Energy*, 39(16), pp.8271–8282.
- Edrisi, A., Mansoori, Z., Dabir, B. & Shahnazari, A., 2014. Hydrogen, nitrogen and carbon dioxide production through chemical looping using iron-based oxygen carrier – A Green plant for H₂ and N₂ production. *International Journal of Hydrogen Energy*, 39(20), pp.10380–10391.
- Eller, K., Henkes, E., Roszbacher, R. & Höke, H., 2012. Ammonia. In *Ullmann's Encyclopedia of Industrial Chemistry*. pp. 647–698.
- Evarestov, R.A. & Veryazov, V.A., 1990. The electronic structure of copper oxide crystalline compounds. *Physica Status Solidi B-Basic Research*, 157(I), pp.281–291.
- Fontijn, A. & Kurzius, S., 1971. *Kinetics of iron and aluminium oxidation by oxygen*, Princeton, New Jersey.
- Galvez, M.E., Frei, A., Halmann, M. & Steinfeld, A., 2007. Ammonia production via a two-step Al₂O₃/AlN thermochemical cycle. 2. Kinetic analysis. *Industrial & Engineering Chemistry Research*, 46, pp.2047–2053.
- Granovskii, M., Dincer, I. & Rosen, M.A., 2006. Life cycle assessment of hydrogen fuel cell and gasoline vehicles. *International Journal of Hydrogen Energy*, 31, pp.337–352.
- Hajjaji, N., Pons, M., Houas, A. & Renaudin, V., 2012. Exergy analysis : An efficient tool for understanding and improving hydrogen production via the steam methane reforming process. *Energy Policy*, 42, pp.392–399.
- Han, T., Hong, H., He, F. & Jin, H., 2012. Reactivity study on oxygen carriers for solar-hybrid chemical-looping combustion of di-methyl ether. *Combustion and Flame*, 159(5), pp.1806–1813.
- Hanak, D.P., Biliyok, C., Yeung, H. & Bialecki, R., 2014. Heat integration and exergy analysis for a supercritical high-ash coal-fired power plant integrated with a post-combustion carbon capture process. *Fuel*, 134, pp.126–139.
- He, X. & Hägg, M.B., 2012. Membranes for environmentally friendly energy processes. *Membranes*, 2(4), pp.706–726.

- Heo, E., Kim, J. & Cho, S., 2012. Selecting hydrogen production methods using fuzzy analytic hierarchy process with opportunities, costs, and risks. *International Journal of Hydrogen Energy*, 37(23), pp.17655–17662.
- HSC Chemistry. *Outotec*. Available at: <http://www.outotec.com/HSC> [Accessed October 5, 2015].
- Hunt, L.B., 1958. The ammonia oxidation process for nitric acid manufacture. *Platinum Metals Rev.*, 2(4), pp.129–134.
- Hydrogen generation market by geography, by mode of generation & delivery, by applications and by technology - Global trends & forecasts to 2019. *MarketsandMarkets Analysis*. Available at: <http://www.marketsandmarkets.com/PressReleases/hydrogen.asp> [Accessed May 28, 2015].
- Il'chenko, N.I., 1976. Catalytic oxidation of ammonia. *Russian Chemical Reviews*, 45(12), pp.1119–1136.
- Jabłońska, M., Chmielarz, L., Węgrzyn, A. & Witkowski, S., 2012. Mixed metal oxides Mg-Cu-Fe obtained from hydrotalcites as catalysts for selective oxidation of ammonia to nitrogen and water vapour (SCO). *Chemik*, 66(7), pp.750–757.
- Jockers, K., Krauss, K. & Theobald, H., 1970. Production of high percentage nitric oxide. U.S. Patent No. 3489515, 13 January 1970.
- Joesten, M.D., Hogg, J.L. & Castellion, M.E., 2006. *The World of Chemistry: Essentials: Essentials*, Thomson Brooks/Cole, USA.
- Kabir, G., Sadiq, R. & Tesfamariam, S., 2013. A review of multi-criteria decision-making methods for infrastructure management. *Structure and Infrastructure Engineering: Maintenance, Management 2013, Life-Cycle Design and Performance*, pp.37–41.
- Kalamaras, C.M. & Efstathiou, A.M., 2013. Hydrogen production technologies : Current state and future developments. In *Conference Papers in Energy*. Hindawi Publishing Corporation.
- Kebede, M., Varner, M.E., Scharko, N.K., Gerber, R.B. & Raff, J.D., 2013. Photooxidation of ammonia on TiO₂ as a source of NO and NO₂ under atmospheric conditions. *Journal of the American Chemical Society*, 135(23), pp.8606–8615.
- Khaleduzzaman, S.S., Saidur, R., Mahbulul, I.M., Ward, T.A., Soheli, M.R., Shahrul, I.M., Selvaraj, J. & Rahman, M.M., 2014. Energy, exergy, and friction factor analysis of nanofluid as a coolant for electronics. *Industrial & Engineering Chemistry Research*, 53, pp.10512–10518.
- Kirova-Yordanova, Z., 2011. Application of the exergy method to the environmental impact estimation: The nitric acid production as a case study. *Energy*, 36(6), pp.3733–3744.
- Kiselev, V.F. & Krylov, O. V, 1989. *Adsorption and Catalysis on Transition Metals and their Oxides* 1st ed., Berlin Heidelberg: Springer-Verlag.
- Kolbitsch, P., Bolhar-Nordenkamp, J., Proll, T. & Hofbauer, H., 2009. Comparison of two Ni-Based oxygen carriers for chemical looping combustion of natural gas in 140 kW continuous looping operation. *Industrial & Engineering Chemistry Research*, 48, pp.5542–5547.

- Koroneos, C., Dompros, A., Roumbas, G. & Moussiopoulos, N., 2005. Advantages of the use of hydrogen fuel as compared to kerosene. *Resources, Conservation and Recycling*, 44(2), pp.99–113.
- Koroneos, C., 2004. Life cycle assessment of hydrogen fuel production processes. *International Journal of Hydrogen Energy*, 29(14), pp.1443–1450.
- Koroneos, C. & Rovas, D., 2012. A review on exergy comparison of hydrogen production methods from renewable energy sources. *Energy & Environmental Science*, 5, pp.6640–6651.
- Koroneos, C., Spachos, T. & Moussiopoulos, N., 2003. Exergy analysis of renewable energy sources. *Renewable Energy*, 28(2), pp.295–310.
- Kosaki, Y., Miyamoto, A. & Murakami, Y., 1982. Bifunctional oxidation of ammonia with metal oxide-Pt/Al₂O₃ by Mechanical mixtures. *Bulletin of the chemical society of Japan*, 55, pp.63–68.
- Kosaki, Y., Miyamoto, A. & Murakami, Y., 1979. Oxidation of ammonia with lattice oxygen of metal oxides by pulse reaction technique. *Bulletin of the chemical society of Japan*, 52(2), pp.617–618.
- Kotas T J, 1995. *The Exergy Method of Thermal Plant Analysis* Reprint., Krieger Publishing Company, Malabar, Florida.
- Kothari, R., Buddhi, D. & Sawhney, R.L., 2008. Comparison of environmental and economic aspects of various hydrogen production methods. *Renewable and Sustainable Energy Reviews*, 12, pp.553–563.
- Lee, S.K., Mogi, G. & Kim, J.W., 2008. The competitiveness of Korea as a developer of hydrogen energy technology: The AHP approach. *Energy Policy*, 36(4), pp.1284–1291.
- Leigh, G.J., 2004. *The world's greatest fix: a history of nitrogen and agriculture*, USA: Oxford University Press.
- Li, K., 2013. Comparison of geothermal with solar and wind power generation. In *Thirty-Eighth Workshop on Geothermal reservoir Engineering*. Stanford: Stanford University.
- Lyngfelt, A., 2014. Chemical-looping combustion of solid fuels – Status of development. *Applied Energy*, 113, pp.1869–1873.
- Mansilla, C., Baurens, P., Noirot, I., Carles, P., Duhamet, J., Leybros, J., Saturnin, A., Gilardi, T., Poitou, S., Naour, F., Robin, J. & Yvon, P., 2010. Performance and economic competitiveness comparison of advanced hydrogen production processes. In *18th World Energy Conference 2010*. pp. 503–508.
- Michalsky, R., Parman, B., Amanor-Boadu, V. & Pfromm, P., 2012. Solar thermochemical production of ammonia from water, air and sunlight: Thermodynamic and economic analyses. *Energy*, 42(1), pp.251–260.
- Michalsky, R. & Pfromm, P., 2011. Chromium as reactant for solar thermochemical synthesis of ammonia from steam, nitrogen, and biomass at atmospheric pressure. *Solar Energy*, 85(11), pp.2642–2654.
- Miyamoto, A., Kosaki, Y. & Murakami, Y., 1978. Synergy in the oxidation of ammonia

- with metal oxide-Pt/Al₂O₃ mechanical mixtures. *Chemistry Letters*, pp.397–400.
- Modarresi, A., Kravanja, P. & Friedl, A., 2012. Pinch and exergy analysis of lignocellulosic ethanol, biomethane, heat and power production from straw. *Applied Thermal Engineering*, 43, pp.20–28.
- Moghtaderi, B., 2012. Review of the recent chemical looping process developments for novel energy and fuel applications. *Energy and Fuels*, 26(1), pp.15–40.
- Mueller-Langer, F., Tzimas, E., Kaltschmitt, M. & Peteves, S., 2007. Techno-economic assessment of hydrogen production processes for the hydrogen economy for the short and medium term. *International Journal of Hydrogen Energy*, 32(16), pp.3797–3810.
- Nam, C.H., Pfeffer, R., Dave, R.N. & Sundaresan, S., 2004. Aerated vibrofluidization of silica nanoparticles. *AIChE Journal*, 50(8), pp.1776–1785.
- Neelis, M., 2004. Exergetic life cycle analysis of hydrogen production and storage systems for automotive applications. *International Journal of Hydrogen Energy*, 29(5), pp.537–545.
- Niazi, S.K., 2012. Multiuse reactors and related methods. U.S. Patent No. 0231504 A1, 13 September 2012.
- 2019 Nitric oxide Industry (CAS 10102-43-9) Analysis For World and China. *Market Research*. Available at: <http://www.solarplaza.com/pressrelease/2019-nitric-oxide-industry-cas-10102-43-9-analysis>.
- Noelker, K., Ruether, J. & GmbH, U., 2011. Low energy consumption ammonia production : baseline energy consumption, options for energy optimization motivation. In *Nitrogen + syngas Conference*. Duesseldorf, pp. 1–14.
- Paniagua, I.L., Martin, J.R., Fernandez, C.G., Alvaro, A.J. & Carlier, R.N., 2013. A new simple method for estimating exergy destruction in heat exchangers. *Entropy*, 15, pp.474–489.
- Papalexandrou, M.A., Pilavachi, P.A. & Chatzimouratidis, A.A., 2008. Evaluation of liquid bio-fuels using the Analytic Hierarchy Process. *Process Safety and Environmental Protection*, 86(5), pp.360–374.
- Perkins, C. & Weimer, A.W., 2004. Likely near-term solar-thermal water splitting technologies. *International Journal of Hydrogen Energy*, 29, pp.1587–1599.
- Peters, M., Timmerhaus, K.D. & West, R.E., 2003. *Plant Design and Economics for Chemical Engineers*. McGraw-Hill Chemical Engineering Series.
- Pilavachi, P.A., Chatzipanagi, A.I. & Spyropoulou, A.I., 2009. Evaluation of hydrogen production methods using the Analytic Hierarchy Process. *International Journal of Hydrogen Energy*, 34(13), pp.5294–5303.
- Quevedo, J.A., Omosebi, A. & Pfeffer, R., 2010. Fluidization enhancement of agglomerates of metal oxide nanopowders by microjets. *AIChE*, 56(6).
- Ramsden, T., Steward, D. & Zuboy, J., 2009. *Analyzing the Levelized Cost of Centralized and Distributed Hydrogen Production Using the H2A Production Model , Version 2 Analyzing the Levelized Cost of Centralized and Distributed Hydrogen Production Using the H2A Production Model , Version 2*, Colorado.

- Ray, J.D. & Ogg, R.A., 1956. A new method of preparing nitric oxide. *Journal of the American Chemical Society*, 78 (23)(1), pp.5993–5993.
- Roeb, M., Sattler, C., Klüser, R., Monnerie, N., de Oliveira, L., Konstandopoulos, A.G., Agrafiotis, C., Zaspalis, V.T., Nalbandian, L., Steele, A. & Stobbe, P., 2006. Solar hydrogen production by a two-step cycle based on mixed iron oxides. *Journal of Solar Energy Engineering*, 128(2), p.125.
- Rosen, M.A. & Scott, D.S., 1998. Comparative efficiency assessments for a range of hydrogen production processes. *International Journal of Hydrogen Energy*, 23(8), pp.653–659.
- Saaty, T. & Vargas, L., 2000. *Models, Methods, Concepts and Applications of the Analytic Hierarchy Process*, Boston: Kluwer Academic Publishers.
- Saaty, T.L., 1990. How to make a decision: The Analytic Hierarchy Process. *European Journal Of Operational Research*, 48, pp.9–26.
- Saaty, T.L., 1980. *The Analytic Hierarchy Process*, New York: McGraw Hill.
- Sadykov, V., Isupova, L., Zolotarskii, I., Bobrova, L.N., Noskov, A.S., Parmon, V.N., Brushtein, E., Telyatnikova, T.V., Chernyshev, V.I. & Lunin V.V., 2000. Oxide catalysts for ammonia oxidation in nitric acid production: properties and perspectives. *Applied Catalysis A: General*, 204(1), pp.59–87.
- Simpson, A.P. & Lutz, A.E., 2007. Exergy analysis of hydrogen production via steam methane reforming. *International Journal of Hydrogen Energy*, 32, pp.4811–4820.
- Skúlason, E., Bligaard, T., Gudmundsdóttir, S., Studt, F., Rossmeisl, J., Abild-Pedersen, F., Vegge, T., Jónsson, H. & Nørskov, J., 2012. A theoretical evaluation of possible transition metal electro-catalysts for N₂ reduction. *Physical chemistry chemical physics: PCCP*, 14(3), pp.1235–45.
- Sorin, M. & Paris, J., 1999. Integrated exergy load distribution method and pinch analysis. *Computers & Chemical Engineering*, 23(4-5), pp.497–507.
- Spath, P.L. & Mann, M.K., 2001. Life cycle assessment of hydrogen production via natural gas steam reforming. *Energy*, (February), pp.NREL/TP-570-27637.
- Steinberg, M. & Cheng, H.C., 1989. Modern and prospective technologies for hydrogen production from fossil fuels. *International Association for Hydrogen Energy*, 14(11), pp.797–820.
- Steinfeld, A., Sanders, S. & Palumbo, R., 1999. Design aspects of solar thermochemical engineering—a case study: two-step water-splitting cycle using the Fe₃O₄/FeO redox system. *Solar Energy*, 65(1), pp.43–53.
- Steinfeld, A., 2002. Solar hydrogen production via a two-step water-splitting thermochemical cycle based on Zn/ZnO redox reactions. *International Journal of Hydrogen Energy*, 27, pp.611–619.
- Steinfeld, A., 2005. Solar thermochemical production of hydrogen - A review. *Solar Energy*, 78(5), pp.603–615.
- Stephens, R. & Pease, N., 1950. Kinetics of the non-catalytic oxidation of ammonia : Flow Experiments by Edgar. *Journal of the American Chemical Society*, 72 (3)(5), pp.1188–

1190.

- Sullivan, K., Piekielek, N., Wu, C., Chowdhury, S., Kelly, S., Hufnagel, T., Fezzaa, K. & Zachariah M., 2012. Reactive sintering: An important component in the combustion of nanocomposite thermites. *Combustion and Flame*, 159(1), pp.2–15.
- Szargut, J., Valero, A., Stanek, W. & Valero, A., 2005. Towards an international reference environment of chemical exergy. *Elsevier Science*, pp.1–21.
- Taheri, K., Gadow, R. & Killinger, A., 2014. Exergy analysis as a developed concept of energy efficiency optimized processes: The case of thermal spray processes. *Procedia CIRP*, 17, pp.511–516.
- Tavares, F. V., Monteiro, L.P.C. & Mainier, F.B., 2013. Indicators of energy efficiency in ammonia production plants. *American Journal of Engineering Research*, 2(07), pp.116–123.
- The Essential Chemical Industry. Available at: <http://www.essentialchemicalindustry.org/chemicals/nitric-acid.html> [Accessed November 5, 2015].
- The Ostwald process for making nitric acid from ammonia: Its proposed combination with the manufacture of calcium cyanamide. *Scientific American Supplement*, LXXVI(1967), pp.161–163.
- Thengane, S.K., Hoadley, A., Bhattacharya, S., Mitra, S. & Bandyopadhyay, S., 2014. Cost-benefit analysis of different hydrogen production technologies using AHP and Fuzzy AHP. *International Journal of Hydrogen Energy*, 39(28), pp.15293–15306.
- Theodore, A., Production of Nitric Oxide. U.S. Patent No. 5478549, 26 December 1995, pp.54–56.
- Thiemann, M., Scheibler, E. & Wiegand, K.W., 2012. Nitric Acid, Nitrous Acid, and Nitrogen Oxides. In *Ullmann's Encyclopedia of Industrial Chemistry Volume 24*. Wiley-VCH Verlag GmbH & Co. KGaA, Weinheim, pp. 177–223.
- Tong, A., Sridhar, D., Sun, Z., Kim, H.R., Zeng, L., Wang, F., Wang, D., Kathe, M.V., Luo, S., Sun, Y. & Fan, L.S., 2013. Continuous high purity hydrogen generation from a syngas chemical looping 25 kW_{th} sub-pilot unit with 100% carbon capture. *Fuel*, 103, pp.495–505.
- Tsatsaronis, G. & Cziessla, F., 2004. Exergy analysis of simple processes. In *Exergy, Energy System Analysis and Optimization*. Encyclopedia of Life Support Systems, pp. 1–9.
- Wang, H.P. & Yeh, C., 1983. On the reduction of copper oxide. *Journal of Chinese Chemical Society*, 30, pp.139–143.
- Wank, J.R., George, S.M. & Weimer, A.W., 2004. Nanocoating individual cohesive boron nitride particles in a fluidized bed by ALD. *Powder Technology*, 142(1), pp.59–69.
- White, A. & Melville, W., 1888. The decomposition of ammonia at high temperatures. *Journal of Chemical Society*, 45, pp.373–385.
- Winebrake, J.J. & Creswick, B.P., 2003. The future of hydrogen fueling systems for transportation : An application of perspective-based scenario analysis using the analytic hierarchy process. *Technical Forecasting & Social Change*, 70, pp.359–384.

- Zawadzki, J., 1950. The mechanism of ammonia oxidation and certain analogous reactions. *Discussions of the Faraday Society*, 8(140), p.140.
- Zhao, Q., Sun, L., Liu, Y., Su, S., Xiang, J. & Hu, S., 2008. Adsorption of NO and NH₃ over CuO/ γ -Al₂O₃ catalyst. *J. Cent. South Univ. Technol. (Engl. Ed.)*, 15(6), pp.830–834.
- Zhu, C., Liu, G., Yu, Q., Pfeffer, R., Dave, R.N. & Nam C.H., 2004. Sound assisted fluidization of nanoparticle agglomerates. *Powder Technology*, 141, pp.119–123.
- Zhu, Y., Mimura, K. & Isshiki, M., 2002. Oxidation mechanism of copper at 623-1073 K*. *Materials Transactions*, 43(9), pp.2173–2176.

LIST OF PUBLICATIONS

Journal Papers

Thengane, S.K., Hoadley, A., Bhattacharya, S., Mitra, S., Bandyopadhyay, S. (2014) Cost-benefit analysis of different hydrogen production technologies using AHP and Fuzzy AHP. *International Journal of Hydrogen Energy*, 2014, 39, 15293-15306
DOI:10.1016/j.ijhydene.2014.07.107

Thengane, S.K., Hoadley, A., Bhattacharya, S., Mitra, S., Bandyopadhyay, S. (2016) Exergy efficiency improvement in hydrogen production process by recovery of chemical energy versus thermal energy, *Clean Technologies and Environmental Policy*
DOI 10.1007/s10098-016-1094-2

Thengane, S.K., Bandyopadhyay, S., Mitra, S., Bhattacharya, S., Hoadley, A. (2016) An alternative process for nitric oxide and hydrogen production using metal oxides, *Chemical Engineering Research and Design*
DOI 10.1016/j.cherd.2016.06.015

Patent

2014900341, Provisional Patent Number, Australian Patent Office, titled “Production Process for Ammonium Nitrate”, filed 5 February 2014 by Orica Mining Services, Newcastle, Australia

International Conference

Thengane, S.K., Hoadley, A., Bhattacharya, S., Mitra, S., Bandyopadhyay, S. (2014) A new alternative process for nitric acid production based on chemical looping approach, Oral Presentation at AIChE Annual Meeting, Atlanta, Georgia (US), 16-21 November 2014

Paper to be submitted

Thermodynamic analysis of chemical looping based nitric oxide and hydrogen production